CHARACTERIZATION STUDIES OF UNMODIFIED AND CHEMICALLY MODIFIED ELECTRODE SURFACES

By

DALE WILLIAM HARAK

Bachelor of Science

Phillips University

Enid, Oklahoma

1989

Submitted to the Faculty of the
Graduate College of the
Oklahoma State University
in partial fulfillment of
the requirements for
the Degree of
DOCTOR OF PHILOSOPHY
December, 1995

CHARACTERIZATION STUDIES OF UNMODIFIED AND CHEMICALLY MODIFIED ELECTRODE SURFACES

Thesis Approved:

Horacio A Mottola

Thesis Advisor

Ziad El Rassi

N Purdie

Huizhen Lu

Thomas C. Collins

Dean of the Graduate College

PREFACE

This thesis concerns the characterization of electrode surfaces, and can be thought of as consisting of three separate parts. *Part One*, consisting of Chapters I and II deals with the characterization of chemically-modified electrode surfaces. Chapter I introduces chemically-modified electrodes and discusses some of their uses in electroanalytical chemistry. Chapter II contains the experimental procedures and results of the research that I have done in this area.

Part Two is composed of Chapters III and IV and treats the characterization of unmodified electrode surfaces. The organization of Part Two follows that of Part One with the introduction of fractal characterization of surfaces being covered in Chapter III and the experimental aspects being covered in Chapter IV.

Part Three contains the overall conclusions for the research projects in Chapter V. Directions for future work are also addressed here.

Pursuing a Ph.D. in chemistry is no easy task; I have had an abundance of help and guidance over these past several years. I would like to take this rare opportunity to express my gratitude all those who helped me in my career path.

I wish to thank my committee members, Dr. Ziad El-Rassi, Dr. Huizhu Lu, and Dr. Neil Purdie for their help and encouragement. A special thank you goes to my advisor, Dr. Horacio Mottola. Dr. Mottola, you are an inspiration to me, not only in the fine aspects of analytical chemistry, but in the aspects of life, in general. Your kind, cheerful, warm-hearted personality has been (and will continue to be) something for which we all should strive to imitate. I expect that your advising duties will not end with my graduation!

Financial support from the Chemistry Department at OSU, the Phillips Petroleum Foundation, Dow Chemical Company, CONOCO, Inc., and the Oklahoma State University Foundation is gratefully acknowledged.

A number of friends here in the lab have helped to make graduate school a learning experience not only in analytical chemistry, but also in the many and varied cultures of the world. The sharing of your cultures and experiences has made this "Oklahoma boy" a much richer person. A heart-felt thank you goes to Lan, Li, Chitra, Rhea, Julio, Juan José, Kiyoshi, Patricia, Chris, Sun Gang, Jianbo, Albahadily, and Paul. I will never forget you and hope that we can stay in touch.

Recognition also needs to be given to Paige Johnson at CONOCO for all of her help and patience with the scanning electron microscopy and X-ray work.

Finally, I want to thank all of my family for all the love and support that they have given me over the years. Mom and Dad, thank you for instilling in me the importance of learning. Without you I could never have gotten this far.

To David and Paula, thanks for always being there when I needed you, and best wishes for you and your new family.

Vicky, its hard to believe all the changes in our lives in the past five years. I want you to know that you and Ethan have given me more joy than words can ever express. Thank you both for all the good times, the understanding when I needed to work late, and the moral support. I love you both with all my heart.

TABLE OF CONTENTS

Chapter Page

I. CHEMICALLY-MODIFIED CARBON PASTE ELECTRODE SURFACES 1

- Introduction 1
- Review of Chemically-Modified Carbon Paste Electrodes 2
- Advantages of Using Carbon Paste Over Other Electrode Materials 3
  - Range of Working Potentials 3
  - Residual Currents of CPE's 4
  - Preparation and Cost of CPE's 6
- Motivation for the Modification of Carbon Paste Electrodes . 7
  - Early History of CPE Modification 7
  - Use of Modifier to Preconcentrate the Analyte 8
  - Use of Modifier to Incorporate an Electrocatalyst . . . 10
  - Use of Modifier to Immobilize Reagents for Electrochemical Reactions 15
  - Modification to Alter the Physical/Chemical Properties of the CPE 19
  - Use of More Than One Type of Modifier in a CPE . . 22
- Means of CPE Modification 23
  - Modification by Adsorption 23
  - Modification by Covalent Attachment 24
  - Modification by Use of a Polymer 29
  - Modification by Direct Admixing 33

Introduction to Surface Analysis Techniques 37

- Electrochemical Techniques 37
- Spectroscopic Techniques 40
  - Auger Electron Spectroscopy 40
  - Infrared Reflectance Spectrometry 41
  - Raman Spectroscopy and Surface-Enhanced Raman Scattering 42
  - X-Ray and Electron Diffraction 43

X-Ray Photoelectron Spectroscopy 43
X-Ray Fluorescence Spectroscopy 44
Extended X-Ray Absorption Fine Structure 45
Secondary Ion Mass Spectroscopy 45
Microscopic Techniques 47
Optical (Light) Microscopy 47
Scanning Probe Microscopy 47
Electron Microscopy 49
X-Ray Microanalysis 54
Summary 56

II. BACKSCATTERED ELECTRON IMAGING OF LIGAND-MODIFIED CARBON PASTE SURFACES BY COMPLEXATION WITH IRON(II) AND/OR CHEMICAL DEPOSITION OF GOLD 59

Chemically-Modified Electrode Characterization 59
Definition of "Characterization" As Applied to Chemically-Modified Electrode Surfaces 59
The Importance of Chemically-Modified Electrode Surface Characterization 60
Experimental 63
Introduction and Background 63
Reagents and Solutions 66
Instrumentation 66
Carbon Paste Surface Preparation 67
Procedure for Ligand Complexation and/or Subsequent Gold
Deposition 70
Results and Discussion 71
Scanning Electron Microscopy and X-ray Microanalysis . . . 78
Scanning Electron Microscopy of the Surface Containing the
Ligand "Spot" 90
Electrochemical Studies 93
Conclusions 96

III. THE CHARACTERIZATION OF UNMODIFIED ELECTRODE SURFACES: SURFACE ROUGHNESS AND REACTIVITY . . . 97

Definition of "Characterization" As Applied To Unmodified Electrode Surfaces 98
Introduction to Fractals and Fractal Geometry 99

Definitions of Fractals, Fractal Geometry, and the Fractal Dimension . . . 99
An Application of Fractal Concepts: How Long is the West Coastline of Great Britain? . . . 103
Types or Degrees of Disorder . . . 105
The Fractal Dimension and Some Theoretical Approaches for its Measurement . . . 106
Inner and Outer Cutoffs for Fractal Behavior . . . 107
Theoretical Models for the Measurement of the Fractal Dimension . . . 108
Box Counting . . . 108
Mass-Radius Method . . . 110
Covering the Object with Spheres . . . 111
Some Experimental Approaches for the Determination of the Fractal Dimension . . . 114
Image Analysis . . . 114
Light Scattering . . . 115
Adsorption Methods . . . 117
Measurements Based on Physical (Electrical) Properties . . . 120
Impedance Analysis . . . 121
Chronoamperometric Techniques . . . 122
Coulometric/Chronocoulometric Techniques . . . 124
An Introduction to the Reaction Dimension . . . 128
Summary . . . 129

IV. IRON(II) COMPLEXES OF THE 1,10-PHENANTHROLINE FAMILY OF LIGANDS AS POTENTIAL PROBES TO CHARACTERIZE ROUGHNESS AND REACTIVITY OF CONDUCTING SURFACES . . . 131

The Importance of Roughness/Reactivity Characterization of Conducting Surfaces . . . 131
Experimental . . . 135
Reagents and Solutions . . . 135
Instrumentation . . . 136
Procedure for Electrode Polishing . . . 137
Procedure for Chronocoulometric Measurements . . . 137
Determination of the Density of the Iron(II) Complexes Used for the Calculation of their Cross-Sectional Areas . . . 140
Results and Discussion . . . 141
Electrochemical Surface Areas . . . 143
Cross-Sectional Areas of Electroactive Probes . . . 145
Log-Log Plots and Scaling Relationships . . . 146

Chapter Page

Conclusions 153

V. SUMMARY AND CONCLUSIONS 155

BIBLIOGRAPHY 159

LIST OF TABLES

Table Page

I. Area Percent Composition of a Carbon Paste Surface Containing 5% 4,7-diphenyl-1,10-phenanthroline after Immersion in Iron(II) and in Gold(III) Solutions 88

II. Summary of Scaling Equations for the Determination of Fractal Dimensions, D_f, on Various Samples 119

III. Chemical Probes Used in the Reported Studies 144

IV. Values of Molecular Diffusion Coefficients Used in Arriving at Apparent Electrochemical Areas from Chronocoulometric Measurements, Anson Plot Values, and Electrochemical Areas for the Glassy Carbon Electrode . 147

LIST OF FIGURES

Figure Page

1. Potential Windows of Different Electrode Materials in 0.10 M H_2SO_4 5
2. Illustration of Redox Mediation in a Chemically Modified Electrode 12
3. Mechanisms for the Redox-Mediated Reactions of Sulfite Ions with Sulphite Oxidase and Phenolic Compounds with Tyrosinase 18
4. Some Reaction Schemes of Carbon Paste Modification via Covalent Bonding of the Modifier 26
5. Spectrophotometric Observation of Leaching 36
6. Schematic Drawing of the Scanning Electron Microscope Showing the Electron Column, the Deflection System, and the Electron Detectors 51
7. Energy-Dispersive X-Ray Spectrum Showing the Presence of Certain Elements on a Chemically-Modified Carbon Paste Surface; X-Ray Mapping of Gold Deposits on Another Carbon Paste Surface 57
8. Representation of the Size and Spacial Distribution of Modifying Centers (depicted as black spots) for Two Hypothetical Chemically-Modified Electrode Surfaces . . 61
9. Diagram Showing the Pyrolytic Graphite Disk Powder Mount Used in the SEM and its Dimensions . . . 68
10. Scanning Electron Micrographs of a 5% 4,7-Diphenyl-1,10-Phenanthroline-Modified Carbon Paste Surface after Immersion in Iron(II) Solution with Subsequent Immersion in a Gold(III) Solution 73
11. Sequence of Chemical Events Comprising the Tagging of Immobilized Ligand Centers on Carbon Paste Surfaces with Gold 75

Figure Page

12. Results of Scanning Electron Microscopy and X-Ray Microanalysis on a Poorly Admixed 5% 4,7-Diphenyl-1,10-Phenanthroline-Modified Carbon Paste Surface prior to Immersion into Iron(II) and Gold(III) Solutions 79

13. Results of Scanning Electron Microscopy and X-Ray Microanalysis of the Carbon Surface in Figure 12 after Immersion into an Iron(II) Solution 80

14. Results of Scanning Electron Microscopy and X-Ray Microanalysis of the Carbon Surface in Figure 12 after Immersion into an Iron(II) Solution Followed by Immersion into a Gold(III) Solution 81

15. Results of Scanning Electron Microscopy and X-Ray Microanalysis on a Well-Admixed 5% 4,7-Diphenyl-1,10-Phenanthroline-Modified Carbon Paste Surface prior to Immersion into Iron(II) and Gold(III) Solutions 82

16. Results of Scanning Electron Microscopy and X-Ray Microanalysis of the Carbon Surface in Figure 15 after Immersion into an Iron(II) Solution 83

17. Results of Scanning Electron Microscopy and X-Ray Microanalysis of the Carbon Surface in Figure 15 after Immersion into an Iron(II) Solution Followed by Immersion into a Gold(III) Solution 84

18. X-Ray Mapping of a Poorly Admixed 5% 4,7-Diphenyl-1,10-Phenanthroline-Modified Carbon Paste Surface after the Surface had been Immersed in both the Iron(II) and the Gold(III) Solutions 87

19. X-Ray Mapping of a Poorly Admixed 5% 4,7-Diphenyl-1,10-Phenanthroline-Modified Carbon Paste Surface after the Surface had been Immersed in both the Iron(II) and the Gold(III) Solutions 91

20. Backscattered Scanning Electron Micrographs of the Carbon Paste Surface Containing the Ligand "Spot" . . . 92

21. Cyclic Voltammograms Obtained with a 5% 4,7-Diphenyl-1,10-Phenanthroline-Modified Carbon Paste Electrode Immersed in 1.0 M $NaClO_4$ 95

22. Illustration Showing how D_f can be used to Quantify the Irregularity of a Line or of a Surface 102

Figure Page

23. Illustration Showing the Box-Counting Method 109

24. Illustration of D_f Determination Using the Mass-Radius Method 112

25. Measurement of D_f by Covering the Object or Surface with Spheres of Differing Size 113

26. Typical Potential and Charge Profiles in Chronocoulometry 127

27. Illustration Showing Molecular Accessibility of Surfaces 133

28. Typical Cyclic Voltammogram of 1×10^{-3} M Tris(1,10-Phenanthroline)iron(II) Perchlorate 139

29. Comparison between Cross-Sectional Area Values for the Tris(1,10-Phenanthroline)Iron(II) Perchlorate Family of Compounds 148

30. Two-Dimensional Projection of the Average Computer-Optimized, Atom-Based Structure of Tris(5-Phenyl- 1,10-Phenanthroline)Iron(II) Cation 149

31. Typical Log-Log Plot of Electrochemical Surface Area Versus Cross-Sectional Area of Electrochemical Probe for a "Smooth" Glassy Carbon Surface 151

32. Typical Log-Log Plots of Electrochemical Surface Area Versus Cross-Sectional Area of Electrochemical Probe for a "Smooth" Gold Surface 152

CHAPTER I

CHEMICALLY-MODIFIED CARBON PASTE ELECTRODE SURFACES

Introduction

Chapter I is meant to introduce the reader to the broad field of chemically-modified carbon paste electrode surfaces. In order to do this, the first part of this chapter will be devoted to a brief review of the broad field of chemically-modified carbon paste electrodes. The review, though by no means exhaustive, will discuss some of the advantages of using carbon paste electrodes (CPE's) over other electrode materials, the basic reasons for modification of CPE's, as well as the various means of modification. Several illustrative examples will be given from the recent literature so that the interested reader can delve further into the original work. Also, the reader interested in more details on modified CPE's is referred to two excellent review articles by Kalcher [1] and by Ulakhovich *et al.* [2].

Chapter I will conclude with an overview of the current instrumental methods of surface analysis and characterization. In particular, the scanning electron microscope will be discussed as well as some of the special techniques associated with it.

Review of Chemically-Modified Carbon Paste Electrodes

The carbon paste electrode was originally developed by Adams [3] while he was attempting to devise a dropping carbon paste electrode composed of suspended carbon particles [4]. The idea was to make a carbon particle electrode, an analog of the well-known dropping mercury electrode. The conditions for successful operation of the dropping carbon particle electrode were far from ideal, however. It was found that a thick paste, packed in a Teflon or glass tube with an electrical connection via a metal contact was more advantageous and had very good electrochemical properties. The first CPE was made by mixing graphite and bromoform, which acted as a liquid binder.

There are several ideas to keep in mind when constructing a carbon paste electrode. For instance, it is important to use highly pure materials. Both the graphite and the pasting liquid must be free from electroactive impurities to achieve low residual currents. Lower residual currents can also be achieved by the use of small graphite particles. The size of the graphite particles must be in the range of 0.0010 to 0.020 mm in diameter for best performance [1].

The choice of the binder used to make a CPE is also important. The binder must be insoluble in the solution to be analyzed. If the binder is even slightly soluble, the CPE surface will be eventually eroded away, causing severe reproducibility problems. For aqueous applications, paraffin oils, silicone grease, silicone oils and mineral oil are commonly used. When the solution to be analyzed is an organic solvent such as acetonitrile, it is common to use compounds such as polyethylene, teflon, and paraffin wax. When these materials for non-aqueous applications are used, an electrochemical pretreatment or conditioning of the CPE is required for efficient electron transfer rates [5]. The more efficient electron transfer rates are probably due to the formation of electrocatalytic or redox-mediating functionalities on the surface of the electrode [1].

Advantages of Using Carbon Paste Over Other Electrode Materials

There are a number of reasons why the carbon paste electrode has become so popular in recent years. These are discussed below.

Range of Working Potentials.

First and foremost, the range of working potentials (potential window) for the CPE is far wider than most any other electrode material. Electroanalytical measurements must be taken in this potential range to avoid the high background currents caused by the oxidation of the solvent at highly anodic potentials and by the reduction of hydronium ions in the solvent at very low potentials. Figure 1 has been adapted from Hynes [5] and Sun [6] and shows the distinct advantage of carbon paste over platinum and mercury electrodes. As can be seen in this figure, platinum is useful at more positive potentials, while mercury is best used at potentials lower than 0.5 V versus the saturated calomel electrode. Carbon paste spans the entire working range of both the platinum and the mercury electrodes, being useful at highly anodic as well as highly cathodic potentials with little or no interference from background currents.

Residual Currents of CPE's. According to Kalcher [1], graphite powder without a binding liquid (in addition to being difficult to handle)gives a fairly high residual current. This high residual current is most likely the result of non-Faradaic processes such as double layer capacitance charging and the unwanted adsorption of molecules onto the large overall surface area of the graphite. Fortunately, these residual currents are dramatically decreased upon the addition of the binding liquid. In fact, the background current in the anodic potential region is extremely low for a wide variety of electrolyte media [4]. In the cathodic potential region a small residual wave due to adsorbed oxygen reduction increases the residual current to slightly larger levels. Because this residual wave has a long, flat plateau, the reduction waves of electroactive species can usually be superimposed without great difficulty [4].

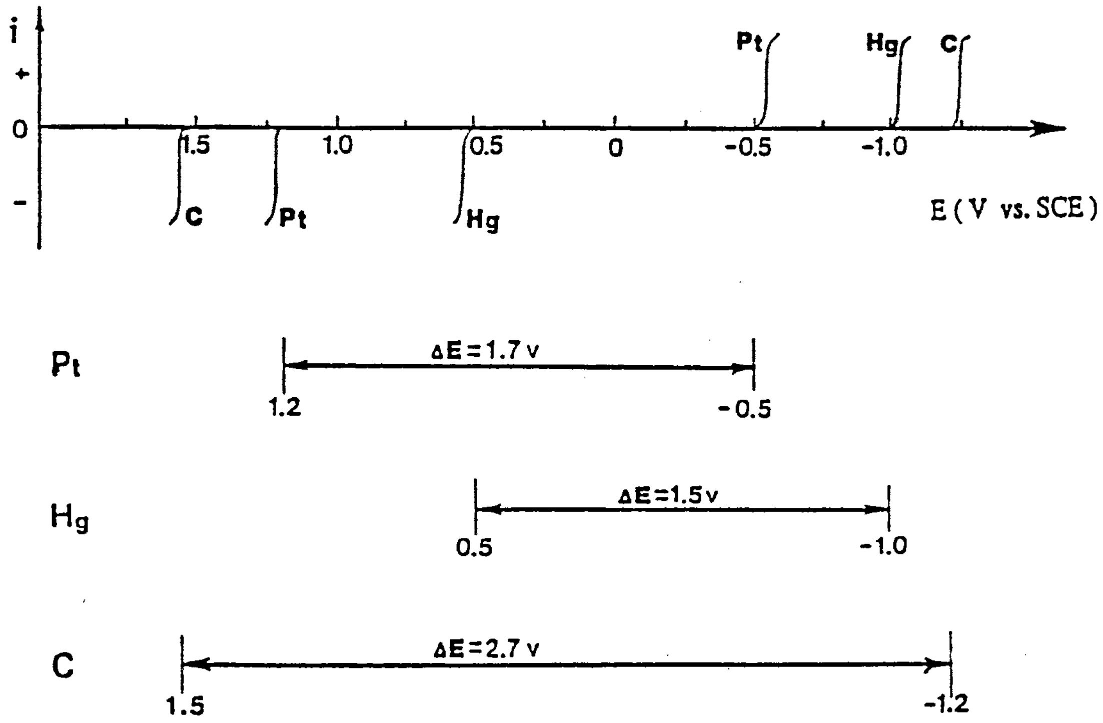
i
+
0
-
1.5
1.0
0.5
0
-0.5
-1.0
C
Pt
Hg
Pt
Hg
C
E (V vs. SCE)
Pt
ΔE = 1.7 v
1.2
-0.5
Hg
ΔE = 1.5 v
0.5
-1.0
C
ΔE = 2.7 v
1.5
-1.2

Figure 1. Potential Windows of Different Electrode Materials in 0.10 M H_2SO_4. Pt, platinum; Hg, mercury; C, carbon [5, 6].

The important idea to note in this discussion is that the carbon paste electrode ordinarily gives very low residual currents within its relatively wide potential window. This means that, for a wide variety of electroactive analytes, low limits of detection can normally be achieved.

Preparation and Cost of CPE's. Another attractive feature of the carbon paste electrode is that the electrode is easily prepared from relatively inexpensive materials. The CPE is readily prepared by thoroughly mixing together in a mortar and pestle the required amounts of purified graphite and the liquid binder. The resulting paste can then be packed into a glass or Teflon electrode body.

The polishing procedure is simple, as well. Unlike the metal-based electrodes, the carbon paste electrode does not require extensive polishing techniques to prepare the surface for various electrochemical procedures. After the carbon paste is packed into the electrode body, all that is needed to polish the surface is to buff the end of the electrode on a smooth, residue-free surface. This procedure produces a shiny, smooth surface that is ideal for carrying out electrochemical measurements.

Because the polishing procedure for CPE's is easily carried out, this makes the renewal of the CPE surface quite straightforward, also. Most laboratories that use CPE's employ special electrode bodies that have a screw-type plunger adjacent to the carbon paste well. To renew the carbon paste surface, the screw is rotated to extrude a small amount of the paste. The surface is then re-polished and the electrode is ready for additional measurements.

Motivation for the Modification of Carbon Paste Electrodes

All electrochemists have, at one time or another, encountered problems that reduce a particular electrode's applicability. Difficulties such as unwanted precipitation or adsorption at the electrode surface, and slow electrochemical reaction kinetics all pose challenges that are most effectively dealt with at the electrode surface [7}. This section will cover some of the early history of the development of modified CPE's, as well as some of the reasons and rationale for the modification of CPE's while citing some specific examples from the recent literature.

Early History of CPE Modification. The first appearances of CPE modification in the literature was some work by Kuwana and French [8] in 1964 and by Schultz and Kuwana [9] in 1965. The modification of the CPE was done by directly mixing organic and organometallic compounds such as ferrocene, anthraquinone, and 5-aminobenzophenone directly into the n-undecane or substituted naphthalene pasting liquid. The idea behind this alteration of the electrode was to be able to study the voltammetric and chronopotentiometric behaviors of water insoluble compounds using a CPE without having to resort to the use of an organic solvent such as acetonitrile to dissolve the compounds. Kuwana [8] hinted, however, that a CPE modified in this way might be useful in electroanalysis. This opened a whole new area of research in this field, and work on modified CPE's for electroanalysis has become quite a popular topic since 1975.

Use of Modifier to Preconcentrate the Analyte. One of the earliest uses of a chemical modifier in a CPE for determinations was the incorporation of ion exchangers, complexing ligands, or adsorbents to preconcentrate a particular analyte at the surface of the electrode. This mode of action has been referred to as bearing formal analogy to trace analysis by the electrochemical technique called anodic stripping voltammetry because the sample species is partitioned from a dilute solution into the modified electrode layer and is subsequently reduced or oxidized by an electrode potential sweep or step [2,7]. Using a modifier which preconcentrates the analyte onto a CPE permits one to allow the analyte to adsorb onto the surface, and then remove the electrode to another solution in which the electrochemical conditions can be optimized for the generation of the analytical signal.

The most common species which are presently determined with CPE's of the "preconcentration" type are the metal cations, a few cationic dyes, complex cations, I^-, NO_2^-, and complex anions. The modifiers are any of a number of cation exchange resins and zeolites, biological modifiers like algae, organic complexing agents such as 1,10-phenanthroline and dimethylglyoxime, or anionic exchange resins. Some organic compounds, e.g. aniline, can be determined with the use of adsorbents as the CPE modifier. Typical adsorbents are clays like sepiolite, hectorite, and bentonite [1].

A notable example from the recent literature of the use of an ionic exchange resin as a modifier in a CPE is the work of Hernández *et al.* [10]. Copper(II) ions were able to be determined down to the 18 nM level by preconcentrating the ions at a Dowex 50W-X8-modified CPE electrode for 2 min with no applied potential. After removing the electrode to an electrolyte solution and using differential pulse voltammetry the analytical signal was produced. The surface of the electrode was regenerated (copper atoms removed to prepare the surface for the next determination) by successive potential sweeps.

The use of organic ligands in CPE's for preconcentration of the analyte is illustrated in the work of Baldwin *et al.* [11], who determined nickel(II) cations at a dimethylglyoxime-modified CPE with very good selectivity. The procedure used was similar to the one used by Hernández, but it was found that conditioning the electrode by repeated immersion in nickel(II) followed by reconditioning (regenerating the surface) in 1.0 M HNO_3 produced an electrode surface which was more efficient in preconcentrating the analyte.

An interesting and unusual modifier that has been used to preconcentrate tetrachloroaurate(III) at the CPE surface is the microscopic algae, *Chlorella* *pyrenoidosa* [12]. Again, the overall procedure included a preconcentration step in which the electrode was placed in the analyte solution for a short period of time, followed by the evaluation step in which the electrode was removed to an electrolyte solution for the differential pulse voltammetric measurement, and lastly, the regeneration step in which the gold-containing ions were removed from the electrode surface by immersion in a 0.05 M sodium cyanide solution. The preconcentration effect was found to be effected by the interaction of the tetrachloroaurate(III) ions with the functional groups present on the surface or within the cellular matrix of the microorganisms.

Preconcentration has also been accomplished using an *in situ* modification, that is, a modification done to a CPE surface by adding the modifier to the analyte solution and not to the CPE directly. Brainina *et al.* [13] were able to preconcentrate I^- and Sb(III) at a graphite rod electrode surface by adding a triphenylmethane dye to the analyte solution. It seems that by holding the electrode at 0 V versus Ag/AgCl, preconcentration of the analyte ions occurs by formation of an insoluble, electrochemically-active adduct which readily adsorbs to the electrode surface. The analyte can then be determined to quite low limits of detection by stripping voltammetry. This preconcentration effect did not take place in the absence of the dye.

Use of Modifier to Incorporate an Electrocatalyst. Another important reason to modify a CPE is to include a species on the electrode surface which can act as a "redox mediator" in an electrochemical reaction between the electrode and the analyte. The function of such a species, called an electrocatalyst, is to lower the energy of activation for the electrochemical reaction by lowering the energy pathway between the reactants and the electrochemical products [14].

There are several different proposed mechanisms for the operation of an electrocatalyst immobilized on a CPE surface. According to Bonakdar and Mottola [15], one of these proposed mechanisms is a chemical reaction of the analyte with the immobilized redox mediator on the electrode surface, followed by the regeneration of the catalyst to its former oxidation state by exchange of electrons with the electrode, the so-called CE mechanism. Figure 2 depicts the reduction of an analyte species in the presence of an electrocatalyst by a CE mechanism and has been taken from Sun [6].

The utility of incorporating electrocatalysts onto electrode surfaces is that the electrode kinetics of an analyte are faster. The oxidation orreduction of the analyte occurs at a potential that is much less positive or negative, respectively, than the expected thermodynamic potential. In other words, the overpotential required to induce an electrochemical reaction is reduced. Because of the lowered overpotential, a determination based on an electrode with an incorporated redox mediator is often much more sensitive and selective for the analyte than a determination at a naked or unmodified electrode.

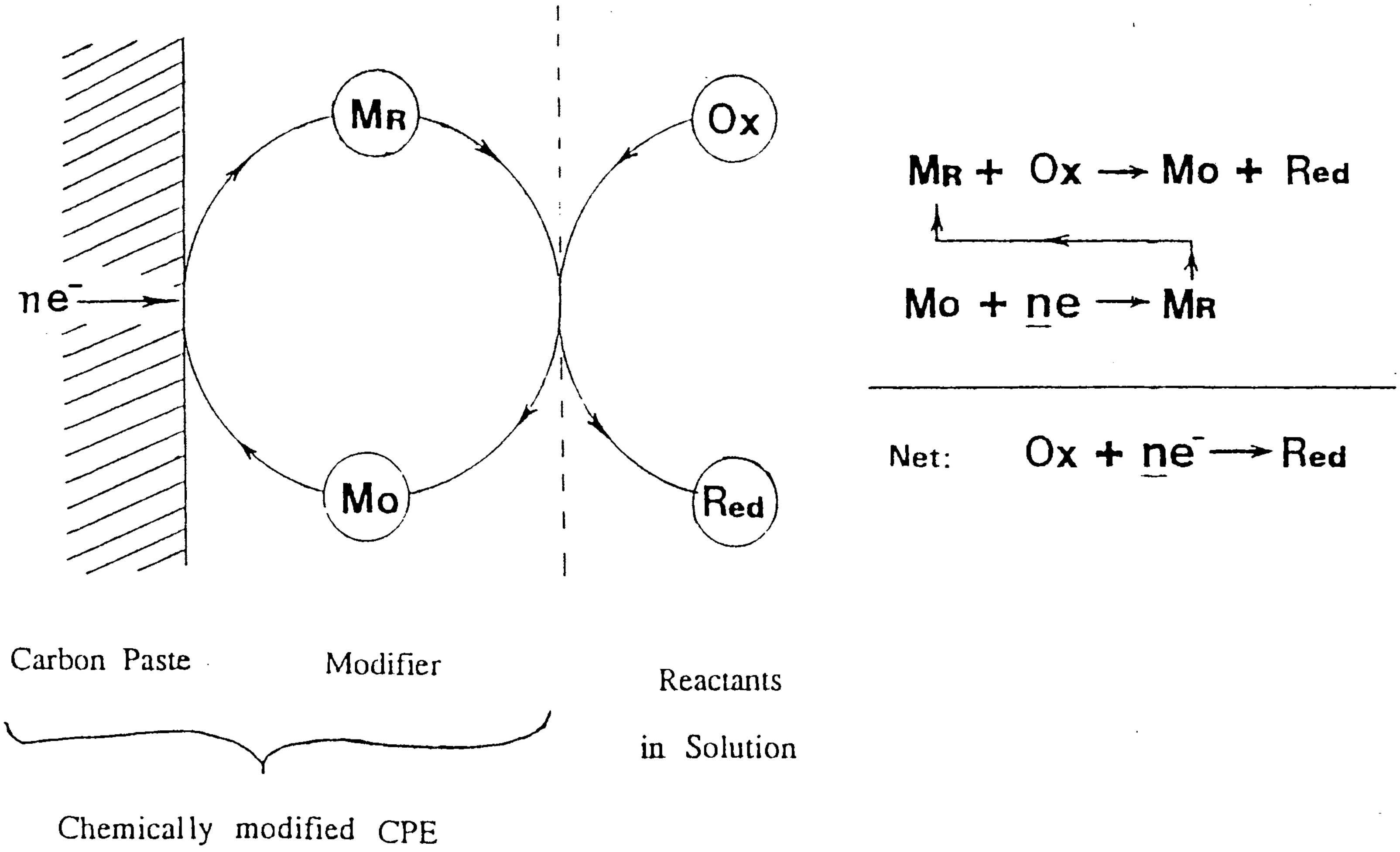
MR
MO
Ox
Red
ne⁻
Carbon Paste
Modifier
Reactants
in Solution
Chemically modified CPE
MR + Ox → MO + Red
MO + ne → MR
Net: Ox + ne⁻ → Red

Figure 2. Illustration of Redox Mediation in a Chemically Modified Electrode [6]

The most common type of modifiers used in CPE's to impart electrocatalytic properties are organometallic complexes such as cobalt pthalocyanine or tris-(4,7-diphenyl-1,10-phenanthroline) iron(II) salts. Other modifiers include electroactive organic compounds and ion exchange resins with electrostatically immobilized transition metals or complex ions. The analytes that have been determined using electrodes with immobilized electrocatalysts vary widely and range from amino acids and carbohydrates to O_2 and compounds of environmental interest like NO and NO_2.

Examples of analytical applications of CPE's modified with electrocatalysts abound in the literature. One example of the use of an ion exchange resin to immobilize the electrocatalyst is the work by Geno *et al.* [16], who electrostatically immobilized $Fe(CN)_6^{-4}$ ions on poly(4-vinylpyridine) at low pH. They incorporated this into a CPE for the catalyzed oxidation of ascorbic acid. In this work it was shown that the rate constants for the oxidation of ascorbic acid were much larger than the corresponding rate constants in homogenous solution, showing the important result that immobilization of the electrocatalyst often improves the efficiency of the catalyst because diffusional restrictions are removed when the modifier is in close contact with the electrode surface.

A dramatic illustration of the lowering of overpotential in the determination of an analyte was given in the work of Linders *et al.* [17].

This paper reported the results of the determination of cysteine in 0.05 M H_2SO_4 at a cobalt pthalocyanine (CoPc)-modified CPE. The potential required to oxidize cysteine at an unmodified CPE was 1.380 V, whereas the potential required for the same reaction at the CoPc-modified CPE was only 0.710 V, giving a measurement which was much more selective. The importance of choosing an electrocatalyst with a formal potential near that of the analyte was also stressed in this paper. For instance, in the determination of cystine the formal potential is only slightly higher than that of cysteine, but this slight increase in formal potential renders the reaction with the CoPc mediator thermodynamically unfavorable and thus unable to catalyze the oxidation of cystine.

In other work by Bonakdar *et al.* [18], and by Hynes *et al.* [19], the amperometric performance of a tris(4,7-diphenyl-1,10-phenanthroline) iron(II) perchlorate-modified CPE in the determination of NO_2 was discussed. Hydrodynamic voltammograms showed that the electrocatalytic effect was indeed at work. The flow of current due to the oxidation of NO_2 was much higher at lower potentials for the modified CPE versus an unmodified CPE, illustrating the improvement of both selectivity and sensitivity when the immobilized modifier is present on the electrode surface.

Use of Modifier to Immobilize Reagents for Electrochemical Reactions. Another important reason to modify the surface of a CPE is to immobilize reagents such as electrochemical reactants or catalysts (excluding electrocatalysts, which were covered in the previous section). By immobilizing electrochemical reagents on the electrode surface, one can greatly reduce the amount of reagent waste, and subsequently, expense. This type of CPE modification is particularly useful for application in flow systems such as continuous flow analysis or chromatography, where reagents must continuously be added to the system flow for operation.

Among the species that make good candidates for immobilization on a CPE surface are enzymes, particularly those enzymes which will catalyze the transformation of an non-electroactive analyte into an electroactive product. Enzymes, being very selective in the types of reactions that they can catalyze, often lend that selectivity to the electrochemical measurement when they are incorporated into a CPE. An important drawback of using enzymes, however, is that many enzymes are quite expensive to obtain commercially. As a result, much research has been conducted to try to minimize the amount of enzyme consumed in a determination.

Among the most studied enzymes glucose oxidase, which catalyzes the oxidation of glucose into gluconic acid and hydrogen peroxide in the presence of dissolved oxygen. The use of this enzyme as a modifier for a CPE is an example of the transformation of the analyte (glucose), which is not readily detectable electrochemically, into an electroactive product (H_2O_2). Matuszewski and Trojanowicz [20] used glucose oxidase in a CPE to determine glucose in soft drinks and fruit juices down to 20 μM levels.

It should be noted at this point that when enzymes are used as modifiers in CPE's, special care must be taken to preserve the activity of the enzymes. Often this is done by working at carefully controlled pH's and by the deliberate storage of the electrode in buffered solutions at reduced temperatures when not in use. Even with these precautions, the activity of the enzyme in the electrode usually goes down with time. The error in the determination of a particular species due to decreasing activity of the enzymes in often controlled by judicious re-calibration. For glucose oxidase, it was found that the activity of the enzyme in the CPE actually increased for the first few days of use, then remained at a relatively constant level for about 3 weeks [20].

Often, the incorporation of a particular enzyme into a CPE necessitates the addition of a co-enzyme such as NAD^+, and/or an electrocatalyst. In the determination of primary alcohols by oxidation with a CPE modified with baker's yeast [21], the active enzyme, alcohol dehydrogenase, required the co-enzyme NAD^+, which was added to the analyte solution. The electroactive product of the enzyme reaction, NADH, is more readily detected in the presence of the electrocatalyst hexacyanoferrate(III), and so this too was added to the analyte solution. The detection limit for ethanol using this system was found to be 2×10^{-6} M with a linear dynamic range of 0.02 to 0.2 mM.

The co-enzyme and/or the electrocatalyst species can be added directly to the analyte solution, but these species seem to make good candidates for immobilization onto the CPE surface as well. Depending on the mechanism of the enzyme reaction, co-immobilization of the auxiliary species may or may not be possible. This will be illustrated in the following two examples.

Abu Nader *et al.* [22] used a CPE modified with sulfite oxidase for the determination of SO_3^{-2}, HSO_3^-, and SO_2 in a continuous-flow system utilizing hexacyanoferrate(III) as a redox mediator. The enzyme was first immobilized on a cross-linked agarose, and was then incorporated into the carbon paste. It was found that the redox mediator could not be co-immobilized with the enzyme in the carbon paste because the mechanism of the enzyme reaction required that the mediator be in intimate contact with the enzyme. Figure 3 depicts this reaction scheme.

In other cases the electrocatalyst and the enzyme can be co-immobilized into the carbon paste. An example of this is the use of tyrosinase and hexacyanoferrate(II) as the redox mediator in the modified carbon paste for the determination of phenol [23]. As shown in Figure 3, the redox mediator reacts with a product of the enzyme reaction, not the enzyme itself. Thus, close contact of the mediator and the enzyme is not necessary. The limit of detection

$$E + SO_3^{2-} \longrightarrow E{-}SO_3^{2-}$$

$$E{-}SO_3^{2-} + H^+ \longrightarrow HE{-}SO_3^-$$

$$HE{-}SO_3^- + H^+ \longrightarrow HESO_3H$$

$$HESO_3H + H_2O \longrightarrow H_2E + SO_4^{2-} + 2\,H^+$$

$$H_2E + 2\,Fe(CN)_6^{3-} \longrightarrow 2\,Fe(CN)_6^{4-} + 2\,H^+ + E$$

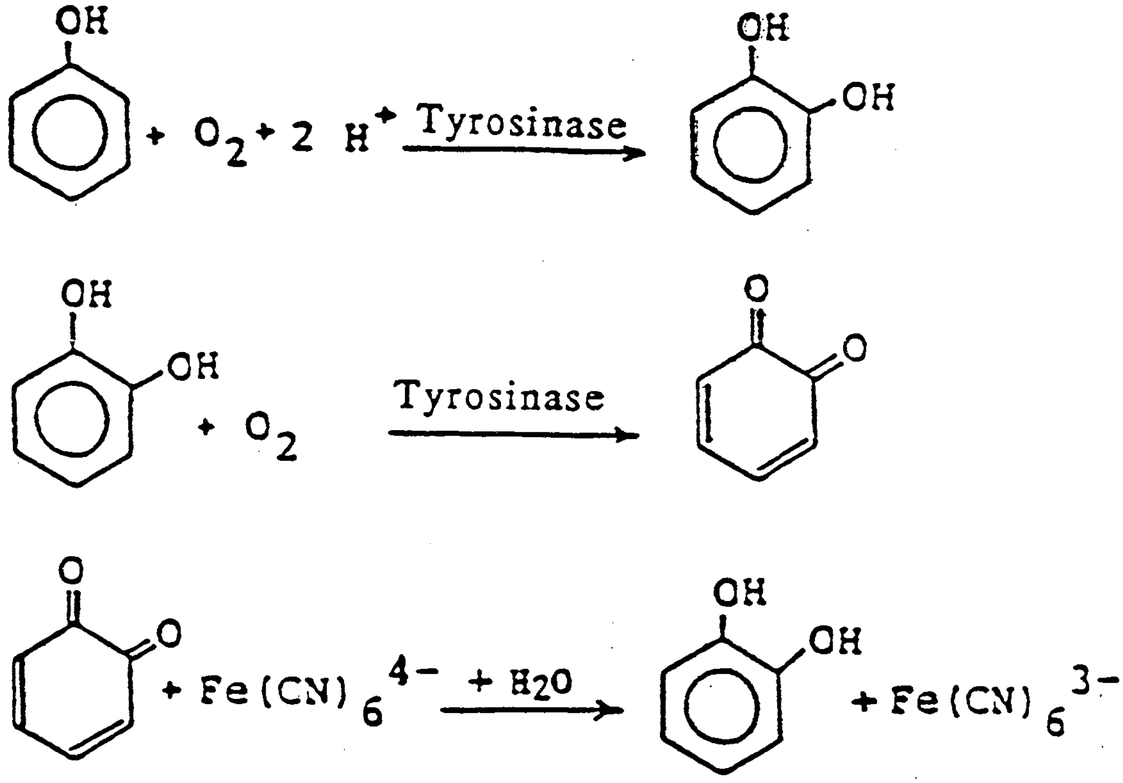
OH
+ O2 + 2 H+
Tyrosinase
OH
OH
OH
OH
+ O2
Tyrosinase
O
O
O
O
+ Fe(CN)6 4-
+ H2O
OH
OH
+ Fe(CN)6 3-

Figure 3. Mechanisms for the Redox-Mediated Reactions of Sulfite Ions with Sulphite Oxidase and Phenolic Compounds with Tyrosinase [22, 23]

for phenol using this system was 14 ppb with a linear dynamic range up to 2.5 ppm in phenol.

Modification to Alter the Physical/Chemical Properties of the CPE. The last main reason to modify a CPE surface is to change the physicochemical properties of the surface. Alteration of the properties of a CPE can provide advantages such as electrode "activation", discrimination against interferences, and protection of the electrode surface from "poisoning".

The types of modifiers used to alter the physical/chemical properties vary widely and range from graphite sprays and silica gel to electropolymerized films and stearate salts. It is important to note that a CPE surface can be modified not only chemically, but it can also be modified by electrochemical pretreatments. Work that has been done in this regard will be discussed, also.

The first example from the literature is not really a modification at all, making it difficult to classify into one of the above "reasons for modification". In a process called extractive accumulation, Wang and Freiha [24] have shown that certain organic compounds can be extracted from an aqueous analyte solution into the pasting liquid of the carbon paste, thus preconcentrating the analyte at the electrode surface. Chlorpromazine was shown to have an affinity for silicone grease used as the binder in one CPE, and hydroxyanisole showed a like affinity for Nujol used as the pasting liquid in another CPE. Work in this area also proved that extractive accumulation causes preconcentration of the analyte species at not only the electrode surface but also in the interior regions of the carbon paste. Studies done in which the voltammetric current was measured before and after removal of a thin section of the CPE surface confirm this. As could be predicted, the preconcentration effect was found to be enhanced by increasing the percentage of the pasting liquid or binder in the carbon paste and also by increasing the time in which the electrode was immersed in the analyte solution.

Another way to modify a CPE surface is to use electrochemical means. Ravichandran and Baldwin [25] applied an electrochemical pretreatment to a plain CPE in a manner similar to a scheme used by Engstrom and Strasser [26] for a glassy carbon electrode. Ravichandran and Baldwin treated the CPE by applying a voltage of 1.75 V versus Ag/AgCl to the electrode for a period of 5 min, and by following this with a 10 s pulse at -1.20 V versus Ag/AgCl. This pretreatment produced an electrode which gave faster electron exchange than before the pretreatment; this was evidenced by the more reversible electrochemical reactions of hydroquinone and ascorbic acid. The mechanism for this effect is not clearly understood, and the formation of electrocatalytic moieties on the electrode surface was not confirmed by cyclic voltammetry as was the case for the work done on the glassy carbon electrode. It should be noted that the improvement in the rate of electron exchange was short-lived in these electrodes, especially for applications in flow systems.

In some cases the modifier used to alter the CPE surface can greatly reduce interferences by other species present in the analyte solution. An example of this is some work done by Ormonde and O'Neill [27], who used a stearate-modified CPE to determine dopamine in brain tissue extracts. Ordinarily, interferent species are present in the extracellular fluid in large excess over the dopamine analyte. Interferences such as ascorbic and uric acids and metabolites often mask the electrochemical signal originating from the analyte. The mechanism for the operation of the stearate modifier seems to be one of electrostatic attraction and repulsion. At pH 7.4 in the analysis, the stearate carboxylic acid moieties are ionized, giving a negatively-charged surface which repels the interferent ascorbic and uric acids, which are also ionized at this pH. The dopamine analyte has a protonated amine group at this pH, and so is attracted to the electrode surface where it can be readily detected. Although electrodes of this type were useful *in vitro*, later studies have shown that they are not useful *in vivo* because of physiological surfactant action on the pasting liquid [28].

One last example of the modification of a CPE to alter its chemical/physical properties an approach used by Abu Nader *et al.* [29] in which an electropolymerized film of 4-hydroxybenzaldehyde and formaldehyde was used to coat the surface of a glassy carbon electrode, protecting the surface from the usual poisoning problems when electrodes of this type are used to determine phenolic compounds. This approach was also applied to a wax-based CPE with the successful formation of a polymer film on this surface, as well. Although the electrochemical characterization and possible applications of this wax-based electrode were not reported, the CPE modified in this way would be expected to behave similarly to other modified CPE's and to the polymer-coated glassy carbon electrode, which was extensively characterized and applied to chromatographic detection systems [29b].

Use of More Than One Type of Modifier in a CPE. It should be noted here that the use of one type of modifier does not exclude the use of another type of modifier in the same electrode. Indeed, the current trend is to incorporate more than one modifier in a given electrode. An example of such a system is the addition of an enzyme and an electrocatalyst into the same carbon paste preparation. The enzyme reacts with the analyte in a specific way which may produce an electroactive product. The electrocatalyst serves to lower the overpotential for the electrochemical detection of the electroactive product. Hale *et al.* [30] have immobilized ferrocene (an electrocatalyst) onto two different siloxane polymers and admixed these preparations into a carbon paste with glucose oxidase for the determination of glucose. Other researchers [31] admixed an insoluble derivative of ferrocene into carbon pastes, and then entrapped either galactose oxidase, glycolate oxidase, or L-amino acid oxidase beneath a polycarbonate membrane on the surface of the polished CP electrode surface.

Means of CPE Modification

The following section will discuss the various methods commonly used to modify CPE's and will also address some of the advantages and disadvantages using each method.

Modification by Adsorption. Although adsorption of an analyte on an electrode surface is often detrimental to the measurement, adsorption is a very convenient way to attach a modifier. In fact, convenience is the most important advantage to using this method of modification. Carbon, especially activated carbon, is by nature a very good adsorbent, readily lending itself to physical adsorption of various modifiers. In addition, the pasting liquid can serve as an organic phase for the extraction of organic-based modifying species onto the electrode surface.

A representative sample of work done to immobilize CPE modifiers by adsorption is an immobilization of glucose oxidase by Ikeda *et al.* [32]. The authors mixed *p*-benzoquinone, a redox mediator, with a carbon paste and packed the mixture into an electrode body. The CPE surface was smoothed, and a drop of a glucose oxidase solution was placed on the surface. After evaporation of the solvent, a 1:4 mixture of Collodion-ethanol was spread on the surface to form a thin film of nitrocellulose which stabilized the adsorbed enzyme. The presence of the redox mediator on the electrode surface allowed determinations of glucose to be done that were independent of the concentration of dissolved O_2 in the analyte solution.

The biggest problem in using adsorption to attach a modifier is that the modifier is often not held as tightly to the electrode surface as one might like. Electrodes modified in this way have very limited application in flow systems like continuous-flow analysis and chromatography because the modifier can be continually swept off of the surface by the incoming stream. It is thus extremely important that the modifier be insoluble in the analyte matrix so that this phenomenon is lessened or does not occur.

Modification by Covalent Attachment. Another important means of CPE modification is by the chemical attachment of the modifier to the CPE. The usual procedure is to treat the CPE surface with a coupling or an activating agent which introduces the required functional groups onto the graphite surface for the subsequent covalent binding of the modifier.

The molecular structure of graphite is one of stacked sheets of fused aromatic rings. Whenever this structure is terminated, such as at a perimeter, dangling valencies become satisfied by reaction with oxygen and water. This produces edge-planes with a large number of various functionalities such as phenolic, quinone, carboxylic, lactone, and other ketonic groups. These reactive groups represent "anchors" for the attachment of coupling agents and/or CPE modifiers. Many researchers have attempted to increase the number of oxygen-containing functionalities on the carbon surface by oxidation of the graphite via RF-induced oxygen plasma ashing, wet chemical oxidation with mixtures of HNO_3 and H_2SO_4, and by heating at very high temperatures in the presence of O_2.

As can be imagined, there are numerous protocols that have been developed for the covalent attachment of a wide variety of species to carbon paste surfaces. The majority of these involve the formation of amide-type linkages between the carboxylic functionalities on the graphite surface and an amine moiety on the modifier. In these reactions the carboxylic groups on the CPE must usually be activated by reacting them with thionyl chloride, acetyl chloride, or a carbodiimide. The carbodiimide activation is preferred by many researchers because of the mild reaction conditions necessary for the subsequent attachment of the amine group-containing modifier. Figure 4 summarizes some of these modification schemes.

One example of the covalent attachment of a modifier onto a CPE by an amide linkage is a procedure developed by Cheek and Nelson [33], who attached diethylenetriamine to a CPE to preconcentrate and determine Ag^+ ions down to 10^{-11} M levels. The immobilization was carried out by reacting graphite, diethylenetriamine, and dicyclohexylcarbodiimide together in methylene

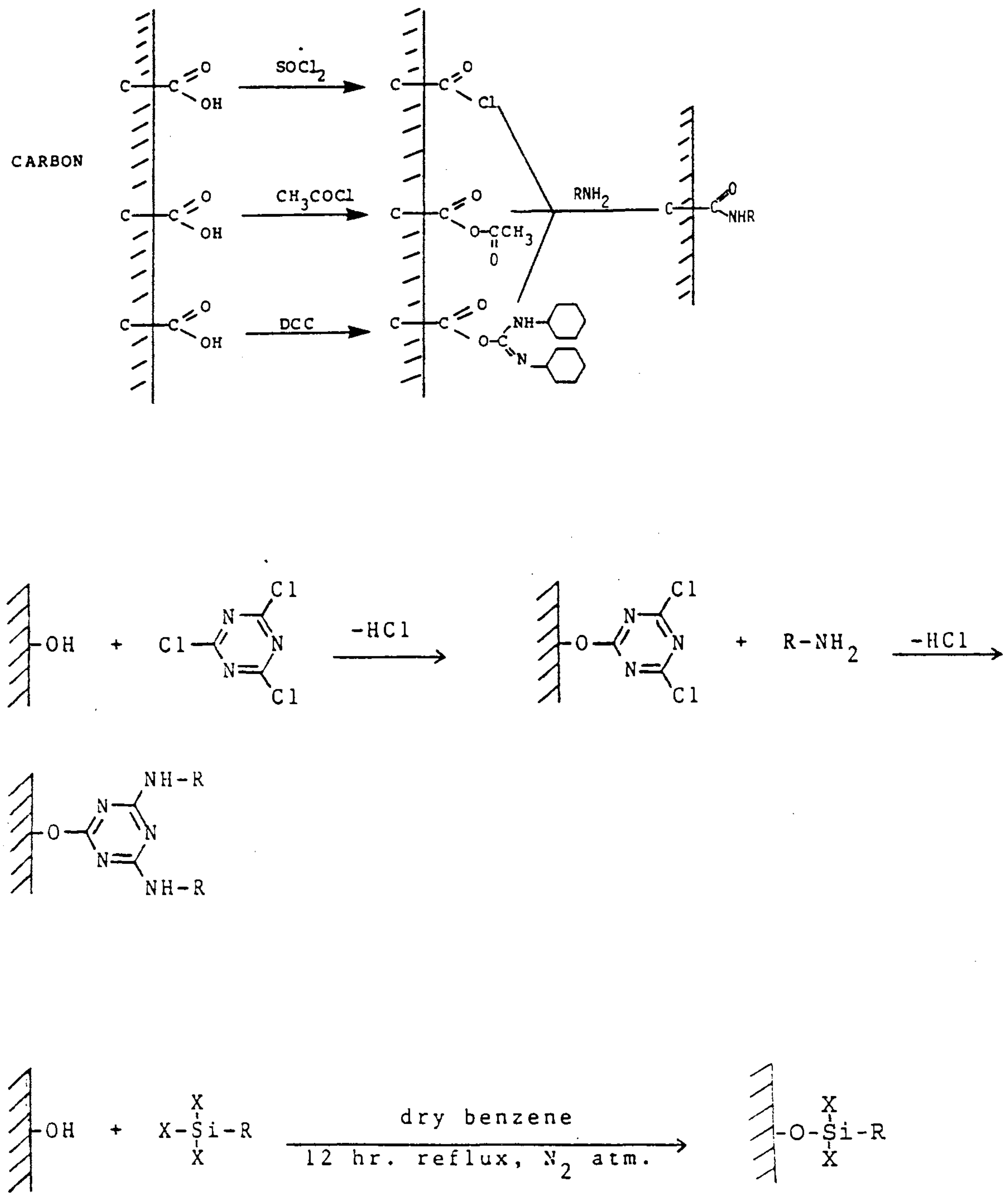
CARBON
SOCl2
CH3COCl
DCC
RNH2
-HCl
R-NH2
-HCl
dry benzene
12 hr. reflux, N2 atm.

Figure 4. Some Reaction Schemes of Carbon Paste Modification via Covalent Bonding of the Modifier [5]

chloride for several hours. After several washings and evaporation of the solvent, the modified graphite was mixed with a liquid binder and packed into an electrode body.

Another method for a covalent attachment of a modifier onto a CPE and utilizing a diimide was one used by Kamin and Wilson [34] to immobilize the glucose oxidase enzyme on a CPE. In order to increase the number of carboxylic moieties on the graphite surface, these authors opted to use a wet oxidation of the graphite prior to the immobilization procedures. The oxidized graphite was mixed with a fine Teflon powder, packed into an electrode body and wetted with a phosphate buffer. The electrode surface was then reacted with 1-ethyl-3-(3-dimethyl aminopropyl) carbodiimide and rinsed again with buffer. The derivatized electrode surface was finally reacted with a solution of glucose oxidase in the phosphate buffer for the covalent attachment of the enzyme to the electrode surface by reaction with free amino groups on amino acid residues in the enzyme. The authors then went on to study the kinetic behavior of the bound enzyme.

In other work electrocatalysts have been immobilized on CPE surfaces. Albahadily [35] has successfully immobilized 5-amino-1,10-phenanthroline and its iron(II) complex on CPE surfaces. The immobilization was begun by oxidizing the graphite by heating in the presence of O_2 or by wet oxidation. The resulting carboxylic groups on the surface were activated (converted to acyl chlorides) by heating with thionyl chloride in dry benzene for 30 min. With the addition of 5-amino-1,10-phenanthroline or its iron(II) complex in dimethylformamide, the covalent attachment of the modifier was complete.

Other covalent attachments of modifiers have been done by reaction of the hydroxyl groups on the CPE surface, though the majority of this work has been done on glassy carbon or pyrolytic graphite surfaces. These modifications involve the attachment of cyanuric chloride or organosilanes to the surface hydroxyl groups to act as bridges for subsequent coupling of amines, alcohols, Grignard reagents, and hydrazines [36].

One last example is a covalent attachment of a modifier to a CPE without using an amide linkage [37]. Yao and Musha's approach for the immobilization of the co-enzyme nicotinamide adenine dinucleotide (NAD^+) was to add n-octaldehyde to the graphite/liquid paraffin binder mixture. By packing this mixture into an electrode body and dipping the electrode into an NAD^+ solution, the co-enzyme was immobilized by the formation of a Schiff base linkage between aldehyde functionalities on the CPE surface with the free amino groups present on the NAD^+ molecule.

The most important advantage to using covalent bonding to immobilize a modifier on a CPE surface is that the modifier is usually held quite tightly to the CPE surface, even for modifiers that are soluble in the analyte solution. In addition, the close proximity of the modifier to the CPE surface greatly enhances electron "communication" between the modifier and the electrode, which should give faster electron transfer rates. The last advantage is that unlike immobilization by adsorption, electrodes modified by covalent attachment are excellent candidates for use in flow systems.

The main disadvantage for covalent immobilization of CPE modifiers is that the procedures are often long and complicated, sometimes requiring the application of harsh conditions to increase the number of functionalities on the graphite surface. Also, it is difficult to control the extent of surface modification.

Another important disadvantage is that in some cases CPE surfaces modified by covalent attachment are not easily renewable. An example of this would be the immobilization of a modifier at a CPE surface after packing the paste into an electrode body, rather than the immobilization of the modifier on the graphite particles in bulk. In such a case, the modifier would have to be re-attached each time the electrode is polished.

Modification by Use of a Polymer. The use of polymers to modify CPE's is widespread in the literature. The vast amount of work that has been done in this area is probably due to the following facts: 1) polymers provide many varied functions on the electrode surface, and 2) there are many techniques available for polymer attachment to the electrode surface.

The polymer, usually applied as a thin layer on the electrode surface, can have many functions. One of the most common uses is the use of the polymer film as a protective layer. The polymer layer can act as a barrier to species which would normally foul or poison the naked electrode surface. An example of this was the work by Abu Nader *et al.* [29], which was described in the section on changing the chemical/physical properties of the surface. These authors electropolymerized a substituted phenol and formaldehyde on glassy carbon and carbon paste electrodes to protect the electrode surfaces from poisoning in the electrochemical determination of phenol.

A more common function of a polymer on a CPE surface is to entrap a modifier on the electrode surface to prevent solubilization of the modifier into the analyte solution. Almeida and Mulchandani [38] were able to determine L-glutamic acid using a CPE containing tetrathiafulvalene as a redox mediator. The tetrathiafulvalene-containing carbon paste was packed into an electrode body and the CPE surface was polished. L-glutamate oxidase was cross-linked with glutaraldehyde, and this solution was dropped onto the electrode surface. After solvent evaporation, the enzyme was entrapped on the surface by placing the electrode into a solution of resorcinol and 1,3-phenylenediamine and repeatedly applying potential sweep cycles between 0 and 0.6 V versus Ag/AgCl to electropolymerize a polymer film on top of the enzyme. The thin polymer film prevented the loss of enzyme into the analyte solution while allowing the L-glutamic acid analyte to diffuse through for interaction with the enzyme.

In other work horseradish peroxidase [39] (for the determination of aniline) and glucose oxidase [40] (for the determination of glucose) were mixed into carbon pastes and placed into electrode bodies. After polishing, the enzymes were anchored into the pastes by applying a thin layer of Nafion (a sulfonated fluoropolymer from Du Pont) onto the respective CPE surfaces. It was reported that enzymes entrapped by this method of placing the polymer film **over** the enzymes showed improved kinetic behavior over other methods in which the enzymes are entrapped **within** polymer matrices. This is probably due to the inability of the enzymes to freely change conformations when they are immobilized inside the entangled polymer chains typically found in a polymer matrix.

In the above examples the function of the polymer film is merely to act as a barrier, either to incoming species which could poison the electrode surface, or to modifiers which could leach out of the carbon paste due to inherent solubility of the modifier in the analyte solution. There has also been much research done in which the polymer film itself acts as the true modifying species. The use of a polymer film as the modifier usually involves the incorporation of electrocatalytic species such as ruthenium or iridium complexes into the film. Murray [36] has classified polymers with electrocatalytic properties into 2 types.

These are: 1) the "redox polymers" which contain the electroactive centers as a part of the polymer chain backbone or in which the electroactive centers are coupled to a functionalized group on the polymer, or 2) the "ion exchange polymers" which electrostatically bind ionic redox substances from their solutions into the film as counterions. In either case the vast majority of the accomplishments in this field of electrode modification has been on metal and glassy carbon surfaces. However, an example of the modification of a CPE with a "redox polymer" follows.

Yu [41] electropolymerized tris[5-amino-1,10-phenanthroline] iron(II) perchlorate onto a wax-based CPE. The 40% paraffin wax/60% graphite electrode was immersed in a solution of the complex, followed by the application of cyclic voltammetric conditions for several cycles over a potential range of 0.0 V to 2.0 V versus Ag/AgCl at a scan rate of 50 mV/s. The shiny, blue polymer which formed on the CPE surface exhibited electrocatalytic behavior, and the CPE modified with this polymer film was found to be useful for the determination of NO_2, phenol, Cl_2, H_2S, and SO_2.

The advantage to using a polymer or polymerization techniques to modify an electrode surface is that the immobilization procedures are usually quite easy to do. Electropolymerization is very readily done on working electrode surfaces, and the use of pre-formed polymer gels is also quite convenient. Another advantage is that polymer films, when used as the true modifying species, can contain a larger quantity of mediator sites than a corresponding monolayer, and better electrocatalytic efficiency may result.

The use of a polymer on an electrode surface also has some drawbacks. When used as an electrocatalytic modifier, attention must be paid to the ion and solvent permeability within the film, the permeability of electroactive species, and the migrating ability of electrons in the polymer film. The limited permeability of some polymer films has prompted many researchers to use polymeric materials which swell in the analyte solvent, giving an open structure more easily accessible to analyte and electrolyte species.

Permeability is also important to polymer films used for entrapment of modifiers. The film must be impermeable to the modifier, but allow free passage to analyte species. This cannot be done in practice, and the result is slower kinetic behavior of many entrapped enzyme systems.

Modification by Direct Admixing. The last main method of CPE modification is by directly admixing the modifier into the carbon paste preparation; this is easily the most popular modification method due to its simplicity and effectiveness.

There are two basic ways to modify a carbon paste by direct admixing. The first is to dissolve the modifier into the pasting liquid, which works well for those modifiers that have lipophilic characteristics. The other is to add the modifier to an already-prepared carbon paste.

Examples of modification by direct admixing abound in the literature. The work of Wang and Chen [42] and Wang *et al.* [43] illustrate both the utility of direct admixing of modifiers as well as the use of more than one modifier in a given CPE.

Wang and Chen [42] prepared a CPE by mixing graphite, mineral oil, potassium hexacyanoferrate (II) (an electrocatalyst), horseradish peroxidase, and disodium ethylenediaminetetraacetate (EDTA) together. The idea was to be able to determine hydrogen peroxide or organic peroxides like 2-butanone peroxide in the presence of metal ions such as cobalt(II), nickel(II), or manganese(II), which are known to have inhibitory effects on the peroxidase enzyme. The function of the EDTA was to bind the metal cations, preventing them from interacting with the enzyme.

Wang *et al.* [43] admixed yeast alcohol dehydrogenase and NAD^+ into a carbon paste composed of mineral oil, graphite, and a ruthenium-dispersed graphite containing ruthenium as an integral part of the graphite particles. The utility of using a ruthenium-dispersed graphite was that dissolution problems were avoided and that electrochemical communication between the ruthenium and the detected enzyme product, NADH, was improved over other methods.

The large popularity of direct admixing means that there are several advantages to using this modification technique. Direct admixing is the easiest and fastest means of achieving modification of CPE's in the laboratory.

Furthermore, the degree of modification is easily regulated by adjusting the weight percentage of the modifier in the paste. Another distinct advantage is that since the modification is done to the carbon paste as a whole, it is a trivial matter to renew the electrode surface.

The last main advantage is that there is a large variety of modifiers that can be incorporated into carbon pastes in this manner. The principle requirement is that the modifier must not be soluble in the analyte solutions to be measured, or at least adsorb strongly to one of the components in the paste. In addition, the modifier should not undergo electrochemical transformations within the potential range of the voltammetric response of the analyzed species (except for electrocatalytic applications) which could cause high background currents.

Among the disadvantages of direct admixing is the requirement of modifier insolubility in the analyte medium. Even slight solubility can cause a slow leaching of the modifier into the analyte solution, giving results that seriously affect reproducibility. The extent of modifier leaching from a CPE modified by direct admixing is commonly studied in characterizing electrode behavior. Figure 5 is a spectrophotometric observation of modifier leaching done by Hynes [5], and it demonstrates the need for insoluble modifiers. Curve A represents the leaching of a highly soluble 1,10-phenanthroline iron(II) complex from a directly-admixed carbon paste, while curve B shows the

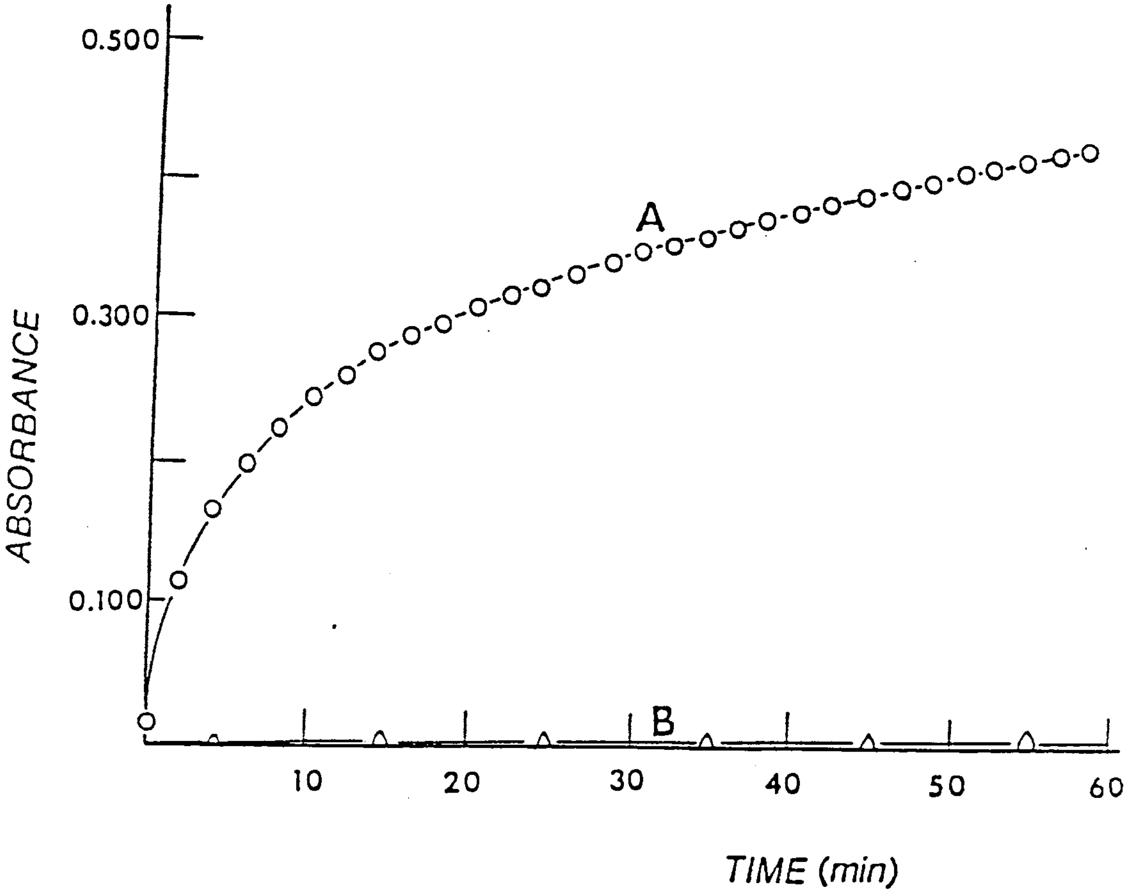

Figure 5. Spectrophotometric Observation of Leaching. Curve A: tris(1,10-phenanthroline)iron(II) cation, monitored at 512 nm; Curve B: tris(4,7-diphenyl-1,10-phenanthroline)iron(II) cation, monitored at 543 nm; 16.8% w/w of appropriate complex, 1.0 M KCl, stirring conditions, no applied potential [5].

leaching of the highly insoluble 4,7-diphenyl-1,10-phenanthroline iron(II) complex from the same directly-admixed paste.

Reproducibility of results from directly-admixed carbon pastes is also very dependent on the homogeneity of the paste. Care must be taken in the preparation of the pastes so that the concentration of the modifier on the CPE surface is similar in analogous experiments.

Introduction to Surface Analysis Techniques

This last section of Chapter I will briefly discuss some of the current techniques available for the study of surfaces. Many of these techniques require sophisticated and very expensive equipment, which is not always widely available. For ease of discussion the various techniques have been grouped together into three separate areas: electrochemical, spectroscopic, and microscopic. The techniques are discussed only to the point to give an overview of the field, to explain some of the basic operating principles of selected techniques, and finally to make the point that surface analysis can be approached in a number of different ways.

Electrochemical Techniques

There are several different electrochemical techniques that can be used to analyze modified (and unmodified) electrode surfaces. Potential step, potential sweep, controlled current, alternating current, and hydrodynamic methods have all been used to study electrode surfaces and processes. Regardless of the specific technique used, however, the information about the nature of an electrode surface that can be obtained from these various techniques is somewhat limited. From a general standpoint electrochemical techniques can determine: 1) the potentials at which species at the electrode surface (either free or adsorbed) can oxidize or reduce, 2) the active surface area of the electrode surface, 3) surface area coverage of an electroactive modifier or adsorbed species, and 4) kinetic parameters of specific electron transfer processes taking place at the electrode surface.

One important electrochemical technique of relevance to this particular research project is a linear potential sweep method known as cyclic voltammetry. This technique typically utilizes a 3-electrode system consisting of a working or indicator electrode (the electrode of interest), a reference electrode (a nearly ideal nonpolarizable electrode), and a counter or auxiliary electrode (electrode which allows the passage of current between it and the working electrode with a negligible amount of current passing through the reference electrode). Cyclic voltammetry measures the amount of current flowing through an electrochemical cell at a working electrode as a function of a "saw-tooth" shaped potential/time ramp applied to the working electrode. Electroactive species in the immediate vicinity of or on the working electrode surface can become oxidized or reduced as the potential applied between the working electrode versus the reference electrode is swept to higher or lower levels, respectively.

Cyclic voltammetry is used mainly to determine formal oxidation and reduction potentials of various electroactive species, but the technique's usefulness does not end there. The shape of the current versus potential waveform is useful for the elucidation of electrochemical mechanisms as well as the rate of electron exchange and associated electron transfer kinetic parameters. The magnitude of the current peaks in cyclic voltammetry can also be used to quantify the amount of electroactive analytes in solution or those present on the electrode surface.

As stated earlier, electrochemical methods are somewhat limited in terms of the kinds of information that can be obtained about electrode surfaces. Specifically, the acquisition of information about surface molecular structure or about locations, size, and distribution of modifying species on an electrode surface is lacking. For this reason electrochemical methods will not be discussed further so that more emphasis can be placed upon spectroscopic and microscopic techniques, which will be much more important for this research.

Spectroscopic Techniques

The aim of this section is to introduce the reader to the various spectroscopic techniques that are commonly used to investigate the nature of solid surfaces. In general the basic operating principle of most spectroscopic surface analysis instruments is that the sample is bombarded by a beam from a source (electrons, ions, or photons). The interaction of this beam with the sample surface produces electrons, ions, photons, or neutrons which are focused into the entrance aperture of an analyzer. The analyzer separates the signal particles on the basis of energy or mass and the particles are then sent to a detector such as an electron multiplier [44].

Auger Electron Spectroscopy. Auger electron spectroscopy is a spectroscopic technique that allows the qualitative and sometimes quantitative identification of elements existing on a surface. In this technique the surface to be analyzed is bombarded with an electron beam. As these so-called primary electrons interact with the surface atoms, there are many possible processes that can develop.

The particular process that produces Auger electrons occurs when the impinging electrons eject a core-level electron from one of the surface atoms. The atom, now in an excited state, fills the core-level vacancy with an electron from an outer shell. By falling into the vacant core position, the outer shell electron must lose a quantum of energy before it can enter the lower energy, core-level shell. The energy released in this process is absorbed by another outer shell electron with the subsequent ejection of the electron. This electron is called an Auger electron, and its emission is favored for those elements with low atomic number [45].

Each Auger electron is released from a surface atom with a characteristic kinetic energy which is related to the binding energies of the three electron shells involved in the overall Auger process of the surface atom [46]. The plotting of a typical Auger spectrum (usually dN/dE versus E, where dN/dE is the first derivative of the number of Auger electrons of a given energy with respect to the electron energy, E) gives fairly well-defined peaks which can be used for the elemental analysis of a surface.

Infrared Reflectance Spectrometry. For surfaces that reflect infrared (IR) radiation relatively well, methods exist whereby the IR radiation reflected from a surface can be used to generate an IR spectrum. The spectrum can be used and interpreted in much the same way as conventional IR spectra to identify the presence of polyatomic inorganic ions as well as organic entities on a surface. The thicknesses of films can also be determined in some cases. Typically, a special reflectance attachment is placed into the sample beam path. The attachment deflects the IR radiation to the surface being analyzed. After reflection from the sample surface, the beam is then directed back into the instrument for detection [47].

Raman Spectroscopy and Surface-Enhanced Raman Scattering.

Raman spectroscopy is based on the Raman scattering effect in which certain molecules inelastically scatter incident light. The light that is scattered by the molecules is of a different frequency than the incident light, and these frequency shifts are due to changes in the polarizability of bonds in the molecule as the bond undergoes transitions in its vibrational energy state. Raman scattering intensity is dependent upon the polarizability of bonds in the scattering molecule, the symmetry properties of the polarizable bonds during a vibration of those bonds, and the intensity of the incident light source [47].

Raman scattering has also been found to give much higher intensities when the scattering species are adsorbed on certain metal surfaces such as silver and gold [46, 47]. The technique known as *surface-enhanced Raman spectroscopy* exploits this fact, but requires the use of specially-designed cells that can house both the metal surface and the adsorbing species. In most cell designs the metal surface (which can be an electrode) is positioned so that it is parallel to a flat, optical window. A space between the metal surface and the optical window allows for the interaction of the metal surface with a solution containing the adsorbate. The incident light beam, usually from a laser, is focused directly adjacent to the surface but parallel to it. The scattered radiation is then analyzed at 90 degree angles to the metal surface through the optical window.

X-Ray and Electron Diffraction. These two methods involve the bombardment of the sample surface with either X-rays or low energy electrons. The diffraction patterns of the X-rays or of the electrons is then studied to calculate spacing of the surface atoms in the lattice. Such information can then be used to determine the orientation of the surface and/or any adsorbed species on the surface [46]. Usually, conditions such as the angle of incidence of the incoming X-rays or electrons is adjusted so that only the outermost layer of atoms on the surface is involved in the diffraction process. Traditionally, these methods required the sample to be placed in ultra-high vacuum conditions, but recently *in situ* techniques have been developed which can allow study of electrode surfaces while under electrochemical conditions.

X-Ray Photoelectron Spectroscopy. This type of spectroscopy is useful in the identification of elements present on a surface. In this technique the sample surface is bombarded with a stream of monochromatic X-rays. Because of the high energy of these incident photons, electrons from the inner cores of atoms absorbing the X-rays will be ejected with an energy equal to the difference between the incident photon energy and the binding energy of the ejected electron in its respective shell [46]. The energies with which the core electrons are ejected are characteristic of each particular element, and this serves as a basis for elemental analysis of a surface. It should be noted that X-ray photoelectron spectroscopy is also sensitive to the oxidation states of atoms. For instance, the technique can differentiate between iron(III), iron(II), and iron(0) due to the shifts in the X-ray photoelectron spectrum. These shifts are thought to be due to increases in the binding energies of the core electrons as the charge on the atom becomes more positive, and the shifts could prove very useful in the study of electrode surfaces.

X-Ray Fluorescence Spectroscopy. When an atom is excited by an incident X-ray, another way it can relax is by emitting another X-ray, which is characteristic of the element. This forms the basis for X-ray fluorescence spectroscopy and allows the qualitative as well as the quantitative analysis of the elements comprising a sample [45]. The sample is bombarded with a polychromatic X-ray beam, and the subsequent fluorescence (secondary X-rays) is recorded by detectors capable of resolving the energies and intensities of the fluorescent signal.

One of the disadvantages to this technique is that since secondary X-rays can originate from any depth down to around 100 micrometers, the analysis is of the bulk rather than of the surface. Another drawback is that the detection sensitivity varies depending on the element detected. Low atomic weight elements are generally detected with higher sensitivity than are elements with higher atomic weights.

Extended X-Ray Absorption Fine Structure. The principle involved in surface analyses of this type is the study of the fine X-ray absorption structure on the high energy side (up to 100 eV) of an X-ray absorption edge. The absorption edge is a certain X-ray energy at which the sample atoms begin to absorb X-ray photons. The fine structure of the X-ray absorption spectrum occurs because of the scattering of photons from surrounding atoms back toward the excited atom at the origin and because of interference between the outgoing wave and the backscattered wave. Fine structure information allows one to calculate bond lengths and geometric structure [45, 46].

Ordinarily, the sample is very thin so that the X-ray intensity transmitted through the sample can be readily measured. Modifications to the technique are usually done for the analysis of surfaces, and this includes the use of a grazing angle of incidence for the incoming X-ray beam or the detection of the X-ray fluorescence relaxation products emanating from the sample atoms rather than the detection of the primary X-ray itself.

Secondary Ion Mass Spectroscopy. In secondary ion mass spectroscopy the sample surface is placed in an evacuated chamber and is bombarded with high energy (5-10 keV) particles or ions. These high energy particles, usually

Ar^+, are made to strike the surface causing ionization and removal (sputtering) of surface atoms. The charged ions that are ejected from the surface are accelerated in an electric field into a mass analyzer, which allows only those particles with a certain mass/charge ratio to pass through the mass selecting sector and thus reach the detector. By changing the conditions (magnetic and/or electric fields) inside the mass analyzer, particles with differing mass/charge ratios can be selected for detection, allowing the collection of intensity versus mass/charge spectra. Such spectra are quite useful for identifying atoms and molecules present on a surface, and in some cases quantitative information can be obtained although this type of analysis is complicated [48].

A related mass spectrometry technique that has been recently developed is known as spatially multidimensional secondary ion mass spectrometry. Instruments such as these allow the imaging of surfaces by bombarding the sample surface with a primary beam of ions. The secondary sample ions that sputter from the surface are focused so that there is a lateral correspondence between the original surface and the virtual image. The virtual image is mass analyzed and is reconstructed at the detector. Only those areas of the surface with a given mass appear in the final image. Such information can be quite useful in characterizing the atomic and molecular make-up of a surface. Rüdenauer has written an enlightening review article on this subject [48].

Microscopic Techniques

In many instances the microscopic techniques have proved most useful for the study of surfaces. This section will highlight the various types of microscopy including scanning electron microscopy and the associated X-ray microanalysis techniques, which are particularly relevant to the research at hand.

Optical (Light) Microscopy. In this, the most common and oldest type of microscopy, the sample is illuminated with light in the visible region of the spectrum, and the image of the sample surface is magnified through a set of optical lenses. There are several types of optical microscopy such as bright field (ordinary), dark field, phase contrast, interference, polarizing, and fluorescence microscopies, each suited to particular kinds of surface materials [49].

Optical microscopy is not as useful for the purposes of this research since it is not capable of visualizing individual modifying centers on carbon paste surfaces. In other words, a modified carbon paste surface and an unmodified carbon paste surface appear to be identical when viewed using an optical microscope. Because of this limitation, the discussion will proceed to more relevant and useful types of microscopy.

Scanning Probe Microscopy. Scanning probe microscopy has become quite popular in recent years because of the atomic resolution possible with many of these instruments. Although there are many types of scanning probe microscopes such as scanning tunneling microscopy and atomic force microscopy, the basic operating principle is the same. Magnified images are obtained by using a scanning probe to obtain information on an object. Variations in the interaction of the probe tip with the sample surface allow the imaging of the surface with the help of electronic data collection. The interactions between the sample surface and the probe tip can range from attractive to repulsive atom-atom interactions (atomic force microscopy) to the exchange of electrons through quantum mechanical tunneling (scanning tunneling microscopy) [50].

Several researchers have used scanning probe microscopy to investigate the nature of carbonaceous surfaces. McCreery *et al.* [51] used scanning tunneling microscopy to study unmodified glassy carbon electrodes. Specifically, the effect of surface morphology on the electrode kinetics and capacitance was compared. Other researchers [52] have been able to characterize activated graphite electrode surfaces using both scanning tunneling microscopy and atomic force microscopy. These techniques were able to locate active sites on the graphite surface due to the differing conductivity and atomic environments surrounding the active centers. Scanning tunneling microscopy has also been used to image colloidal gold [53] and thermally evaporated gold islands [54] on pyrolytic graphite surfaces.

Electron Microscopy. This field has enjoyed a great deal of success in the last 50 years, more than likely a result of the incredible depth of field and resolving power of the electron microscope. The first electron microscopes were of the transmission type, which can be thought of as the electron microscope analog of the ordinary light microscope. In transmission electron microscopy, electrons (sometimes called primary electrons) are focused by magnetic fields so that they pass through and interact with a thin sample film (50-200 Å in thickness). The resulting image is magnified and focused via magnetic fields onto a fluorescent screen or photographic plate for viewing [55]. As in all types of electron microscopy, the sample and electron path must be placed under high vacuum to avoid electron interaction with air molecules.

The limitation of having to use thin samples in transmission electron microscopy was one of the reasons for the development of the scanning electron microscope (SEM). The fundamental difference between the transmission electron microscope and the SEM is the fact that rather than form an image by directing primary electrons **through** the sample, the SEM uses secondary electron emission from the sample and backscattered primary electrons for imaging [56]. Secondary electrons are those electrons produced when electrons from the sample atoms are dislodged as a result of being bombarded by the primary electrons from the microscope's electron gun. The secondary electrons are usually of low energy, but are of great utility in forming an image of the specimen surface. Backscattered primary electrons are also useful for imaging. These electrons originate from the electron gun, and are simply those electrons that have been elastically scattered by the specimen surface.

Figure 6 shows a simple schematic diagram of a scanning electron microscope. The SEM operates by focusing (via electromagnetic lenses) a fine beam of electrons upon the specimen. The electrons have been energized by acceleration in an electric field, and these electrons typically have energies of up to 40 keV. The result is that a very small spot on the specimen surface (usually less than 10 nm in diameter) is bombarded with primary electrons. Other electromagnetic lenses (called the scan coils) move the small electron spot across the specimen surface so that a rectangular raster is generated. The signal intensity (amplified secondary or backscattered electron current) is measured simultaneously with each specific location of the small electron spot on the specimen surface. Variations in signal occurring as the beam moves over the specimen surface provide the intensity changes we see on the viewing screen as an image [56]. The degree of magnification is defined as the ratio of the linear size of the viewing screen to the linear size of the electron raster. Therefore, to achieve high magnification one simply decreases the size of the rectangular electron raster by adjusting the scan coils.

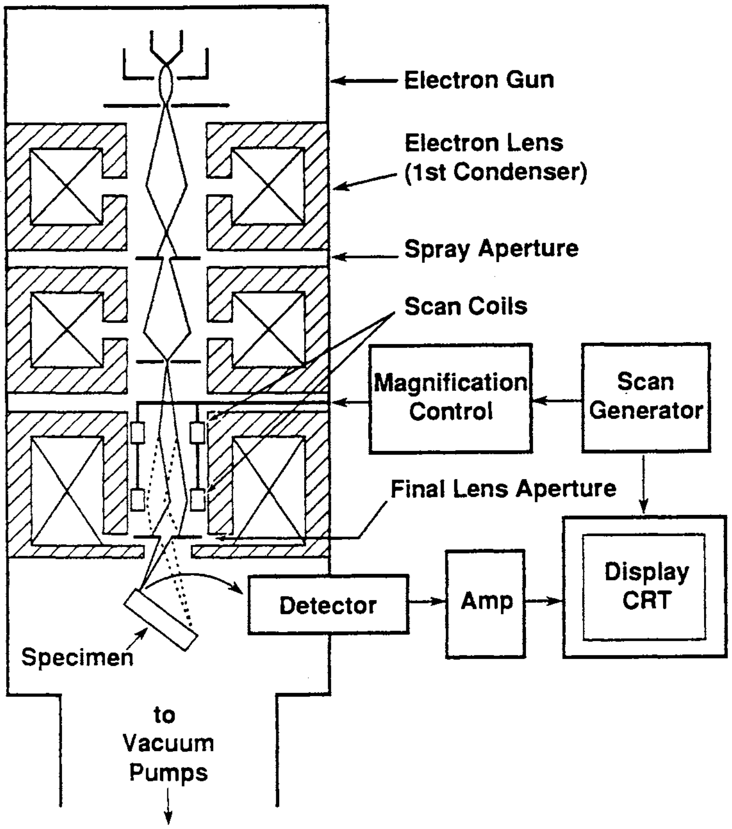
Electron Gun
Electron Lens
(1st Condenser)
Spray Aperture
Scan Coils
Magnification Control
Scan Generator
Final Lens Aperture
Display CRT
Detector
Amp
Specimen
to
Vacuum
Pumps

Figure 6. Schematic Drawing of the Scanning Electron Microscope Showing the Electron Column, the Deflection System, and the Electron Detectors [55, 56]

There are many processes that occur as a result of bombarding a specimen surface with energetic electrons, and these processes produce a number of signals that can be measured to gain qualitative andquantitative information about the specimen surface. Secondary electrons, backscattered primary electrons, and X-ray signals are all commonly used to study surfaces in a scanning electron microscope.

Secondary electrons originating from the specimen itself are quite sensitive to surface topography, and are thus the most commonly used signal for SEM surface imaging. The secondary electrons are usually of low energy after they emerge from the sample surface, and as a result, most commercial SEM manufacturers employ a secondary electron detection system utilizing a positively charged electron collector that draws the low-energy secondary (and a few backscattered) electrons into it for detection [56, 57]. As Figure 6 shows, the detector is usually located to the side of the specimen at small to medium angles to the plane of the specimen. In addition, the specimen is often tilted slightly toward the detector to increase the brightness of the image. Brightness increases because the zone of secondary electron emission (directly surrounding the impinging primary electron spot) increases as the angle at which the primary electron beam strikes the specimen varies from the perpendicular [57].

Backscattered primary electrons, as stated earlier, are simply those electrons from the primary beam that are elastically scattered by the specimen surface. Backscattered electrons are quite useful in SEM imaging and particularly in this research because they respond to specimen characteristics such as surface composition and, to a lesser extent, surface topography. Backscattered electron production shows a strong correlation with the atomic number of the specimen atoms, and this forms the basis for high contrast modes in scanning electron microscopy. Since the backscattering efficiency increases with atomic number, an element of higher atomic number will show stronger emission, resulting in brighter areas on the viewing screen [57]. This, as will be shown in Chapter II, will be very important to the viewing of modifying centers marked with gold on a carbon paste electrode surface.

The backscattered electron detector is located directly over the specimen. This is because, unlike secondary electrons, backscattered primary electrons are fairly high in energy and travel in straight paths, being unaffected by low voltage electric fields such as is found in the positively-biased secondary electron collector. Only those backscattered electrons with trajectories in line with the detector will produce a signal. Because the backscattered electron signal is weak (due to the small number of backscattered electrons directly reaching the detector), interfering secondary electrons must be deflected away. This is commonly done by applying a slightly negative bias on the collector of the backscattered electron detector [56, 57].

The last type of signal that will be discussed here and that is used in conjunction with scanning electron microscopic imaging is the characteristic X-ray signal. X-rays are emitted as a product of the stabilization process of a specimen atom following ionization of the atom by the primary electron beam. In a typical scenario an electron from an inner atomic shell is dislodged by the primary electron beam and an electron from an outer shell fills the vacancy. Because energy must be released for such an electron to drop to a lower shell, an X-ray photon is emitted with an energy equal to the difference between the energy levels of the final and initial states of the transitional electron [57]. Since all atoms have various electron shells with characteristic amounts of energy, each atom will emit X-rays of certain characteristic wavelengths when the atom is bombarded by a beam of high-energy, primary electrons or by another means of excitation. This forms the basis for the SEM-related technique called "X-ray microanalysis". It should be noted that X-rays of widely varying wavelengths can also be produced when primary electrons are decelerated in the electric fields of the specimen atoms. These X-rays (called continuum, Bremsstrählung, or white X-rays) are not characteristic of particular elements, but are always present and must be dealt with as background noise.

X-Ray Microanalysis. This SEM-related technique is capable of qualitatively and sometimes quantitatively determining which individual elements are present in a given specimen. Elemental evaluation can be done using two different X-ray analysis systems. *Wavelength dispersive X-ray spectrometry* works by "counting" X-rays of a given wavelength for a given period of time. This system has the advantages of higher sensitivity and applicability to elements from beryllium to uranium [57]. The other system, *energy dispersive X-ray spectrometry*, is a compact, low cost system which is capable of rapid, simultaneous multi-element analysis of the full X-ray spectrum. It is the more commonly used system and will be briefly described below.

Energy dispersive X-ray spectrometry operates by allowing X-rays from the specimen to strike a semiconductor crystal which has a high bias voltage across it. As a result of X-ray bombardment, the atoms of the crystal each absorb a given amount of energy and release electrons (an ionization process), which then migrate in the semiconductive material. The higher the energy of the X-ray, the greater the number of electrons are ionized. The strength of the current from the crystal is thus proportional to the energy of the X-rays striking the crystal. These electrical pulses are digitized and are sent to a multi-channel analyzer which sorts these signals and counts the number of X-rays at each energy level that strike the crystal. The analysis of X-rays using this system does not involve the actual separation of wavelengths, but does require computer processing of the data. The overall elemental analysis of the specimen sample is much more rapid because many X-ray wavelengths are processed at the same time [57].

The speed of the energy dispersive analysis spectrometer allows the processing of data in two different ways, both of which were very important to the present research. The first is the generation of a X-ray intensity versus X-ray energy spectrum, an example of which is shown in Figure 7. Another way to use X-ray data is to produce an image or map. This is done by selecting only a given energy range for X-ray detection. The specimen is scanned (rastered) by the primary electron beam, and when an X-ray is detected in the selected energy range, the corresponding beam location on the synchronously-scanned viewing screen is marked with a dot. Regions of high concentration are therefore characterized by a high dot intensity. An X-ray map of this type is also shown in Figure 7.

Summary

This chapter was meant to introduce the reader to a wide variety of topics, all of which are relevant to the research at hand. The chapterbegan with a review of modified carbon paste electrodes, citing several methods of carbon paste modification as well as analytical applications of modified CPE's.

To give an overview of the different techniques currently available for surface analysis, a number of surface analysis techniques were discussed, highlighting their basic operating principles. Some detail was given concerning

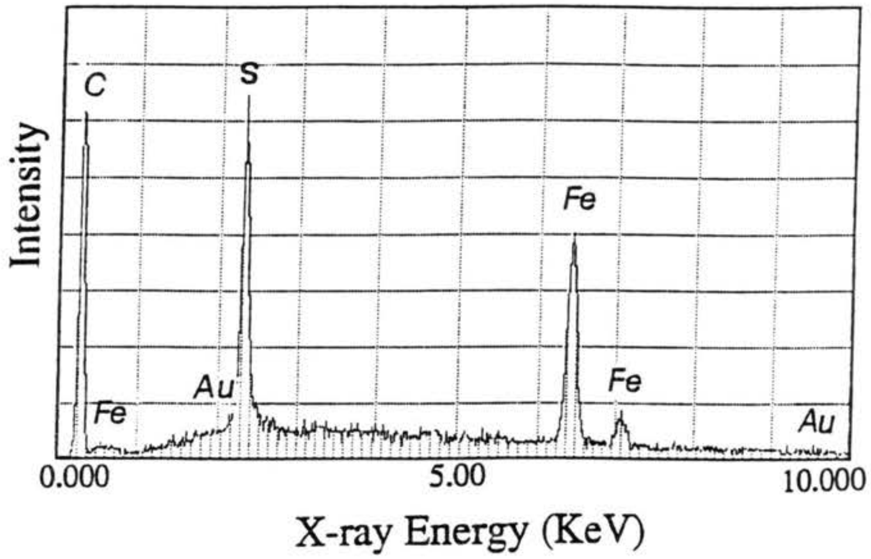

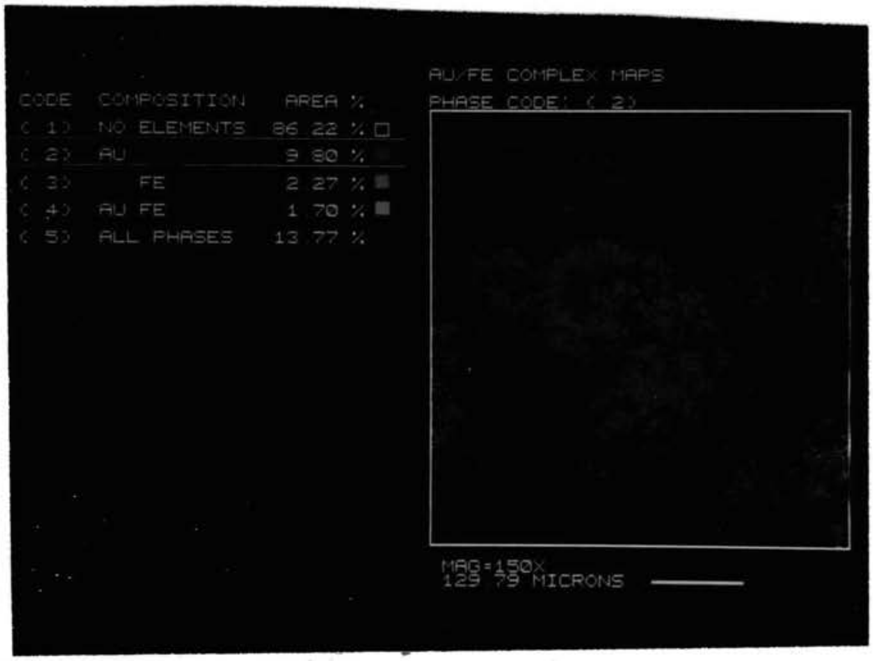

CODE	COMPOSITION	AREA %	
(1)	NO ELEMENTS	86 22 %	☐
(2)	AU	9 80 %	■
(3)	FE	2 27 %	■
(4)	AU FE	1 70 %	■
(5)	ALL PHASES	13 77 %	

AU/FE COMPLEX MAPS
PHASE CODE: (2)

MAG=150X
129 79 MICRONS

Figure 7. Energy-Dispersive X-Ray Spectrum Showing the Presence of Certain Elements on a Chemically-Modified Carbon Paste Surface; X-Ray Mapping of Gold Deposits on Another Carbon Paste Surface.

scanning electron microscopy and X-ray microanalysis, since these were the chief techniques used for this research.

CHAPTER II

BACKSCATTERED ELECTRON IMAGING OF LIGAND-MODIFIED CARBON PASTE SURFACES BY COMPLEXATION WITH IRON(II) AND/OR CHEMICAL DEPOSITION OF GOLD

Chemically-Modified Electrode Characterization

The focus in this chapter is to define the word "characterization" as it is applied to chemically-modified electrode surfaces in this thesis, to discuss the importance of and the motivation for the present work, and to give some experimental details of how carbon paste electrodes modified with 4,7-diphenyl-1,10-phenanthroline or its iron(II) complex can be "characterized".

Definition of "Characterization" As Applied to Chemically-Modified Electrode Surfaces

The word "characterization" has become very widely used and has also been given many different meanings. It is therefore imperative that an exact definition be given to the word as it is to be used in this chapter to avoid ambiguity.

"Characterization" will be used in this chapter to depict that process whereby one can locate or map the individual modifying centers on a chemically-modified electrode surface. By doing this, one can gain much needed information on both the size of and the spacial distribution of the modifying centers on the electrode surface. This information is important to the electroanalytical chemist because it is well known that the size of and the spacial distribution of modifying centers on a chemically-modified electrode surface greatly influence the performance of the electrode in analytical applications.

The Importance of Chemically-Modified Electrode Surface Characterization

Figure 8 is a representation of the size and spacial distribution of modifying centers (depicted as black spots) for two hypothetical chemically-modified electrode surfaces. The top diagram shows a surface in which the modifying centers are large and poorly distributed, indicating poor homogeneity of the centers on the electrode surface. The bottom diagram exhibits the opposite extreme; the modifiers are uniformly distributed, and the centers themselves are small (indicating good homogeneity). Most electroanalytical

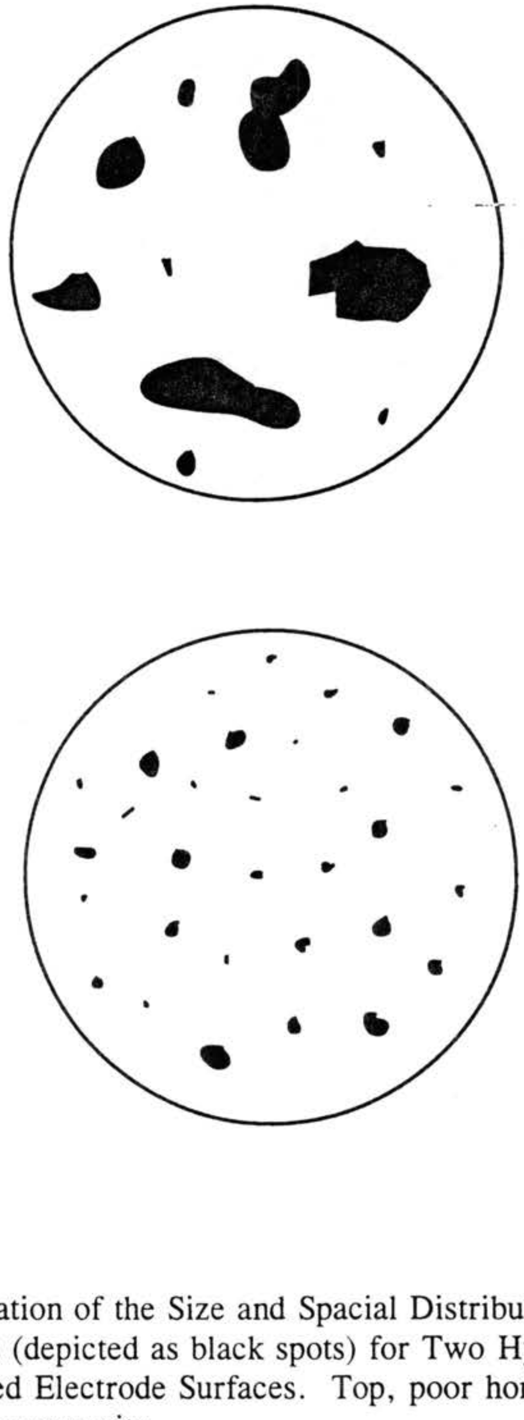

Figure 8. Representation of the Size and Spacial Distribution of Modifying Centers (depicted as black spots) for Two Hypothetical Chemically-Modified Electrode Surfaces. Top, poor homogeneity; bottom, good homogeneity.

chemists will agree that in a comparison of performance, the electrode with good homogeneity will effect better results in analytical applications.

There are two basic reasons for the improvement in performance of a modified electrode with the homogeneity of the modifier. First of all, an analyte will have, from a statistical standpoint, a better chance of coming into contact and interacting with a modifying center if those centers are more uniformly distributed across the electrode surface. Secondly, the surface distribution of the active modifying centers must be similar in analogous electrodes to obtain reproducible and comparable results. The reproducibility of the modified electrode surface is usually improved by the homogeneous placement of the modifying centers. This idea is particularly relevant to CPE's modified by the method of direct admixing, in which truly analogous electrodes can be difficult to prepare. The best results are obtained when the modifier is well mixed into the carbon paste preparation.

Until now, there was no simple and effective method for the experimentalist to "see" the distribution of the modifying centers on the surface of the electrode. One was forced to use either specialized surface analysis techniques or to rely on indirect means of acquiring knowledge of the distribution of the modifying centers by analyzing electrode performance. Chapter II will focus on the experimental details of how modifying centers can be located on an electrode surface by the use of redox chemistry and scanning electron microscopy techniques.

Experimental

The experimental details of the characterization of carbon paste electrodes modified with 4,7-diphenyl-1,10-phenanthroline or its iron(II) complex will be presented after a brief introduction and literature survey.

Introduction and Background

Ligands such as 1,10-phenanthroline and its derivatives, dimethylglyoxime, dithizone, thenoyltrifluoroacetone, and others [1,2] are commonly used as modifiers on carbon paste electrodes to preconcentrate metals on the electrode surface or to act as redox mediators after complexation with a metal ion. Under given experimental conditions, many of these immobilized ligands at the surface of the electrode can form stable complexes with iron(II) or iron(III), and this complexation followed by a reaction with gold(III) [as tetrachloroaurate(III), ($AuCl_4^-$)] provides the basis for a mapping of the active centers with scanning electron microscopy via backscattered electron imaging. Other ligands, which may or may not have an affinity for iron cations, but which bear intrinsic or induced positive charges can also be mapped in this manner by marking the ligands with $AuCl_4^-$ to form ion-pairs with the ligands.

Mappings such as these can thus serve as an indication of the degree and homogeneity of surface modification of the carbon paste.

Recently, a number of researchers have attempted to understand the rather complex nature of carbonaceous electrode surfaces using scanning electron microscopy. Wang *et al.* [58], for example, have studied the distribution and homogeneity of mercury-coated carbon foam composite electrodes. Mercury(0), which was used to preconcentrate trace metals such as lead on the electrode surface, introduces highly conductive domains which are readily discernible by the scanning electron microscope. This allowed the direct mapping of the mercury(0) modifier on the electrode surface. Bodalbhai and Brajter-Toth [59] have electrodeposited copper(0) onto glassy carbon and pyrolytic graphite electrode surfaces for the scanning electron microscopic mapping of the active sites on the electrode surfaces. They found that the particle density of the copper(0) sites on the surface correlated well with the electrochemical reactivity of the surfaces. Still other researchers have been able to tag the active carboxylate groups for the scanning electron microscopic mapping of these groups on a carbon fiber electrode [60]. This was done in a multistep derivatization with carbodiimide, biotin, a poly(oxyalkalene)diamine, and avidin-coated colloidal gold particles. The microscopic resolution of the active carboxylate groups was on the submicron scale.

The approach used here for the scanning electron microscopic mapping of 4,7-diphenyl-1,10-phenanthroline-modified carbon paste electrodes takes advantage of the fact that most ligands of this type form stable complexes with iron(II) or iron(III), and that the anchored iron centers exhibit reversible or quasi-reversible electrochemical redox behavior. Consequently, direct complexation with iron(II) [or iron(III) and the subsequent electrochemical reduction of iron(III) to iron(II)] will result in immobilized iron(II) centers at the active points of surface modification. These iron(II) centers on the carbon paste surface can in turn act as reducing centers for gold(III) species.

In a similar way, ligands that can bear a positive charge, can also attach $AuCl_4^-$, a species formed when gold(III) chloride is dissolved in hydrochloric acid. Since gold(0) and gold(III) are revealed equally well when backscattered electron imaging is used in the scanning electron microcope (SEM), both schemes (involving iron complexation followed by a redox reaction with $AuCl_4^-$, or direct ion-pairing with $AuCl_4^-$) can be used to map ligand-modified carbon paste surfaces. In essence, gold(0) and/or gold(III) depositing at the locations of the ligands serve as tagging entities that are revealed by scanning electron microscopy, cyclic voltammetry, and energy-dispersive X-ray microanalysis. This approach to chemical surface characterization is presented and discussed here.

Reagents and Solutions

Gold(III) chloride, 99%, was purchased from Aldrich (Milwaukee, WI). The iron solutions were prepared with $Fe(NH_4)_2(SO_4)_2$ from Mallinckrodt (St. Louis, MO). The 4,7-diphenyl-1,10-phenanthroline and $NaClO_4$ were from GFS Chemicals (Columbus, OH). The water used for solution preparation was deionized and further purified by distillation in an all-borosilicate-glass still with a quartz immersion heater. All other chemicals were reagent grade.

Instrumentation

Electron scanning microscopy was performed at the Scanning Electron Microscopy Facility (CONOCO, Inc., Ponca City, OK) using a Cambridge Stereoscan 250 Mark II microscope (Reichert-Jung Cambridge Instruments Inc, Buffalo, NY) equipped with a Robinson backscattered electron detector and a Traco Northern TN 5500 X-ray detector.

Cyclic voltammetry was carried out using a BAS-100 electrochemical analyzer (Bioanalytical Systems, West Lafayette, IN). The system utilized a Ag/AgCl, 3.0 M NaCl reference electrode and a platinum wire auxiliary electrode.

Carbon Paste Surface Preparation

Carbon pastes were prepared by placing in an agate mortar the required weights of graphite (Ultra Carbon, Bay City, MI), light mineral oil (Fisher Scientific, Fair Lawn, NJ), and 4,7-diphenyl- 1,10-phenanthroline (G. F. Smith, Columbus, OH) to give a mixture which was 70% graphite, 25% mineral oil, and 5% modifier. This mixture was either thoroughly mixed to give a homogeneous paste, or was only partially mixed to obtain a non-homogeneous paste. Both of these pastes were packed into the wells of two separate SEM pyrolytic graphite disk powder mounts (Ernest F. Fullam, Inc., Latham, NY). These powder mounts were 2.54 cm in diameter with an 8 mm diameter by 1.5 mm deep recess on one of the faces (see Figure 9). The carbon paste surfaces were polished by placing the carbon paste-containing powder mounts face down on an index card covered by a sheet of glassine (weighing) paper and gently moving the powder mount back and forth over the paper. The carbon paste surfaces created in this way duplicate typical carbon paste surfaces formed on standard carbon paste electrodes. The use of the SEM graphite powder mounts avoided the problem of having to remove the carbon paste from an electrode body for mounting in the SEM, a step which tended to introduce defects onto the carbon paste surface.

To illustrate that the gold marks or tags only those specific locations on the electrode surface in which a ligand center is present, a carbon paste surface

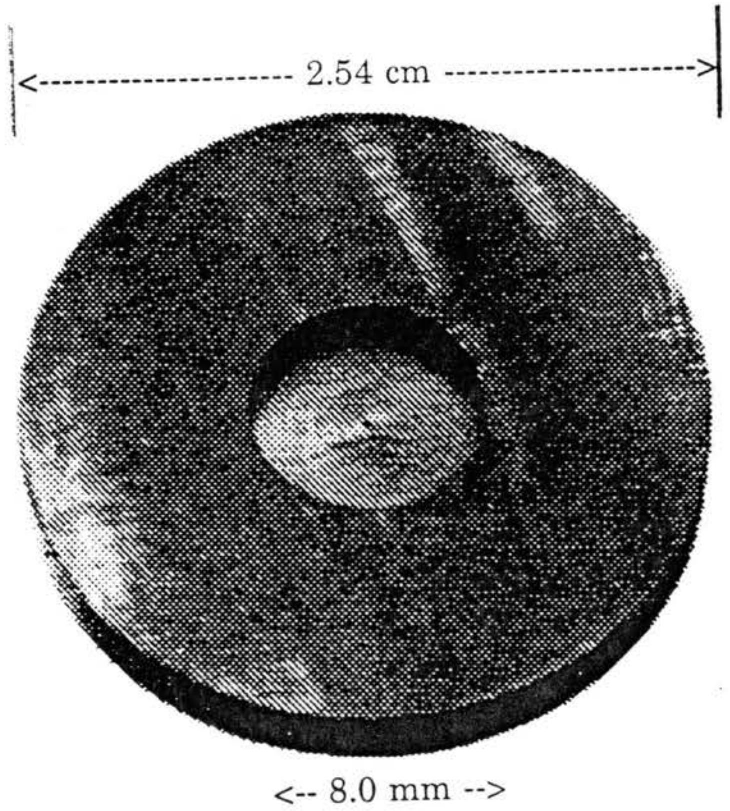

Figure 9. Diagram Showing the Pyrolytic Graphite Disk Powder Mount Used in the SEM and its Dimensions

was prepared in which a single, well-defined ligand center region was deliberately placed at a specific location on the surface. This was done by packing a 70% graphite, 30% mineral oil paste into an SEM powder mount and polishing the surface as described previously. Using a glass capillary tube approximately 1 mm in diameter, a small, cylindrical cavity was introduced byinserting the capillary perpendicularly through the carbon paste surface for the entire depth of the paste. After removal of the capillary, the resulting cavity was carefully packed with a paste of 70% 4,7-diphenyl-1,10-phenanthroline and 30% mineral oil. The resulting carbon paste surface was free of any ligand centers except for the strategically-placed ligand "spot", which was clearly visible with the unaided eye or low-power light microscope.

For the electrochemical studies the working electrode [5, 35] was produced by packing the same modified (homogeneous) carbon paste described earlier into a Teflon electrode body containing a well 4 mm in diameter. The carbon paste surface was polished using the same procedure described above for the SEM powder mounts. Electrical contact to the paste was made via a small brass rod.

Procedure for Ligand Complexation and/or Subsequent Gold Deposition

Complexation of the immobilized ligands was effected by the overnight immersion of the graphite powder mount or Teflon electrode body containing the ligand-modified carbon paste into an unstirred 0.010 M iron(II) ammonium sulfate solution. This iron(II) solution was prepared anew each day since the solution tended to oxidize to iron(III) after long periods.

For gold deposition the preparation of the gold solution for immersion of the iron(II)-modified carbon surfaces is particularly critical. The gold solution was prepared by dissolving the gold(III) chloride powder in aqua regia (1 part concentrated HNO_3, 1 part H_2O, and 3 parts concentrated HCl). The solution was evaporated to near dryness, and more concentrated HCl was added. This step was again repeated to rid the solution of nitric acid. The solution was then evaporated to near dryness and diluted to the appropriate volume with 0.025 M HCl to give a 1.0% gold(III) chloride solution. Finally, the solution was filtered to separate any residual gold particles. The resulting gold(III) solution was protected from light to avoid photoreduction of the gold(III). It should be noted that if the 0.025 M HCl was simply added to the gold(III) chloride powder, some of the gold was immediately reduced to gold(0) before dissolution could occur.

The gold(III) immersion of the various 4,7-diphenyl-1,10-phenanthroline-modified carbon paste surfaces was done by thoroughly rinsing the surfaces with purified water and then placing then into the gold(III) chloride/0.025 M HCl solution at 50°C without stirring. The contact time with the gold(III) solution varied from 1 to 15 min. Long contact times (greater than 15 min) often resulted in gold deposition at rough interfaces (i.e.: edges of cleavage planes on the graphite surface) having no iron centers, an effect which was also more noticeable when the deposition of gold(0) onto the carbon paste surface was carried out in stirred solutions.

Results and Discussion

Nonconducting or poorly conducting specimens examined in the scanning electron microscope need to be coated with a film of conducting material to avoid charging effects that can introduce artifacts onto a scanning electron micrograph. Gold(0) is commonly used in scanning electron microscopy to enhance conductivity and to aid in obtaining better surface topography [56]. It is then reasonable to assume that a chemical deposition of gold [either gold(III) or gold(0)] onto a chemically-modified carbon paste surface could enhance conductivity at the specific ligand centers, giving better contrast in the scanning electron micrographs. In addition, the contrast between the chemically-modified carbon paste surface and the areas of deposited gold can be increased further by using backscattered electrons for the SEM imaging. As stated in Chapter I, the number and energies of the backscattered electrons produced upon irradiation of the sample with primary electrons increases with the atomic weight of the sample target. Thus, areas on the carbon paste surface covered with a layer of gold should show improved contrast with a smaller dependence on surface topography [56]. The improved contrast by using backscattered electron imaging is shown in Figure 10.

In a hydrochloric acid medium, gold is in the form of $AuCl_4^-$, and, as with any gold ionic species, $AuCl_4^-$ is easily reduced [gold(III) is a strong oxidant and comparable to chlorine in oxidation power]. The tetrachloroaurate(III) complex anion is easily reduced to metallic gold by iron(II) in a hydrochloric acid medium according to the following standard formal potentials [61]:

$$AuCl_4^- + 2\,e^- \text{ ----> } AuCl_2^- + 2\,Cl^- \qquad E°' = 0.95\ V$$

$$AuCl_2^- + e^- \text{ ----> } Au(0) + 2\,Cl^- \qquad E°' = 1.13\ V$$

and, apparently, in hydrochloric acid the $AuCl_2^-$ undergoes partial disproportionation according to the following overall reaction:

$$AuCl_4^- + 3\,e^- \text{ ----> } Au(0) + 4\,Cl^- \qquad E°' = 1.01\ V$$

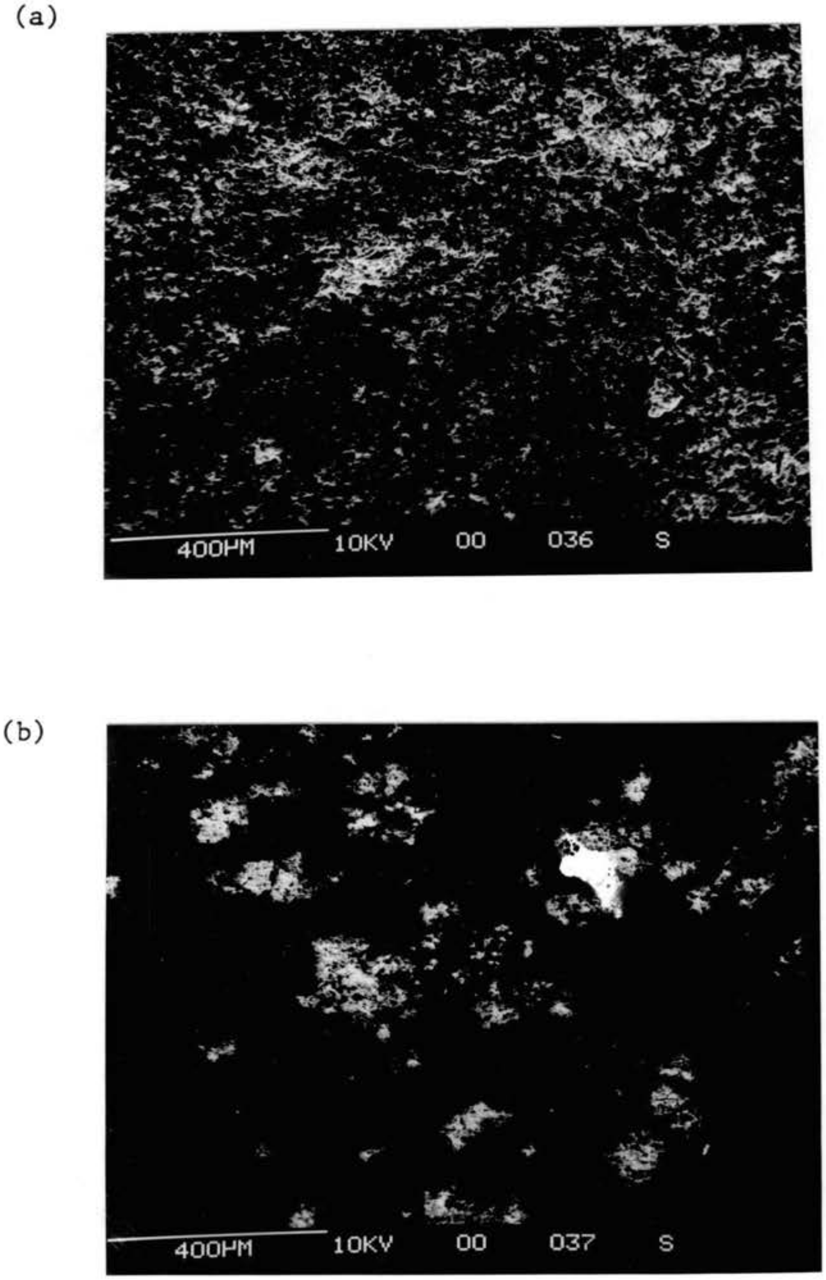
(a)
400PM
10KV
00
036
S
(b)
400PM
10KV
00
037
S

Figure 10. Scanning Electron Micrographs of a 5% 4,7-Diphenyl-1,10-Phenanthroline-Modified Carbon Paste Surface after Immersion in Iron(II) Solution with Subsequent Immersion in a Gold(III) Solution. (a) secondary electron image; (b) backscattered electron image of the same surface in (a).

Mild temperatures above 25°C help the reduction to metallic gold [61]. This reaction, in the presence of iron(II), is favored by the ubiquity of the iron(II)/iron(III) couple in the redox scale; this makes accessible a large number of redox reactions involving this redox couple.

The chemically-based surface characterization proposed here takes advantage of the redox chemistry just discussed, but may also involve an ion exchange process at the ligand or ligand-iron(II) complex centers. Figure 11a illustrates the proposed mechanism of the ion-pairing of protonated ligand centers and $AuCl_4^-$. In this scheme the ligand moieties (which may have no inherent charge) become protonated in acidic media. The protonated ligands are thus positively charged and so can act as centers for ion-pair formation with $AuCl_4^-$, the predominant species in $AuCl_3/HCl$ solutions. The ligands, now tagged with gold, show up well in scanning electron micrographs utilizing backscattered electron imaging. This process was operative in experiments done on 4,7-diphenyl-1,10-phenanthroline-modified carbon paste surfaces that had not been complexed with iron(II). After immersion in solutions of $AuCl_3/HCl$, backscattered electron imaging still showed good contrast at the ligand locations. This work shows that if the immobilized ligand centers bear (or can be induced to bear) positive charges, direct ion-pairing with $AuCl_4^-$ will result in marking the ligand locations with the gold(III) species.

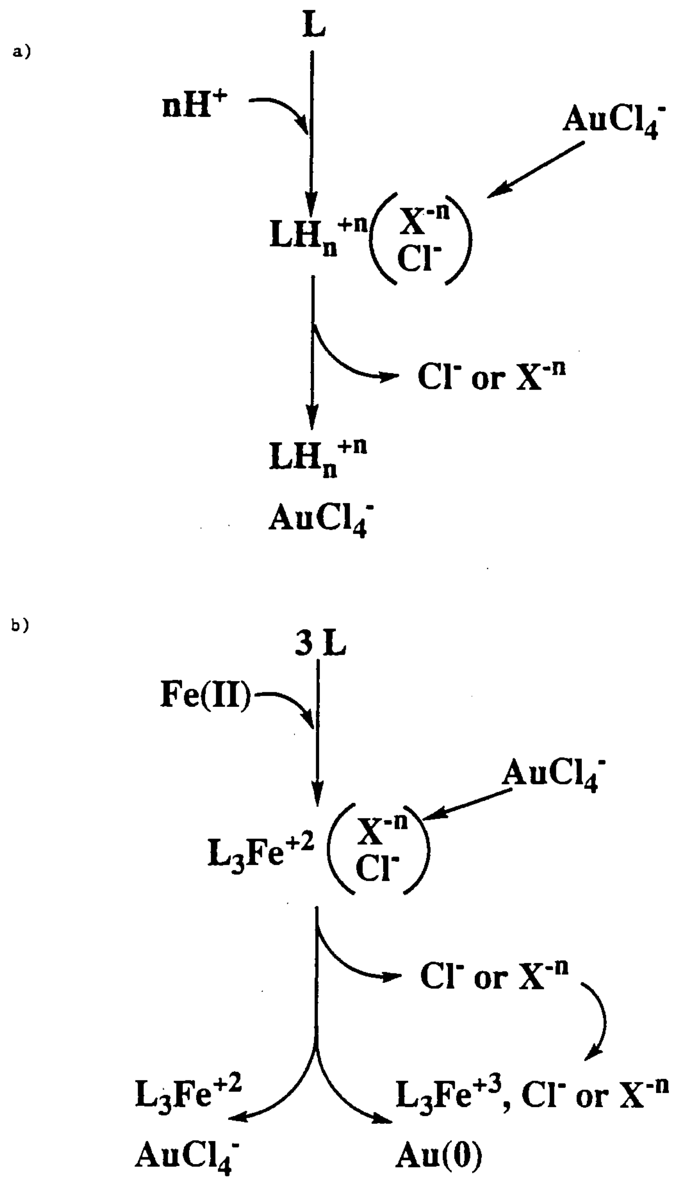
a)
L
nH+
AuCl4-
LHn+n (X-n Cl-)
Cl- or X-n
LHn+n
AuCl4-
b)
3 L
Fe(II)
AuCl4-
L3Fe+2 (X-n Cl-)
Cl- or X-n
L3Fe+2
AuCl4-
L3Fe+3, Cl- or X-n
Au(0)

Figure 11. Sequence of Chemical Events Comprising the Tagging of Immobilized Ligand Centers on Carbon Paste Surfaces with Gold. a) an uncharged ligand that can be protonated at low pH; b) a ligand that can undergo iron(II) complexation.

Figure 11b shows the mechanism of gold reaction via ion-pairing **and** reduction at ligand centers that have been complexed with iron(II), a procedure necessary for those ligands that have no intrinsic positive charge and that will not protonate at low pH. The surface area occupied by the ligands represent different local environments than do the exposed graphite edge planes, which, depending on pH, are probably negatively charged. The ligand is first complexed with iron(II), and since the iron(II) complex is positively charged, an anion, X^-, must be located in its immediate proximity (ion-pair formation) to satisfy electroneutrality. The counteranion, in a solution of iron(II) is chloride or some other anion depending on the medium. In the gold(III) solution, $AuCl_4^-$ can substitute for the counteranion and can be partially reduced to gold(0) by the iron(II) centers. Concomitantly, the free Cl^- ions previously produced again occupy the counter-ion positions. It is possible, however, that some $AuCl_4^-$ units remain unreduced even though they have undergone the ion-exchange reaction. It must be stressed again that this is not a problem because the scanning electron microscope using backscattered electron imaging is quite effective in locating the ligand centers regardless of the oxidation state of the gold species.

Gold deposition by reduction onto the ligand centers should not be impeded by the stoichiometric requirement of 3 iron(II) centers to 1 $AuCl_4^-$ unit because only in rare cases will the homogeneity of the modifier in a directly-admixed carbon paste be such that only 1 or 2 iron(II) complex molecules will be present in any one active iron(II) center. In a majority of cases, the active iron centers will contain many individual iron(II) complex units.

It should be emphasized that the electron exchanges taking place here occur by simple immersion; there is no external potential applied to the surfaces under study. Consequently, the strong dependence on voltage exhibited by the differential capacitance should play a secondary role, if any. The anion exchange processes illustrated in Figures 11a and 11b can possibly occur in the vicinity of the outer Helmholtz plane region, and in the "gray" area located in the boundary between the compact and diffuse layer. In the case of gold deposition by reduction, when the gold chloride complexes and the iron centers are at the appropriate distance, electron transfer (facilitated by the conjugated benzene rings in the ligand molecules) can take place.

Once deposition by reduction starts around an iron(II) center, nucleation around that center may be favored, enlarging and highlighting to some extent the points one is interested in visualizing. Direct observation by conventional light microscopy before and after gold deposition on carbon paste surfaces with large and easily visualized ligand centers confirm that within the recommended contact time, deposition and nucleation is confined around the locations of iron(II) centers.

Scanning Electron Microscopy and X-ray Microanalysis

Figures 12 through 14 show scanning electron micrographs of a 5% 4,7-diphenyl-1,10-phenanthroline modified carbon paste surface in which the ligand modifier was poorly admixed. Figure 12a shows the surface before it was immersed in the iron(II) and the gold(III) solutions. Figure 13a is the same surface after treatment with iron(II). Note that there are no distinctive features, and that the contrast between the ligand centers and the surrounding carbon paste is poor. After immersion in the gold(III) solution and using backscattered electron imaging, the contrast is markedly improved as can be seen in Fig. 14a, which shows highlighted regions of gold(0)/gold(III) covering the modified carbon paste surface. Figures 15a, 16a, and 17a show similar results for a well-admixed 5% 4,7-diphenyl-1,10-phenanthroline modified carbon paste. It should be emphasized that all micrographs shown here are direct exposures without any special sample preparation prior to microscopic observation.

A comparison of Figures 14a and 17a imply that the gold has been deposited directly over the ligand modifying centers because both the spatial distribution and size of the gold deposits agree with the predicted spatial distribution and size of the admixed ligand centers in the carbon paste (refer again to Figure 8). To **verify** that the gold deposits directly over the ligand centers, energy-dispersive X-ray microanalysis was performed on each of the

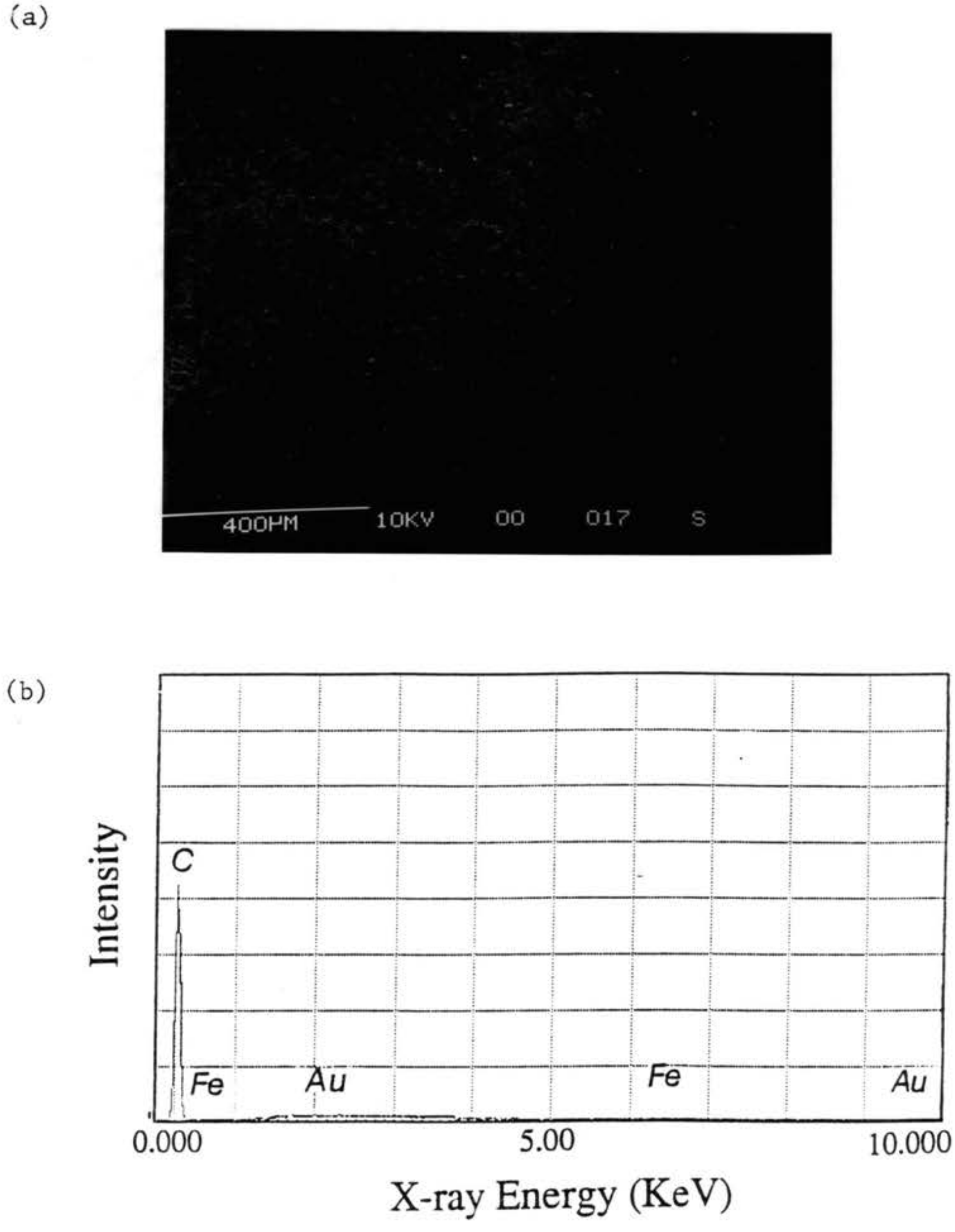

Figure 12. Results of Scanning Electron Microscopy and X-Ray Microanalysis on a Poorly Admixed 5% 4,7-Diphenyl-1,10-Phenanthroline-Modified Carbon Paste Surface prior to Immersion into Iron(II) and Gold(III) Solutions. a) scanning electron micrograph; b) energy-dispersive X-ray spectrum.

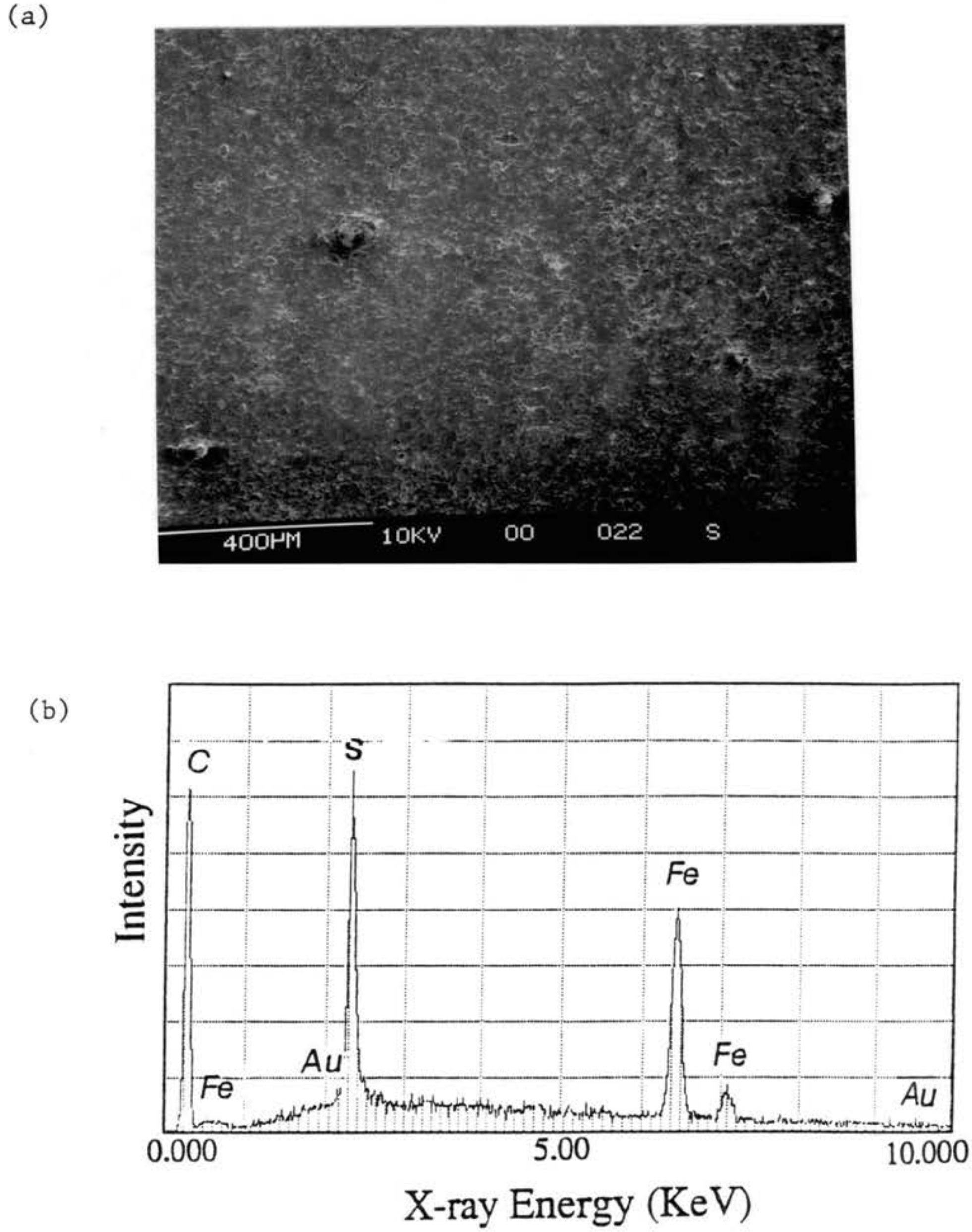

Figure 13. Results of Scanning Electron Microscopy and X-Ray Microanalysis of the Carbon Surface in Figure 12 after Immersion into an Iron(II) Solution. a) scanning electron micrograph; b) energy-dispersive X-ray spectrum.

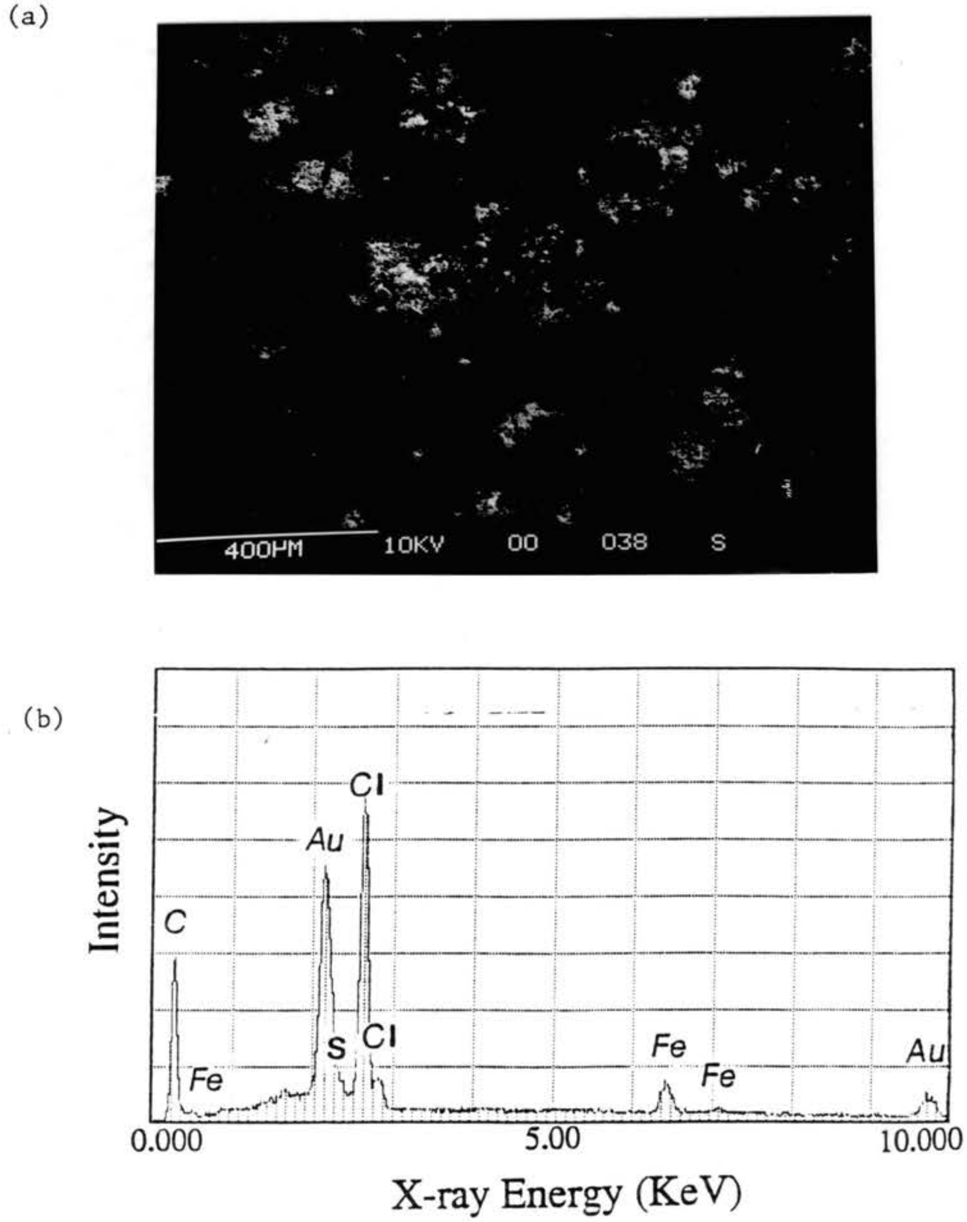

Figure 14. Results of Scanning Electron Microscopy and X-Ray Microanalysis of the Carbon Surface in Figure 12 after Immersion into an Iron(II) Solution Followed by Immersion into a Gold(III) Solution. a) scanning electron micrograph; b) energy-dispersive X-ray spectrum.

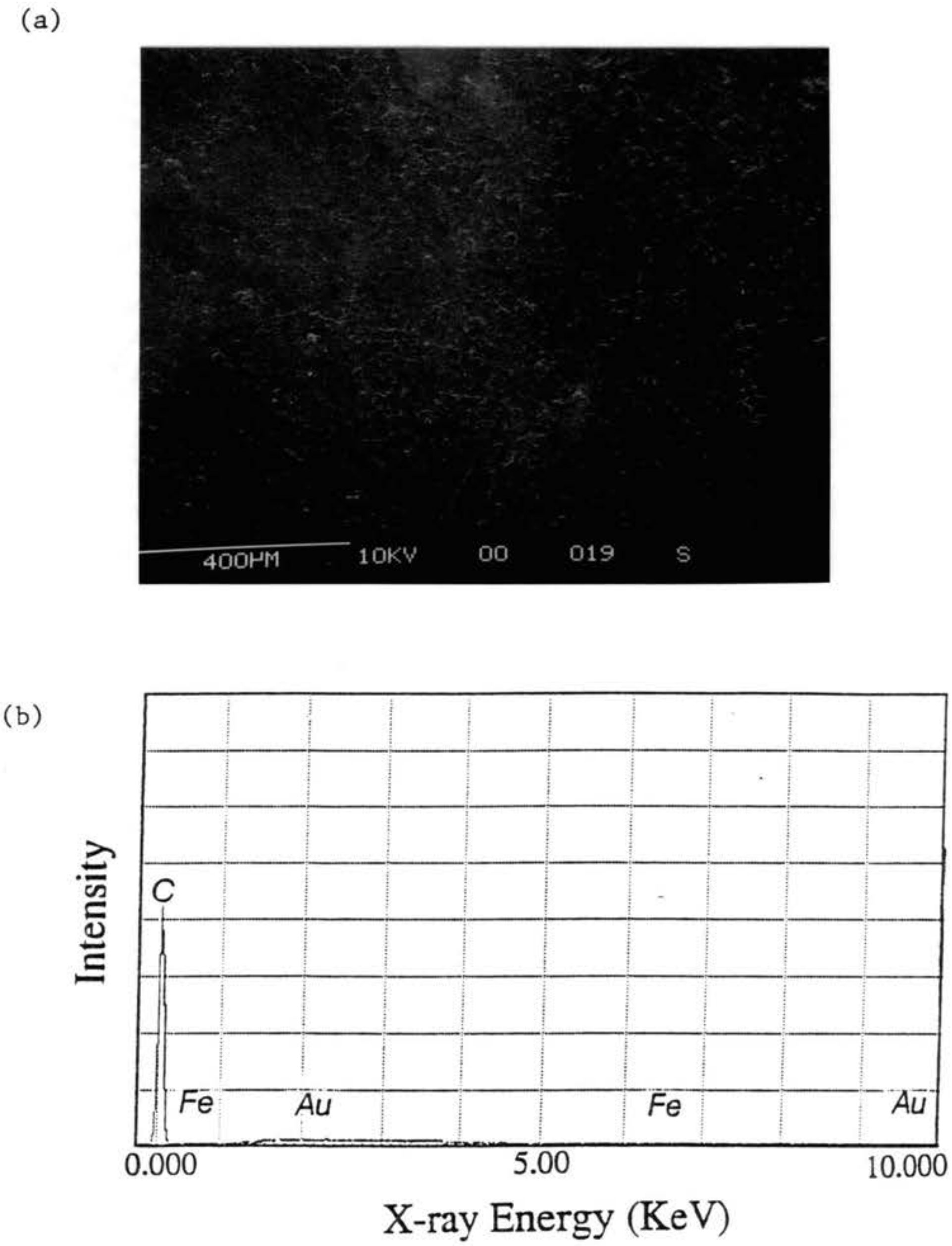

Figure 15. Results of Scanning Electron Microscopy and X-Ray Microanalysis on a Well-Admixed 5% 4,7-Diphenyl-1,10-Phenanthroline-Modified Carbon Paste Surface prior to Immersion into Iron(II) and Gold(III) Solutions. a) scanning electron micrograph; b) energy-dispersive X-ray spectrum.

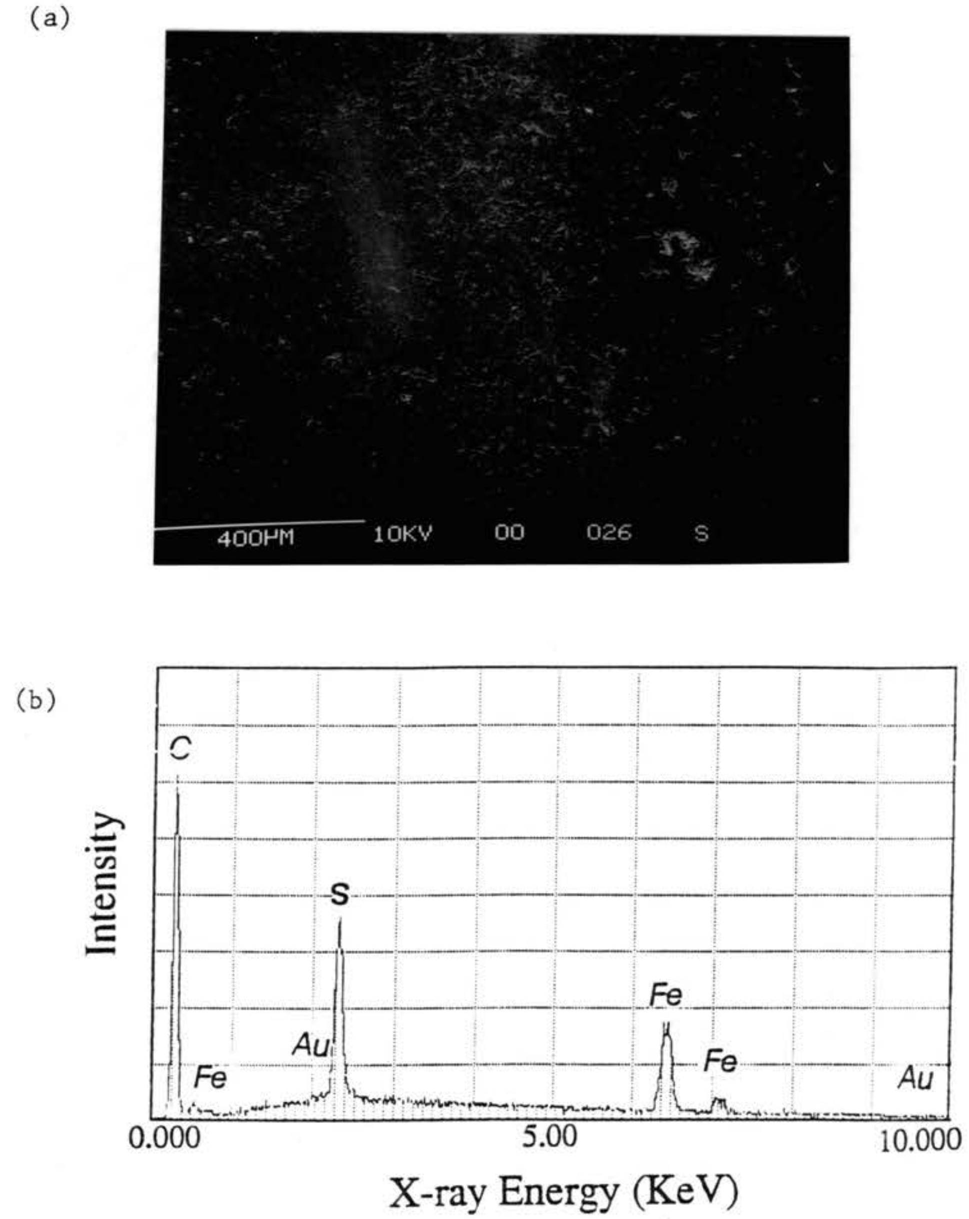

Figure 16. Results of Scanning Electron Microscopy and X-Ray Microanalysis of the Carbon Surface in Figure 15 after Immersion into an Iron(II) Solution. a) scanning electron micrograph; b) energy-dispersive X-ray spectrum.

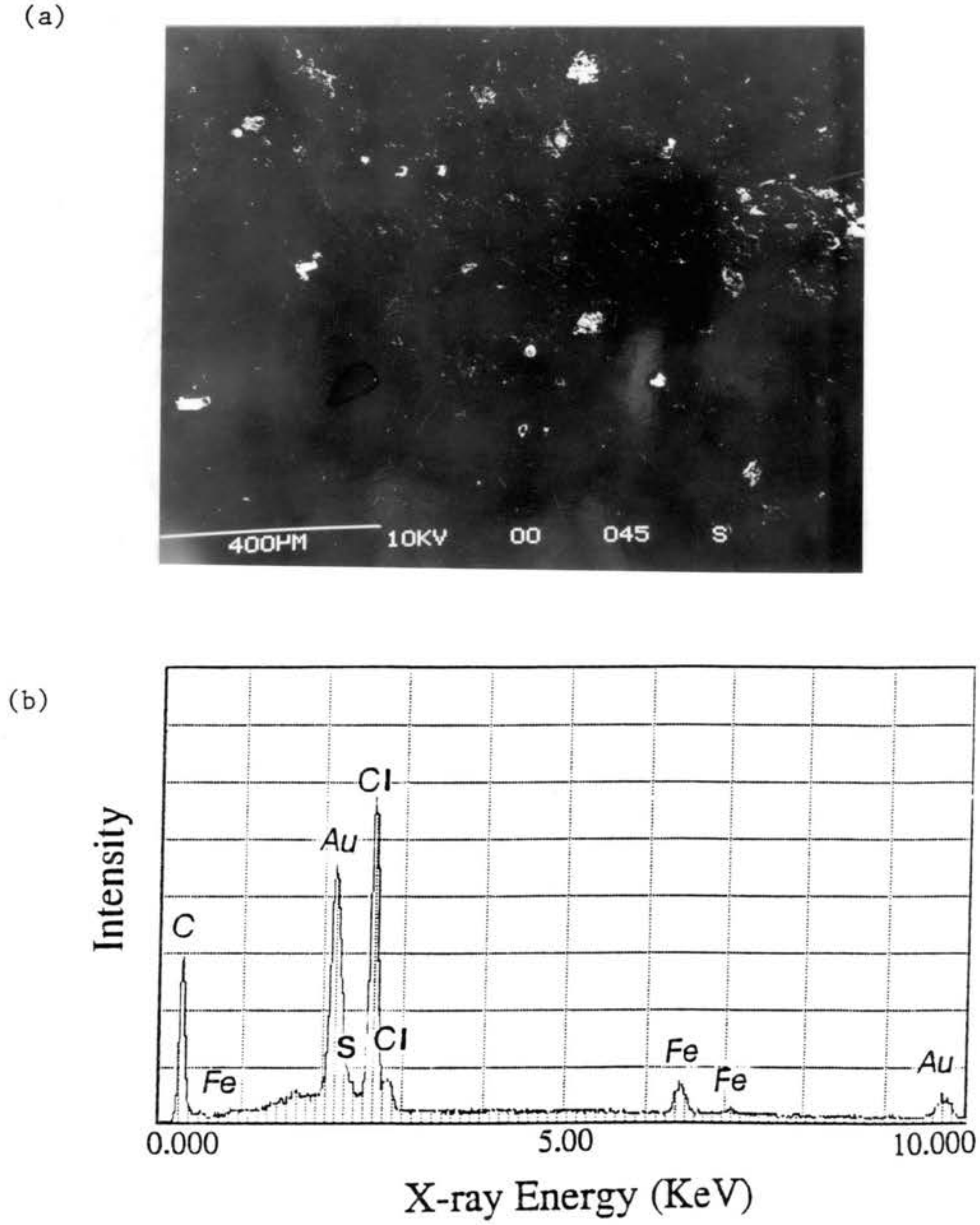

Figure 17. Results of Scanning Electron Microscopy and X-Ray Microanalysis of the Carbon Surface in Figure 15 after Immersion into an Iron(II) Solution Followed by Immersion into a Gold(III) Solution. a) scanning electron micrograph; b) energy-dispersive X-ray spectrum.

modified carbon paste surfaces at each immersion step. These X-ray spectra are shown in part b of Figures 12 through 17.

The X-ray spectra presented in Figures 12b and 15b show only the presence of carbon on each of the surfaces (the 0.3 KeV, K_α line peak) since neither of the surfaces had yet been immersed in iron(II) or gold(III) solutions. Figures 13b and 16b show the same respective surfaces after immersion in iron(II) solution. Note that each of these spectra now shows a strong iron peak (6.4 KeV, K_α line), due to the formation of the iron(II) ligand complexes, and a strong sulfur peak (2.3 KeV, K_α line) due to the presence of sulfate as the counterion to the positively-charged iron(II) complex. When the modified carbon paste surfaces are finally immersed into the gold(III) solution, the X-ray spectra show strong gold peaks (the strong peak at 2.2 KeV, $M_{\alpha+\beta}$ line, and the less pronounced peak at 9.72 KeV, L_α line) as well as chloride counterion peaks (K_α line at 2.7 KeV). These spectra show that there is essentially no iron (very small peaks at 6.4 KeV and 7.1 KeV for the iron K_α and K_β lines) exposed on the surface. The assignment of these peaks in these spectra accurately agrees with the plot of the energy of X-ray emission lines given in [62].

In another experiment, an X-ray image or map (see Chapter I, Figure 7) was obtained from a poorly admixed 5% 4,7-diphenyl-1,10-phenanthroline carbon paste surface after the surface had been immersed in both the iron(II) and the gold(III) solutions. To accomplish this, the X-ray detector was adjusted to detect only those X-rays with certain characteristic energies arising from electron transitions in a given element or elements of interest. The cathode ray tube was scanned synchronously with the electron probe, and the X-ray area map was marked with a dot whenever an X-ray was detected in the selected energy range. Care was taken to avoid peak overlaps.

Separate X-ray area maps of the elements of interest (Fe, Au, and Cl), as well as combinations of these elements, were built up so as to obtain the complete mapping of the modified carbon paste surface. The result of this particular X-ray technique is shown in Figure 18. This X-ray map is typical of the results obtained and is actually a **composite** of 7 individual mappings of the modified carbon paste surface in which the X-ray detector was adjusted to select each of the following elements or combinations of elements: 1) gold alone, 2) iron alone, 3) chlorine alone, 4) gold + iron, 5) gold + chlorine, 6) iron + chlorine, and 7) gold + iron + chlorine. The meaning of X-ray maps in which more than one of the above elements is selected for mapping (i.e.: maps 4, 5, 6, and 7) is that the selected elements co-exist on the carbon paste surface within the pixel resolution used.

Using this X-ray map, the percent composition of the surface was calculated. Table I gives the results of these calculations and shows that approximately 15% of the total surface area was covered by gold. Along with stoichiometric considerations, this points to gold nucleation, which, as stated

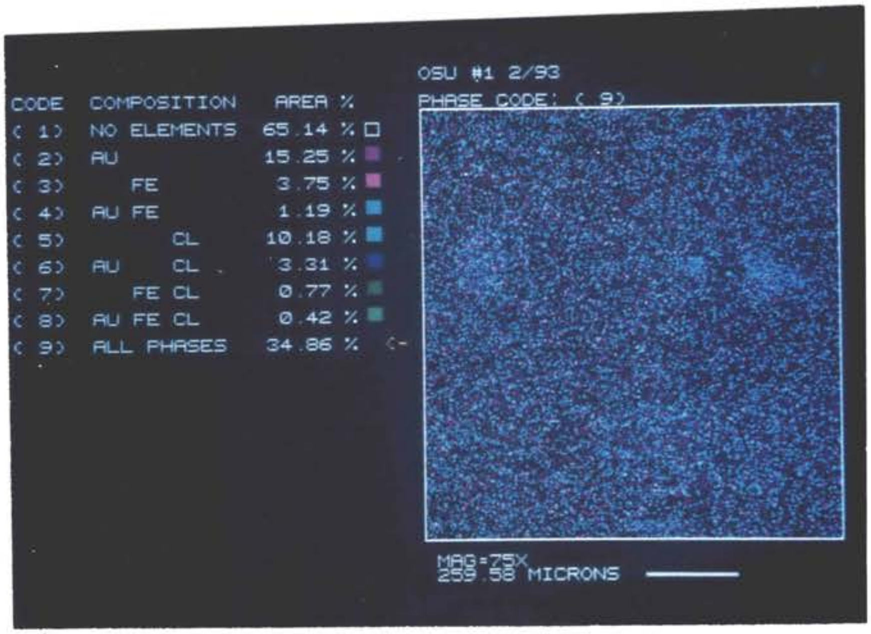

```
                                             OSU #1 2/93
CODE   COMPOSITION    AREA %                 PHASE CODE: ( 9)
( 1)   NO ELEMENTS   65.14 % □
( 2)   AU            15.25 % ■
( 3)      FE          3.75 % ■
( 4)   AU FE          1.19 % ■
( 5)         CL      10.18 % ■
( 6)   AU    CL       3.31 % ■
( 7)      FE CL       0.77 % ■
( 8)   AU FE CL       0.42 % ■
( 9)   ALL PHASES    34.86 %   <-

                                             MAG=75X
                                             259.58 MICRONS  ————
```

Figure 18. X-Ray Mapping of a Poorly Admixed 5% 4,7-Diphenyl-1,10-Phenanthroline-Modified Carbon Paste Surface after the Surface had been Immersed in both the Iron(II) and the Gold(III) Solutions

TABLE I

AREA PERCENT COMPOSITION OF A CARBON PASTE SURFACE CONTAINING 5% 4,7-DIPHENYL-1,10-PHENANTHROLINE AFTER IMMERSION IN IRON(II) AND IN GOLD(III) SOLUTIONS

SPECIES	AREA %
Gold	15.25
Iron	3.75
Chloride	10.18
Gold, Iron*	1.19
Gold, Chloride*	3.31
Iron, Chloride*	0.71
Gold, Iron, Chloride*	0.42
No elements	65.14

* Areas with spots comprising more than one species within the pixel resolution used.

earlier, can result in enlargement and enhancement of the centers of interest. This feature would be quite beneficial in well-admixed ligand-modified carbon pastes in which the active ligand centers would be small.

Table I also includes an area percentage entry for those areas on the surface where both gold and chlorine reside. This value is 3.31%, a number reasonably close to the 5% modification level of the carbon paste preparation. The difference is probably due to the fact that the carbon paste used was prepared by poorly admixing the ligand modifier so that the modifying centers would be large and easily visualized. In addition, the X-ray images obtained here represented only a small part of the entire surface area of the carbon paste surface. Therefore, local variations in the modification level should be expected.

It should also be noted from Table I that the area percentage of the X-ray map produced from iron X-ray energies alone (3.75%) was less than the 5% modifier composition of the carbon paste. This can be explained by the fact that since the iron atoms are effectively covered by a layer of gold, the X-ray intensity produced by the iron atoms should be attenuated to some extent because X-rays would be produced below the surface and would have to propagate through the other atoms in the specimen to escape for detection.

All of these observations support the mechanism proposed earlier (Figure 11b) for the deposition of gold at the iron(II) centers on a modified carbon paste surface. In essence, one should see X-ray signals at any given ligand center arising from the presence of gold, chlorine, and relatively few signals from iron. Figure 19 shows additional X-ray maps of the same surface in Figure 18, and were made by setting the X-ray detector to detect X-ray energies arising from gold + chlorine (Figure 19a), and from gold + iron + chlorine (Figure 19b). Both figures show distinct high-density dot regions corresponding to the expected locations of the active ligand centers as viewed by backscattered electron imaging (not shown) of the same surface.

Scanning Electron Microscopy of the Surface Containing the Ligand "Spot"

In other work the carbon paste surface with the deliberately-placed ligand spot (see the Experimental section) was allowed to complex overnight in the 0.010 M iron(II) ammonium sulfate solution. A scanning electron micrograph was taken of this surface using backscattered electron imaging, and this is shown in Figure 20a. The contrast between the iron(II)-ligand complex spot and the plain carbon paste background is fairly poor, but the micrograph is included to show the general shape of the iron(II)-ligand center. This carbon surface was then immersed into the gold(III) solution in steps for periods of 1, 5, and 10 min intervals with distilled water rinsing and scanning electron microscopy after each step. Figure 20b shows the surface after a total gold(III) immersion time of 5 a)

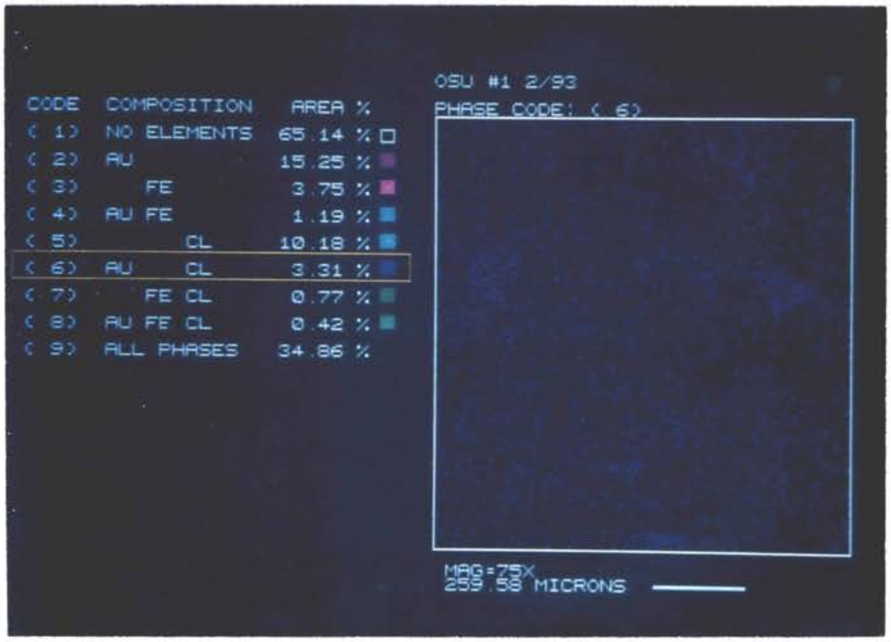

```
CODE  COMPOSITION    AREA %           OSU #1 2/93
( 1)  NO ELEMENTS   65.14 % □         PHASE CODE: ( 6)
( 2)  AU            15.25 % 🟪
( 3)     FE          3.75 % 🟪
( 4)  AU FE          1.19 % 🟦
( 5)        CL      10.18 % 🟦
( 6)  AU    CL       3.31 % 🟦
( 7)     FE CL       0.77 % 🟩
( 8)  AU FE CL       0.42 % 🟩
( 9)  ALL PHASES    34.86 %
                                       MAG=75X
                                       259.58 MICRONS
```

b)

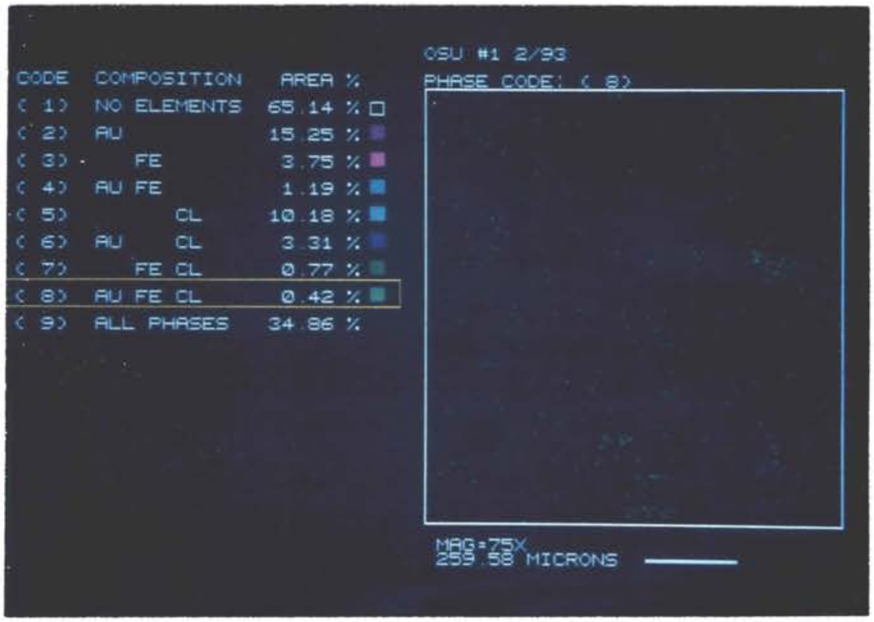

```
CODE  COMPOSITION    AREA %           OSU #1 2/93
( 1)  NO ELEMENTS   65.14 % □         PHASE CODE: ( 8)
( 2)  AU            15.25 % 🟪
( 3)     FE          3.75 % 🟪
( 4)  AU FE          1.19 % 🟦
( 5)        CL      10.18 % 🟦
( 6)  AU    CL       3.31 % 🟦
( 7)     FE CL       0.77 % 🟩
( 8)  AU FE CL       0.42 % 🟩
( 9)  ALL PHASES    34.86 %
                                       MAG=75X
                                       259.58 MICRONS
```

Figure 19. X-Ray Mapping of a Poorly Admixed 5% 4,7-Diphenyl-1,10-Phenanthroline-Modified Carbon Paste Surface after the Surface had been Immersed in both the Iron(II) and the Gold(III) Solutions. a) Map comprised of gold + chloride X-ray energies; b) Map comprised of gold + iron + chloride X-ray energies.

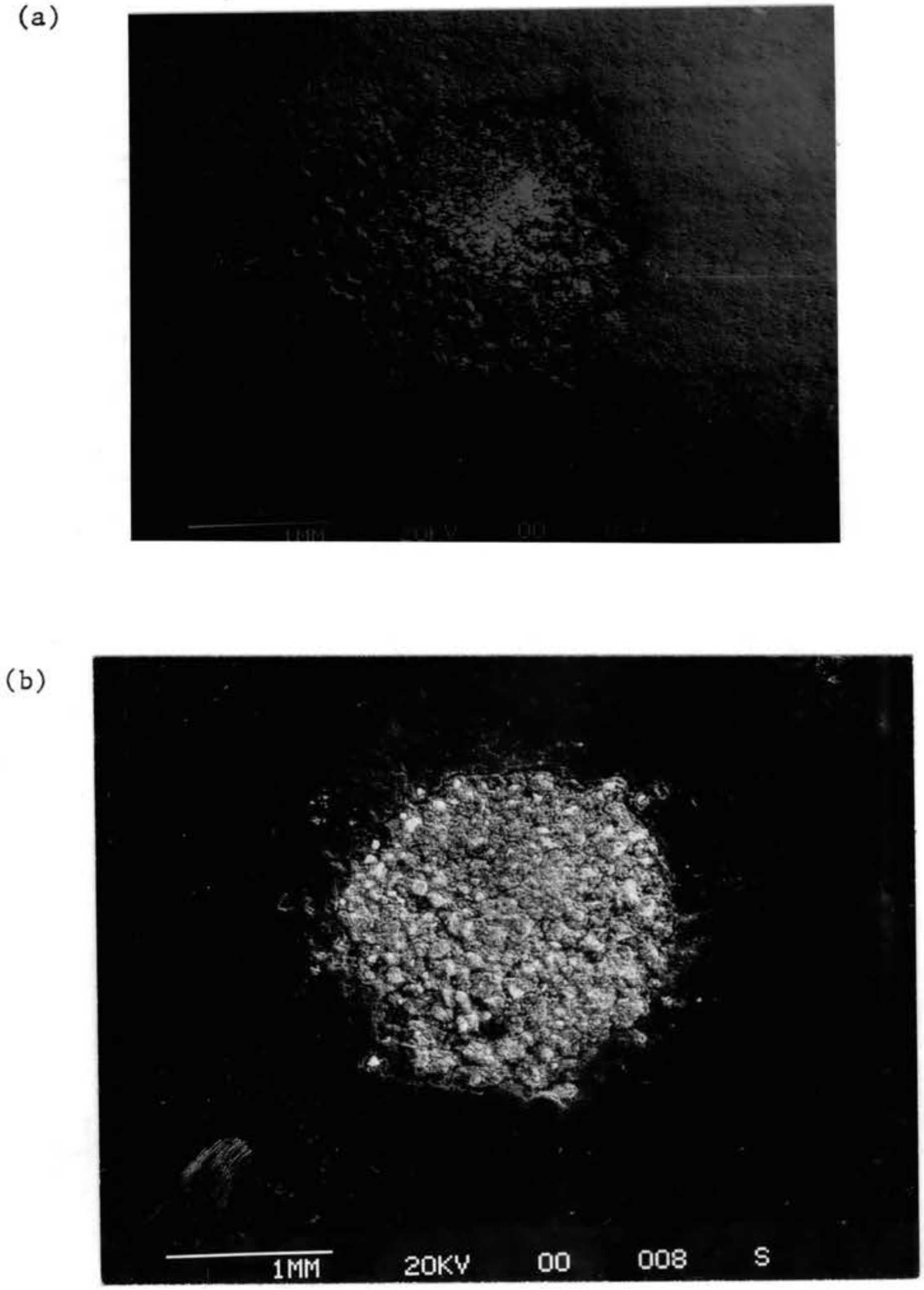

Figure 20. Backscattered Scanning Electron Micrographs of the Carbon Paste Surface Containing the Ligand "Spot". a) ligand spot after complexation with iron(II); b) same surface as in a) after the subsequent immersion into a gold(III) solution for 5 min.

min. Note that with the deposition of gold, the contrast between the iron(II) center and the plain carbon background was much improved. In addition, the shape of the gold deposit closely matches that of the original, confirming the deposition of gold only on locations where there are ligand centers.

Electrochemical Studies

Additional evidence that the deposition of gold occurs over the active iron centers comes from electrochemical studies. The working electrode for this work was a 5% 4,7-diphenyl-1,10-phenanthroline-modified carbon paste electrode. The electrode was immersed in an iron(II) solution using the same conditions as those described for the preparation of the carbon paste surfaces in the SEM powder mounts. Following the complexation of the ligands with iron(II), the electrode was thoroughly rinsed with distilled water, and was then placed into an electrochemical cell containing 1.0 M $NaClO_4$. A cyclic voltammogram was recorded, and this is shown in Figure 21a. The anodic peak at 0.980 V (versus Ag/AgCl, 3.0 M NaCl) and the cathodic peak at 0.741 V are both characteristic of the quasi-reversible couple of the iron(II)-ligand complex present at the electrode surface [5].

This same modified carbon paste electrode was then immersed into the gold(III) solution, again replicating the conditions used for the carbon paste surfaces on the SEM powder mounts. The immersion was again carried out in steps with cyclic voltammograms being recorded between the immersions. The cyclic voltammetry was done by removing the electrode from the gold(III) solution, thoroughly rinsing the surface with distilled water, and then placing the electrode into an electrochemical cell containing 1.0 M $NaClO_4$. Figure 21b shows the voltammogram for the electrode after immersion of the electrode in the gold(III) solution for 1 min. As expected, the current due to the oxidation/reduction of the active iron(II)-ligand complex centers decreased, since these active centers should have begun to be covered with gold(0). The concomitant appearance of a cathodic peak at 0.309 V indicates the presence of gold on the electrode surface. Note that the anodic peak for the oxidation of the iron centers on the electrode surface has broadened and appears to have shifted to more positive potentials. This phenomenon can be explained by the fact that the oxidation of the iron and gold centers under these conditions occurs at potentials that are quite close to one another.

Figure 21c is the cyclic voltammogram for the above electrode after an additional immersion in the gold(III) solution, with a total gold(III) exposure time of 5 min. As can be seen from the figure, the cathodic current at 0.763 V has again decreased, indicating that gold is still depositing on the iron(II) centers. The currents due to the oxidation and reduction of gold have also increased, showing the increased presence of gold on the electrode surface. This same trend of decreasing iron(II) currents and increasing gold currents was

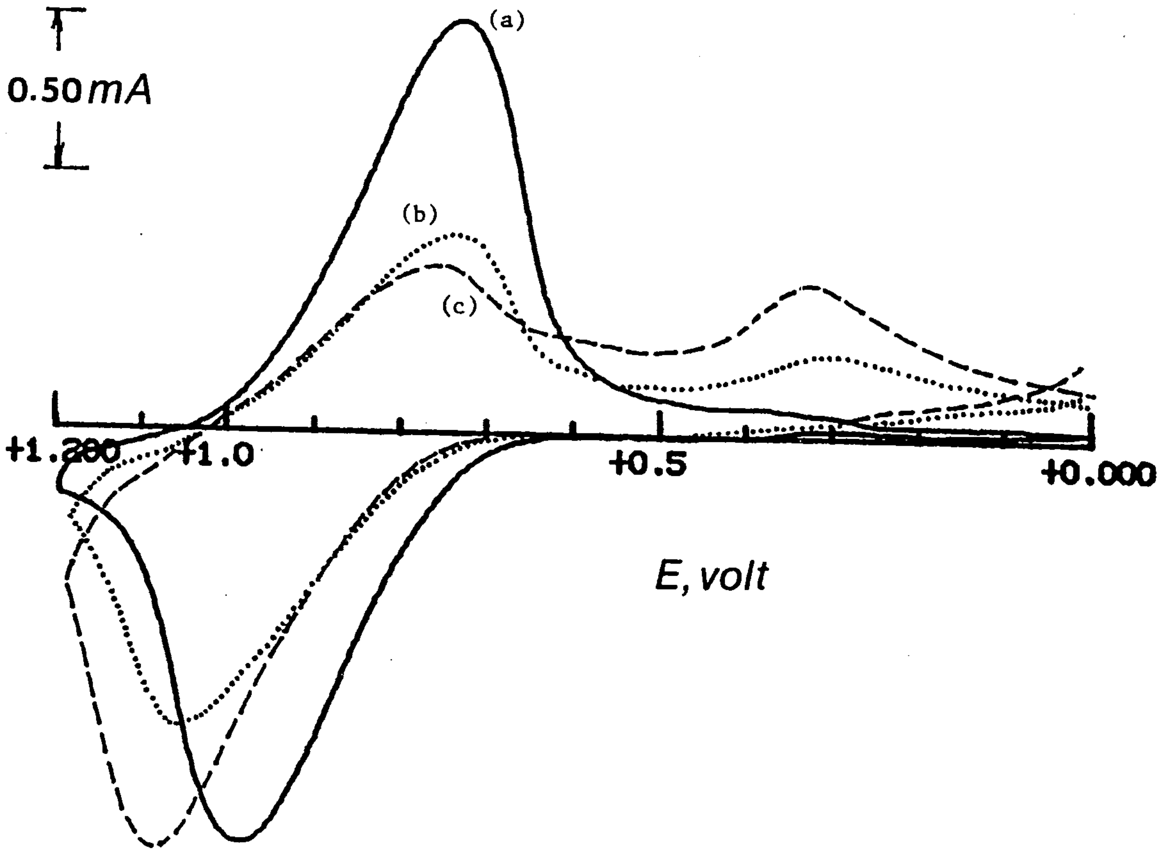

Figure 21. Cyclic Voltammograms Obtained with a 5% 4,7-Diphenyl-1,10-Phenanthroline-Modified Carbon Paste Electrode Immersed in 1.0 M $NaClO_4$. Scan Rate: 0.020 V/s. a) after overnight immersion of the electrode into a solution of iron(II); b) the same electrode as in a) following a 1 min immersion into a gold(III) solution; c) the same electrode as in b) following an additional immersion into the gold(III) solution for a total of 5 min.

found to continue for gold immersion times of up to 11 min, at which time the iron(II) currents become indistinguishable from the background current.

Conclusions

It may be concluded from the data presented here that mapping of active centers on ligand-modified surfaces can be done by the introduction of positively-charged groups on the ligands or by complexation with iron(II), followed by chemical deposition of gold (via anion exchange or redox reaction) and scanning electron microscopy via backscattered electron imaging. Cyclic voltammetry, X-ray energy-dispersive microanalysis and X-ray area scanning (mapping) validate the overall approach used here by showing that the deposition of gold occurs directly over the active modifying centers.

CHAPTER III

THE CHARACTERIZATION OF UNMODIFIED ELECTRODE SURFACES: SURFACE ROUGHNESS AND REACTIVITY

This chapter and the one following it will deal with the characterization of *unmodified* electrode surfaces although the concepts discussed in these chapters could very well be applied to modified electrodes of the type discussed in Chapters I and II. Chapter III will begin with a definition of "characterization" as it is applied in this thesis to unmodified electrode surfaces. Later, an introduction to surface roughness, fractal geometry, and the fractal dimension will be presented which should ease the transition to topics such as the theoretical and experimental approaches for the measurement of the fractal dimension. Several examples from the current literature will be given to illustrate the experimental approaches. The chapter will conclude with a brief discussion of the reaction dimension used in the field of catalysis, which will have some bearing on the experimental results presented in Chapter IV.

Definition of "Characterization" As Applied To Unmodified Electrode Surfaces

The word "characterization" will have a different meaning for Chapters III and IV than it did in previous chapters. For unmodified electrode surfaces, "characterization" will refer to that process whereby one can *quantify* the roughness and reactivity of the surface. Information such as this could be very useful to the electroanalytical chemist, who is often concerned with accurately reproducing electrode surfaces from one experiment to another. Evidence of this concern for reproducible electrode surfaces are the many long and sometimes complicated electrode polishing procedures in use by people in the field.

Another area in which surface roughness and reactivity play a major role is in the determination of the "true" surface area of the electrode. Since the electrode surface area enters many electrochemical equations for the measurement of current, current density, charge, etc., it is important to find out how surface roughness will affect these quantities.

The quantification of roughness and reactivity (characterization) of an electrode surface can be done by determining what is known as a "fractal dimension" for the surface. The ideas embodied in this term originate from a rather new mathematical field known as fractal geometry. This area and related fractal concepts are introduced in the following section.

Introduction to Fractals and Fractal Geometry

This section will introduce fractals and fractal geometry, and will assume that the reader is not familiar with these terms. Therefore, the bulk of the discussion will center on the physical aspects of fractals and fractal behavior and not on the mathematical derivations usually associated with this topic in the literature. The section will begin with a few definitions and then progress into an example of fractal behavior from a classic paper by L. F. Richardson to clearly illustrate fractal aspects and measurements to the reader. Finally, the different types (or degrees) of disorder and irregularity will be discussed.

Definitions of Fractals, Fractal Geometry, and the Fractal Dimension

The area of fractal geometry and its application to a wide array of fields such as the physical sciences, biology, economics, medical sciences, and linguistics [63] has grown tremendously in recent years. Its success has been its ability to describe and model extremely disordered and chaotic systems, a task which would be monumental, if not impossible, using conventional Euclidian geometry.

Although fractal concepts were already being worked on by Hausdorff (by 1919) and Besicovitch (by 1935) [64], the term "fractal" is attributed to B. B. Mandelbrot, who first coined the word in 1975 in a book called "Les objets fractals: forme, hasard et dimension", which was translated to English in 1977. This book, "Fractals: Form, Chance, and Dimension" won great acclaim and is now considered a classic work in this area.

The word "fractal" comes from the Latin adjective "fractus", which means "broken up" [65]. It describes a set or object that seems rough or disordered, and more importantly, remains at the same level of roughness or disorderliness when a part of the object is viewed after successive magnifications. Likewise, if the object is successively contracted (viewed under successively less magnification) the object will again look similar. That the object looks the same regardless of the magnification is an important property of fractals known as "scaling". To state it another way, "when each piece of a shape is geometrically similar to the whole, both the shape and the cascade [of shapes] that generate it are called *self-similar*" [65].

Fractal geometry is the tool that allows us to look at irregular, chaotic sets or objects from a mathematical point of view. According to Preining [63], "fractal geometry is the study of geometric shapes that seem chaotic when compared with those of standard (Euclidian) geometry (lines, spheres, etc.) but exhibit extreme orderliness because they possess the property of invariance under suitable contractions and dilations". Notice again the emphasis on scaling properties of these fractal objects or sets. Fractal geometry modifies and actually upgrades the concepts of Euclidean geometry for reasons that will be revealed next.

There remains one term that will be very important for this discussion and for the experimental aspects to be presented in Chapter IV. The quantity known as the *fractal (Hausdorff-Besicovitch) dimension* can be thought of in two different ways. It can be viewed as an extension of the classical Euclidian (or topological) dimension in which a point was assigned a dimension of 0, a line a dimension of 1, a plane a dimension of 2, and a space-filling volume (such as a cube) a dimension of 3. The fractal dimension, D_f, upgrades this idea by allowing a *non-integral* dimensional representation of an object. For example, Figure 22 illustrates 2 randomly drawn lines. The top line could have assigned a D_f of 1.32 (or any real number between 1 and 2) to describe how the line becomes plane-filling as it becomes increasingly irregular. Another even more random line has a still higher D_f: equal, say, to 1.71. Similarly, a random, corrugated plane could be assigned a D_f of 2.52 (or any real number between 2 and 3) to describe how the plane becomes volume-filling upon increasing irregularity. It has already been intimated that the fractal dimension can be used to *quantify* the irregularity of an object; this is another useful way to think about the physical meaning of the term.

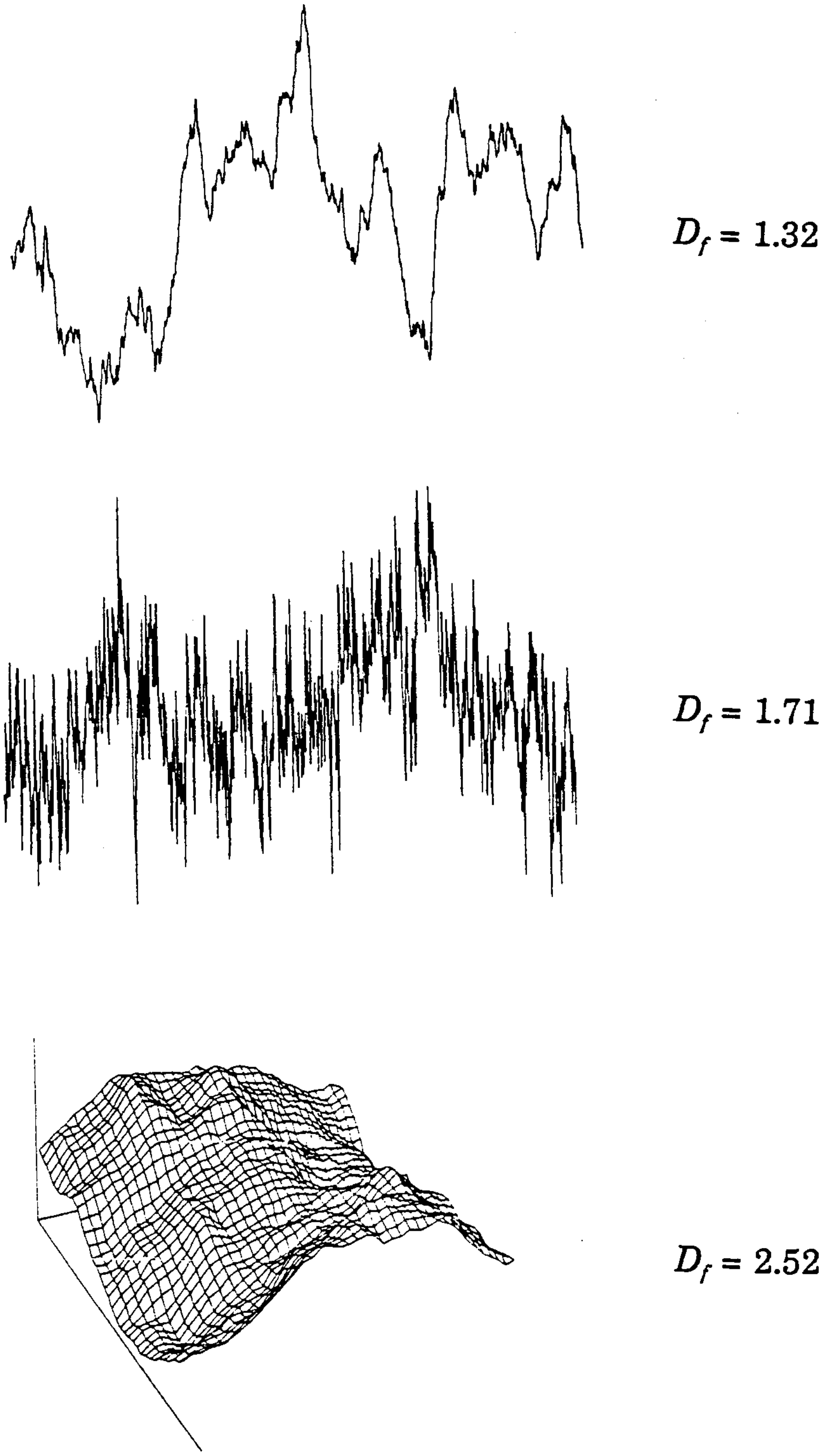

Figure 22. Illustration Showing how D_f can be used to Quantify the Irregularity of a Line or of a Surface [64]

Now that the definitions for the most basic fractal concepts have been examined, an application of these concepts to a practical, real-life problem will be given.

An Application of Fractal Concepts: How Long is the West Coastline of Great Britain?

In a lengthy article [66] concerning the statistics and probability of war among neighboring countries, Lewis F. Richardson asked a supposedly simple question--How long is the western shore of Great Britain? He found that the question had no simple answer.

Richardson took detailed maps of the region, and using dividers set to a fixed length, counted the number of "steps" that it took to "walk" the coastline from Land's End in the South to Duncansby Head in the North. Using the set length of the dividers and the number of "steps" he could calculate the perimeter of the west coast. He then changed the setting on the dividers and repeated the "walking" process. What he found puzzled Richardson, for depending on the set length of the dividers, the calculated lengths of the coast were different; smaller "steps" resulted in increasingly large perimeter lengths. What Richardson observed is common when one attempts to measure the length of a fractal curve. Richardson found that irregularity in the coastline remained even after subsequent attempts to use smaller and smaller divider lengths. Similar results were obtained on the coasts of Australia and South Africa.

The author also found discrepancies in the reported lengths of shared natural boundaries between countries, suggesting that each neighboring country must have used a different "step" size in determining the overall boundary length. Richardson observed this phenomenon only on jagged "natural" boundaries such as rivers.

One of the more interesting and useful parts of the essay was the development of the mathematical relationship between the set length of the dividers (the step size), λ, and the calculated length of coastline, $\Sigma\lambda$. Quite empirically, Richardson found that a plot of log (step size) versus log (length of the coastline) yielded a straight line. This relationship (for the west coast of Great Britain) was shown to have the following mathematical form:

$$\Sigma \lambda \propto \lambda^{-0.25} \tag{1}$$

He realized that the slope of this line and lines drawn using data from other coastlines was directly correlated to the jaggedness or irregularity of the coasts or boundaries. For instance, the irregular west coast of Great Britain showed a fairly large negative slope, while the much smoother coast of South Africa gave only a slight negative slope. Based on Richardson's work, Mandelbrot [65] proposed a more general equation:

$$\Sigma \lambda \propto \lambda^{1-D_f} \qquad (2)$$

where D_f is the fractal dimension. An equation of the type shown above is known as a *scaling equation* and reflects the scaling properties of fractal objects. The corresponding log-log plot, now known as a Richardson Plot in honor of its originator, has become an important tool for the measurement of the fractal dimension. An example of the use of a Richardson Plot can be seen in the experimental results section in Chapter IV.

Types or Degrees of Disorder

There are several different kinds of disorder in fractal-type objects, and these were carefully and clearly spelled out recently by Pfeifer and Obert [67]. Their classification of the types of disorder is based on two different kinds of similarity in an object. Dilation similarity has been already been discussed. This is the idea that when a small part of an object is magnified, the result looks similar to the original object. Translation similarity reflects how the irregularity of an object changes as one moves along the curve or surface at the same magnification level. As will be shown next, it is this property of an object that allows its classification according to Pfeifer and Obert's scheme.

The authors have divided all objects into four different types: no disorder, weak disorder, anisotropic strong disorder (self-affine), and isotropic strong disorder (self-similar). Those objects with *no disorder* have the properties of dilation and translation similarity. An example of this would be a perfectly straight line or a perfectly flat surface. Objects with *weak disorder* still show dilation and translation similarity, but only on a localized basis. An example of this type of object would be a slightly irregular line characterized by long, straight stretches, interspersed by an occasional change of direction. *Self-affine* objects contain even more disorder and have the properties of dilation similarity and macroscopic translation similarity, meaning that there is a great deal of translation irregularity on a local level, but the average translation irregularity over the whole object is fairly minimal. A good example of this could be a noisy baseline drawn with a strip-chart recorder. *Self-similar* objects are considered to be true fractals and contain only dilation similarity--there is no translational similarity at all. Many natural objects exhibit this type of irregularity. Coastlines, mountains, trees, and clouds have all been given as examples of fractal objects [65].

The Fractal Dimension and Some Theoretical Approaches for its Measurement

In this section additional aspects of the fractal dimension will be covered. In addition a few of the theoretical models that are used for the measurement of the fractal dimension will also be addressed.

Inner and Outer Cutoffs for Fractal Behavior

According to Pfeifer and Obert [67], there is always a particular size range (scale) for which *real* objects exhibit fractal behavior. To continue with the example of the length of the coastline of Great Britain, there are lower and upper bounds (inner and outer cutoffs) for the step size, λ, for which the scaling equation is obeyed. The upper limit for the step size in this particular example could be considered to be the overall length of the coastline, $\Sigma\lambda$. Since step sizes larger than this would give $\Sigma\lambda \propto \lambda^1$, this would mean that based on Mandelbrot's equation (2), D_f would be equal to 0, a meaningless value in this context of measuring an irregular line. In this case one would expect a value between 1 and 2.

The lower size limit for the step size requires a bit more analysis. In Richardson's original work, recall that he used detailed maps and dividers for his measurements. The lower limit for the step size in this example could conceivably be somewhere in the range at which the continuous lines of the map become individual dots of ink. The individual dots of ink introduce additional irregularity into the measurement, beyond that of the original problem--the length of a coastline. Therefore, the irregularity would tend to be overstated, and values of D_f would no longer correspond to the irregularity of the coastline only. Another way to think about this is to consider measuring the coastline by physically walking along the shore. If one could take infinitely small steps (with infinitely small feet) one would eventually reach a point where the placement of individual grains of sand would add to the overall measurement of irregularity. This measurement would no longer describe the irregularity of the coastline only, but also of the irregularity of the packing of particles of sand. This would be a different kind of fractality and would require a different scaling equation. On the practical side, for real object applications (as condensed matter), atomic length scales set a lower bound [67].

Theoretical Models for the Measurement of the Fractal Dimension

This section will briefly describe some of the models used as tools to measure or quantify the irregularity of an object. Again, emphasis is placed on the physical aspects without the mathematical background.

Box Counting. This method is commonly used (at least by the mathematicians) to determine the fractal dimension. In this technique a measure is made of the number of boxes needed to cover an area occupied by the object as a function of the box size [64]. The boxes are positioned in an orderly grid over the object. This is illustrated in Figure 23. In addition, the "dimensionality" of the box changes depending on the type of object. For instance, to measure the irregularity of a straight line, the "box" has a dimension

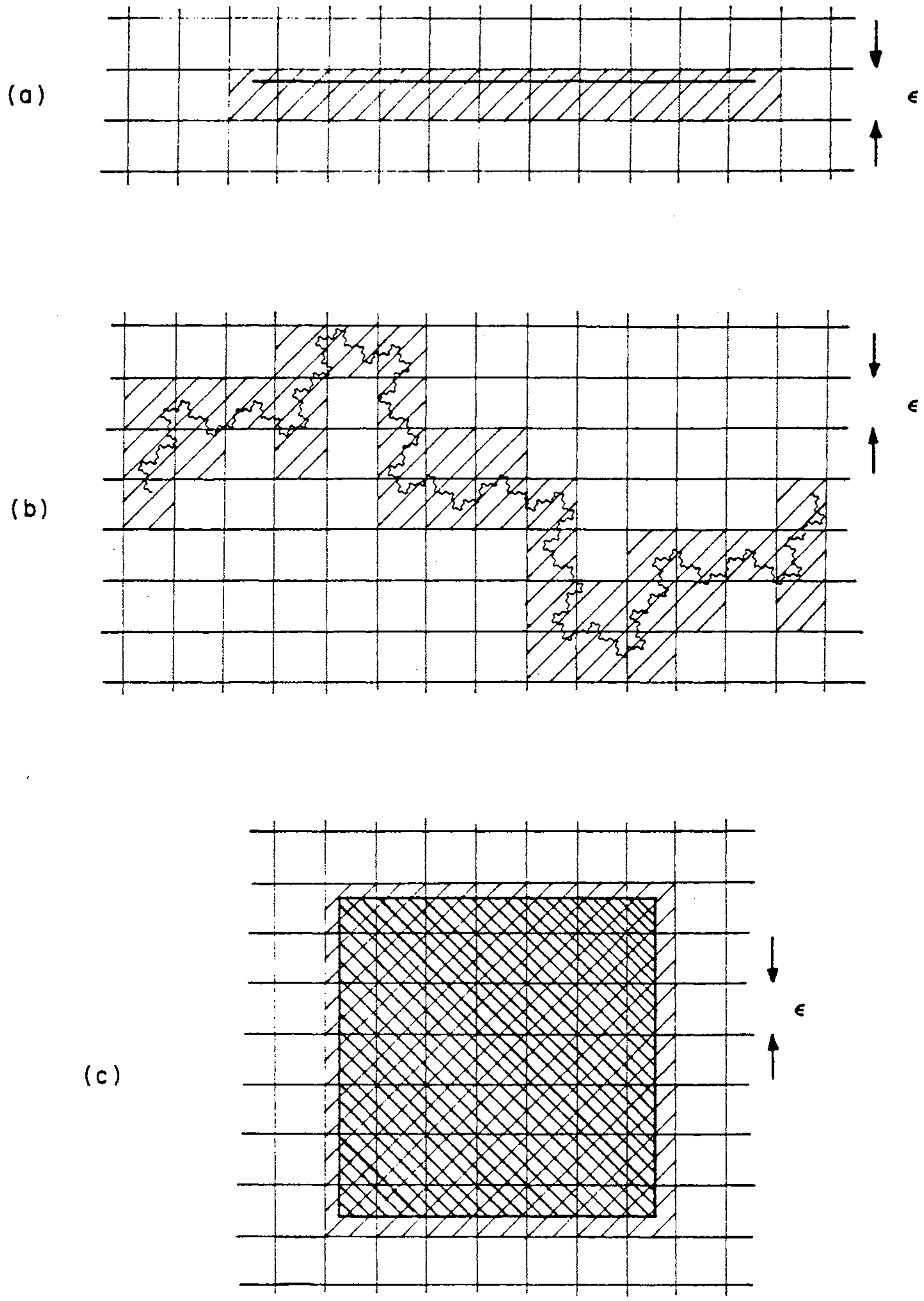

Figure 23. Illustration Showing the Box-Counting Method. Counting of non-empty boxes (shaded) for a) a straight line; b) an irregular curve; c) a square [67].

of 1. To measure the irregularity of a curve or a flat plane, the "box" has a dimension of 2. For an irregular surface, the box has dimensionality of 3. The scaling equation for the relationship between the number of boxes of a certain size, $N_{box}(\epsilon)$, needed to contain an object such as a curve or a surface and the box size itself, ϵ, has been shown by Pfeifer and Obert [67] to be:

$$N_{box}(\epsilon) \propto \epsilon^{-D_f} \tag{3}$$

Unfortunately, this model, as simple as it sounds, has two important drawbacks. For those objects that approach ordinary Euclidean dimensions, the method tends to overestimate lengths, areas, or volumes. The second drawback is that, on an experimental level, the method can usually be implemented only with computer image analysis.

Mass-Radius Method. This method operates by modeling the object with "lattice sites". These sites can be thought of as covering the object with tiny boxes such as those used in the box method. The distance between adjacent sites is denoted by ϵ (as was the box size in the previous model). In the mass-radius method a series of circles (or spheres) of radius, R, each centered on a given lattice site, is constructed and the number of the lattice sites that are contained by each of the circles, $N_{sites}(R)$, is counted as a function of radius size.

This quantity is referred to as the "mass". This method works best when $R >> \epsilon$, as is illustrated in Figure 24. The scaling equation is as follows [67]:

$$N_{sites}(R) \propto R^{D_f} \tag{4}$$

The mass-radius method, like the box counting technique, is best implemented with the aid of a computer, a reliable image of the object, and image analysis software.

Covering the Object with Spheres. The last technique that will be discussed for the determination of D_f is the model in which the object is covered with spheres or balls of differing sizes. This idea is illustrated in Figure 25. The minimum number of these balls, $N_{ball}(r)$, needed to cover the object is counted as a function of ball radius, r. The scaling equation is [67]:

$$N_{balls}(r) \propto r^{-D_f} \tag{5}$$

This approach to determine D_f for an object is very popular, as it is easily implemented experimentally. The balls can, in many cases, be well approximated by real molecules, and the objects covered by the "balls" can be the surfaces of catalysts, adsorbents, and electrodes. As will be seen in the next

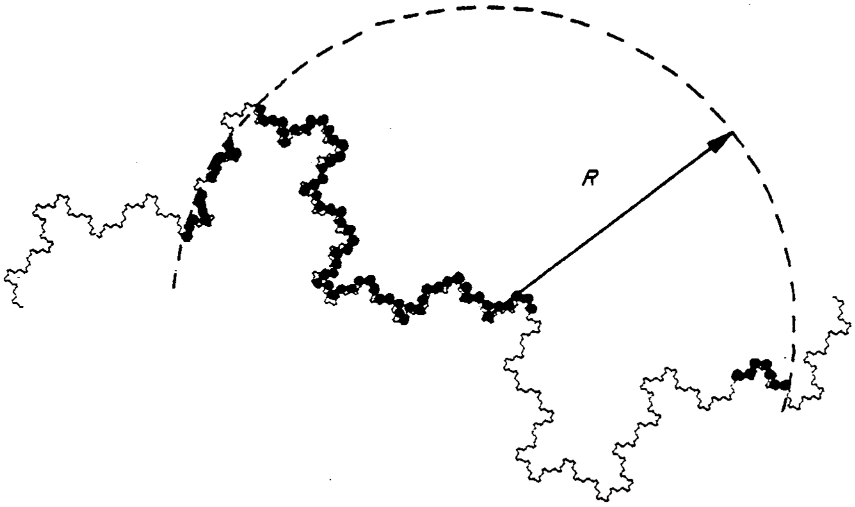

Figure 24. Illustration of D_f Determination Using the Mass-Radius Method. The sites are pictured as adsorbed molecules on a surface [67].

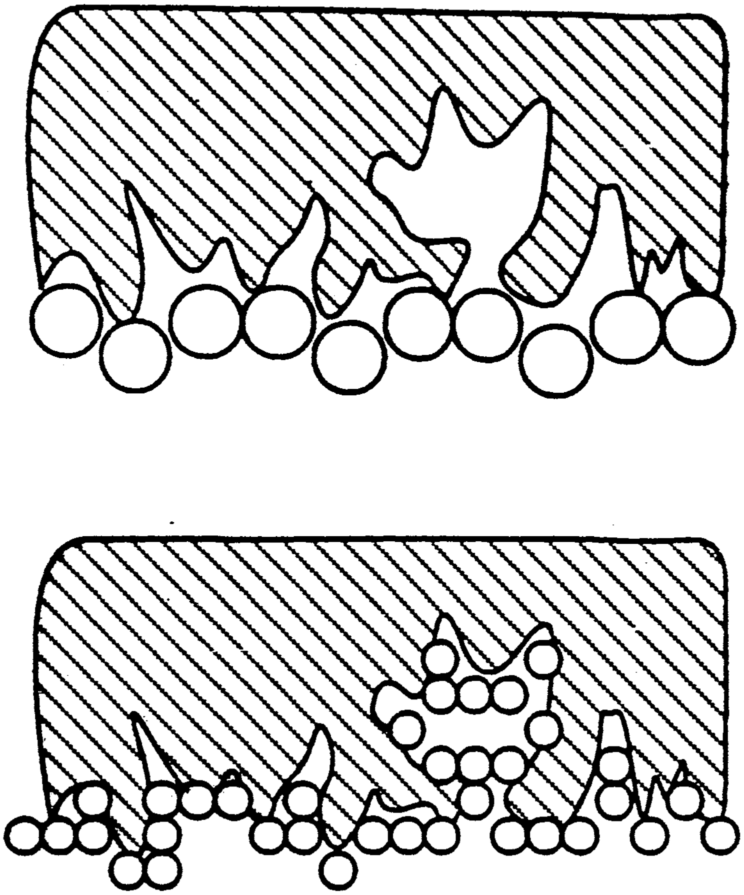

Figure 25. Measurement of D_f by Covering the Object or Surface with Spheres of Differing Size. Note that the surface area accessible to the spheres is different in each case.

section, a great many of the experimental approaches for the determination of the fractal dimension are based upon these theoretical principles.

Some Experimental Approaches for the Determination of the Fractal Dimension

It is the intent of this section to merely introduce some of the experimental methods currently in use for the determination of D_f. The references given, being representative of the work in that particular field, should be consulted for more detailed discussions. A review of work done in the area of D_f determinations can also be found in Avnir *et al.* [68].

Image Analysis

The digitization of an image of a fractal object or surface is a standard way of obtaining quantitative data regarding the object's jaggedness [64]. In this technique an image of the object is made via a photograph or micrograph. The image is digitized by a scanner or video camera and is transmitted to a computer where it is stored as a two-dimensional array of pixels. Various computer programs can then be used to calculate the fractal dimension. Recently, for example, image analysis in this manner was applied to study the topography of the state of Oregon [69]. The majority of the research done in this area, however, is in the development of new computer algorithms to quickly and accurately calculate fractal dimensions from images [70].

Images from scanning electron and scanning probe microscopies are also routinely used for D_f determinations. Many of these methods use a stereo pair of photomicrographs which are digitized for computer analysis. The computer compares the offset at many locations on the two images and calculates heights of surface irregularities on the basis of the parallax angle. The magnification scale can be varied both with the microscope and with the computer; therefore, fractal dimensions can be calculated [71].

Light Scattering

A very powerful method to determine fractal dimensions of individual particles and surfaces is the use of light scattering [69]. In experiments of this type a beam of intensity I_0 is directed on the sample and the scattered intensity is measured as a function of the angle θ between the incident and the scattered beam. In many cases the scattering intensity is measured at relatively small angles. In addition, a wide variety of light sources are used to study scattering. The type of light source used depends on the characteristic length scales associated with the object to be studied.

Although the mathematics of light scattering is involved, the scattered intensity is a function of (among many other things) the shape or structure of the object. In this so-called structure factor lies the fractal dimension. Through suitable mathematical derivations, Vicsek has given the following scaling law [64]:

$$I(q) \approx q^{-D_f} \tag{6}$$

where $I(q)$ is the scattered intensity and q has the form:

$$q = \frac{4\pi}{\lambda}\sin\left(\frac{\theta}{2}\right) \tag{7}$$

where λ is the wavelength of incident light. By plotting log $I(q)$ versus log q, the fractal dimension can be determined from: $slope = -D_f$.

Examples that could be cited in the literature of D_f determinations using light scattering could include Skatkov *et al.* [72], who, using small angle X-ray scattering (SAXS), determined fractal dimension values for porous niobium samples with equations similar to those outlined above. The fractal dimension of SiO_2 samples has also been determined using SAXS by Schmidt *et al.* [73]. Other researchers [74] have determined fractal dimension values on soot samples by using incident laser light and relatively large scattering angles.

Adsorption Methods

This is an extremely large area of research. The popularity of this method of D_f determination is due, in part, to the ease at which the ideas related to the original definitions of D_f can be implemented experimentally. One can see that the idea of covering a fractal object with a monolayer of adsorbed molecules bears strong resemblance to the theoretical method of covering the object with spheres which was discussed earlier. Typically, for adsorption methods, the objects for which the fractal dimension is determined are limited to surfaces and some porous materials.

In many of the adsorption-type methods, one generally determines (by use of an appropriate isotherm) the number of moles, n, of an adsorbate to cover the object in a monolayer. In this way an estimate of the area of the surface can be made. Avnir and Pfeifer [75] have shown that if the adsorbate is varied through a series of spherical molecules of radius, r, the fractal dimension, D_f, can be calculated from:

$$n \propto r^{-D_f} \tag{8}$$

These authors point out that the adsorbate molecules need not be spherical provided that they belong to what is called a *homologous series*. In such a series the square of the radius of each molecule in the series, r^2, divided by its cross-sectional area, σ, is a constant. Substituting σ into equation (8) we obtain:

$$n \propto \sigma^{(-D_f/2)} \tag{9}$$

Since the apparent surface area, A, "seen" by the molecules is equal to $n\sigma$, equation (9) becomes:

$$A \propto \sigma^{(2-D_f)/2} \tag{10}$$

Scaling equations such as this can be derived for a number of different experimental situations. Avnir and Farin [76] have reviewed the various scaling equations that have been derived along with their individual applications. Table II summarizes some examples of chemical interest.

As examples from the literature of this kind of D_f determinations, one could cite the work of Avnir and Pfeifer [77] who were able to determine the fractal dimension of porous silicic acid particles by covering them with monolayers of alcohol molecules of varying size. Using equation (10), the authors determined D_f for their samples to be 2.94, a number which indicates extreme irregularity of the samplesurfaces and pore structure. For their estimation of cross-sectional area, σ, of the covering (probe) molecules, the authors assumed sphericity of the molecules and used molar volume values.

TABLE II

SUMMARY OF SCALING EQUATIONS FOR THE DETERMINATION OF FRACTAL DIMENSIONS, D_f, ON VARIOUS SAMPLES [76]

Sample	D_f	Adsorbates	Scaling Equation
granular activated carbon	2.71	N_2, various organic molecules	$n \propto \sigma^{-D_f/2}$
soil	2.92	malachite green	$n \propto R^{D_f-3}$
porous silicic acid	2.94	N_2, small chain alcohols	$A \propto \sigma^{(2-D_f)/2}$
partially graphitized carbon black	2.04	N_2, methanol, benzene, cyclohexane	$V_m \propto \sigma^{-D_f/2}$
glassy melted rock	2.46	Argon	$A \propto R^{D_f-3}$

In these equations, n and V_m represent monolayer coverage of the adsorbate on the surface (for example, moles of adsorbate per gram adsorbent); σ is the effective cross-sectional area of adsorbate; A is the apparent surface area; R represents radius of the particles.

A recent advance in this particular field is the development of mathematical treatments that allow D_f determinations using a single N_2 isotherm [78]. This was done on non-porous carbon fibers and carbon blacks and involves multilayer coverage of the surface. The utility of this approach is that adsorption experiments do not have to be done for each adsorbate.

It should be pointed out that still other adsorption type methods are available for the determination of D_f. Pfeifer and Avnir [75] also suggest that the use of a single adsorbate molecule, such as N_2, can be used to probe objects or specimens of differing size to quantify the roughness and irregularity of a given sample with the following scaling equation:

$$n \propto R^{(D_f - 3)} \tag{11}$$

where n is defined as before and R is the radius of the sample specimens. An adsorption method based on this approach is best applied to powdered samples which are easily separated into varying particle sizes by means of sieves. Goodwin [79] has determined the fractal dimension of controlled-pore glass samples using this strategy.

Measurements Based on Physical (Electrical) Properties

The physical properties of fractal objects can also be used for the experimental determination of D_f. Many of these involve the measurement of electrical properties such as current, charge, and frequency dependence of impedance of fractal interfaces. Surface roughness or irregularity has been recognized for some time as being an important parameter which can seriously affect the measurement of current and related quantities at electrodes [80]. Several researchers have attempted since then to use these electrical quantities to measure irregularity on electrode surfaces; representative examples from the literature follow.

Impedance Analysis. The application of a small amplitude alternating voltage to an electrode/electrolyte system (in the absence of any Faradaic process) has been used to study interfacial processes. Such data can yield information on rate and diffusion coefficients and double-layer capacitance [81]. One of the problems of impedance analysis, however, is the frequency dependence of the impedance which has been observed at many non-smooth electrode surfaces. It is this property, however, which turns out to be very useful for the quantification of electrode surface roughness. Nyikos and Pajkossy [81] have given the following empirical relation describing the frequency dependence, or constant phase element:

$$1/Z \propto (i\omega)^{\alpha} \tag{12}$$

where Z is the impedance, i is $(-1)^{1/2}$, and ω is the frequency. The exponent, α, was defined by using an "impedance mesh" (an equivalent circuit consisting of an array of resistors and capacitors designed to mimic an irregular electrode surface). The authors studied the effect of spatial magnification (scaling) of the impedance mesh on the admittances, capacitances, and resistances. Based on such scaling arguments, these researchers showed that α is related to the fractal dimension of the electrode surface by:

$$\alpha = \frac{1}{D_f - 1} \qquad \textbf{(13)}$$

It should be mentioned here that equation (13) is not accepted by all of those in the field. In fact, no general relationship between α and D_f seems to prevail. A fairly general feature of the different models, however, is that the larger is D_f, the smaller is α, in accordance with expectations [82].

Chronoamperometric Techniques. Various researchers later moved from impedance analysis to the treatment of diffusion-limited charge transfer across a fractal electrode surface [83]. Again with the use of scaling considerations, Nyikos and Pajkossy have produced a relationship between current density, j, and time, t, which can be formulated as follows:

$$j \propto t^{-\alpha} \tag{14}$$

where

$$\alpha = (D_f - 1)/2 \tag{15}$$

Such equations are considered to be the time-domain equivalent of the constant phase element behavior described in equations (12) and (13). Equations (14) and (15) allow the direct estimation of the fractal dimension by calculating the slope of the line produced by plotting log (current) vs. log t. These ideas were verified experimentally for gold electrodes manufactured to known D_f values and immersed into hexacyanoferrate(III) solutions [84]. Wu *et. al* [85] suggested that the proportionality given in equation (14) be incorporated into a generalized Cottrell equation:

$$i = nFAC^{*}\left(\frac{D}{\pi}\right)^{1/2} t^{-(D_f-1)/2} \tag{16}$$

where i is the current, n is the number of electrons exchanged, F is the Faraday constant, A is the electrode area, C^{*} is the concentration of the electroactive species in the bulk of the solution, D is the diffusion coefficient, π is the constant, and t is time. It should be noted that for smooth electrode surfaces with $D_f = 2$, the equation reverts back to the classic Cottrell case for which $i \propto t^{-1/2}$. This generalized equation was shown to be followed in the case of single crystal and polycrystalline TiO_2 electrodes. Furthermore, fractal behavior ($D_f > 2$) was observed when the diffusion length of the electroactive species to the electrode surface was less that the actual surface irregularities on the electrode surface.

Coulometric/Chronocoulometric Techniques. These techniques are a modification of the amperometric techniques mentioned earlier in which current is integrated with time so that the amount of charge is one of the quantities measured. A few examples from the literature illustrate the use of these techniques.

Crevs *et. al* [86] have used coulometry to determine the fractal dimension of rough silver electrodeposits using the scaling equation:

$$A \propto V^{D_f/3} \tag{17}$$

where A is the surface area of the silver deposit, and V is the volume of the silver deposit. The volume of the deposit was estimated by first calculating the mass of the deposit using the amount of charge required to grow the deposit and Faraday's Law. Dividing this result by the density of solid silver gave the volume of the deposit. The surface area, A, was estimated by measuring the amount of charge required to cover the silver deposit with a monolayer of lead or cadmium and dividing this result by the monolayer charge density for these metal layers on platinum. By plotting log A vs. log V, D_f could be calculated from the slope.

In other work Chen and Jorné [87] used the mass-radius approach as a theoretical basis for their experiments. They determined D_f for zinc electrodeposits at a copper cathode surrounded by an annular zinc anode in a thin-layer cell made of glass. The authors used the scaling equation

$$M(r) \propto r^{D_f} \tag{18}$$

where $M(r)$ is the mass of the electrodeposit and r is the radius of the deposit. $M(r)$ was determined by coulometry, and r was estimated with the aid of a microscope fitted with calibrated reticles. The measurements of both $M(r)$ and r were done over time while the electrodeposit was growing. The slope of the line resulting from a plot of ln $M(r)$ vs. ln r gave D_f directly.

As will be seen in Chapter IV, chronocoulometric techniques can also be used for the determination of D_f. Chronocoulometry is an electrochemical technique in which the potential of the working electrode is stepped from an initial potential where no redox reaction occurs to a final potential where the reaction of interest does occur [88]. The Faradaic portion of the chronocoulometric response can be described by the integrated Cottrell equation, obtained by integration of the signal current between time = 0 and time = t. Typical excitation and signal plots are shown in Figure 26. Because double-layer charging and charge due to adsorbed species on the electrode surface must be taken into account, additional terms must be added to the integrated Cottrell equation [88]:

$$Q = \frac{2nFAD^{1/2}Ct^{1/2}}{\pi^{1/2}} + Q_{dl} + nFA\Gamma \qquad \textbf{(19)}$$

where Q is the total amount of charge, n is the number of electrons, F is the Faraday constant, A is the electrode area, D is the diffusion coefficient, C is the bulk concentration of the electroactive species, t is time, Q_{dl} is the charge due to capacitive charging of the double layer, and Γ is the surface excess of reactant due to adsorption. Since the latter two terms are not time dependent, it can be seen that a plot of Q vs. $t^{1/2}$ should be linear. Such a plot is called an Anson plot, and the line produced should have a slope equal to $(2nFAD^{1/2}C)/(\pi^{1/2})$.

In experiments for the determination of D_f, all the quantities in the above Anson plot slope equation are known or can be estimated except for A, which should reflect changes in surface roughness and reactivity. With reliable values for the other quantities, the *effective* surface area of the electrode can be

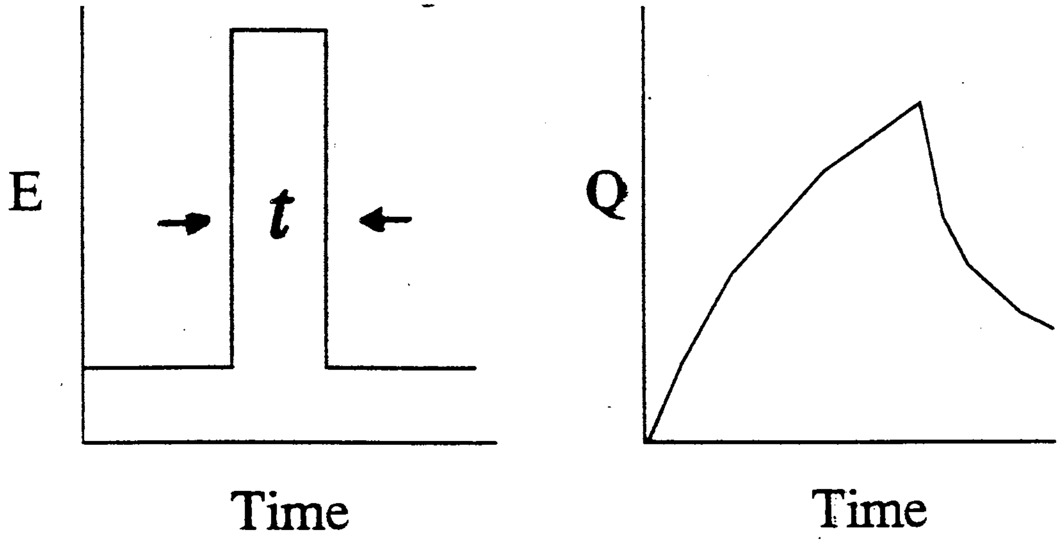

Figure 26. Typical Potential and Charge Profiles in Chronocoulometry. E is potential, t is the pulse time, and Q is total charge.

calculated. Chapter IV will discuss how the effective surface area can be used to determine D_f values for a given electrode surface.

An Introduction to the Reaction Dimension

All of the discussion so far has been concerned with the fractal dimension, D_f, suggesting that there is only one type of fractal dimension to describe a fractal object. While one usually connotes D_f with the geometric irregularity of the surface, Farin and Avnir [89] introduced another type of fractal dimension, the reaction dimension, D_R, which reflects the reactivity of a catalyst with changes in the size of the particle size of the catalyst. In their perusal of the literature dealing with many different kinds of catalysis, they found that activity, *a*, of a given catalyst, and the particle size of the catalyst, *R*, obeyed the following scaling law:

$$a \propto R^{D_R} \tag{20}$$

Their interpretation of D_R was that it provides a quantitative means of the comparative evaluation of the degree of structure sensitivity of a catalyst, or the sensitivity of catalytic processes to changes in scale of the individual catalyst particles. In this light, it becomes clear that there can be many different types of fractal dimension quantities to describe a particular surface. The particular fractal dimension quantity that is determined will depend on the type of reaction taking place at the surface. The authors stated it best in a later paper [68]: "...it is more appropriate to observe a material surface as representing a host of *effective* surfaces for specific surface processes. Thus, one has to replace the discussion of *the* fractal dimension of *a* surface with a fractal dimension of the collection of surface sites which participate in a specific process."

Although the experimental determination of D_f by chronocoulometry (the experimental details of which follow in Chapter IV) does not deal with catalysis, it is important to note that in this work one is dealing with a specific process at a fractal surface--an electrochemical reaction. Therefore, one must also consider that the quantity that has been determined, D_f, also takes into account such things as diffusion to and from a fractal surface and the activity/distribution of active sites on the surface.

Summary

It was the purpose of this chapter to introduce the reader to fractal geometry and fractal concepts, both of which are relevant to the experimental work to be discussed in the next chapter.

Chapter III began with an introduction of fractal geometry in which terms such as the fractal dimension were defined. The fractal dimension was shown to *quantify* the irregularity of an object. It can also be thought of as an extension or upgrading of the dimension concept from classical Euclidian geometry. A few classical problems from the literature (such as the length of a coastline) were discussed in order to clarify the definitions. Next, the various theoretical approaches to the measurement of the fractal dimension were discussed, followed by the actual experimental methods that are presently in use for such determinations of D_f.

In the last section, the reaction dimension was introduced, and the point was made that there may be many different types of fractal dimension quantities that could describe a given surface, depending upon the individual processes/reactions that take place at the surface. In short, the fractal dimension quantity that is determined for a given surface not only is associated with surface roughness and irregularity, but is also related to the *reactivity* of the surface.

The experimental details of the quantification of the surface roughness and reactivity of a glassy carbon electrode surface will now be addressed in Chapter IV.

CHAPTER IV

IRON(II) COMPLEXES OF THE 1,10-PHENANTHROLINE FAMILY OF LIGANDS AS POTENTIAL PROBES TO CHARACTERIZE ROUGHNESS AND REACTIVITY OF CONDUCTING SURFACES

The Importance of Roughness/Reactivity Characterization of Conducting Surfaces

Chapter IV is meant to use the background information presented in Chapter III to show how one can characterize the roughness and reactivity of conducting surfaces. This chapter will discuss the importance of and the motivation for this work, and will also give experimental details of how this was accomplished with glassy carbon and gold [90] electrode surfaces. As stated previously, although the experimental emphasis in this work was placed on *unmodified* glassy carbon surfaces, the ideas expressed here could very well be applied to modified electrode surfaces, as well.

Why is the ability of the electroanalytical chemist to quantify the roughness and reactivity of an electrode surface important? The main answer to this question is to help the chemist with reproducibility problems so prevalent in electrochemical techniques. Quantification of roughness and reactivity could also give the researcher a tool with which to evaluate electrode performance. Figure 27 is a depiction of 2 hypothetical electrode surfaces in contact with molecular species of differing sizes. Figure 27a depicts a relatively smooth surface while Figure 27b depicts a highly irregular surface. Most electrochemists would agree that the rough and smooth electrodes would not perform to equal extents. The most obvious reason for this is that the surface areas of the two electrodes are very different, but there are other reasons, as well.

Among the other reasons one could cite for the different performance levels of the electrode surfaces in Figure 27 are the differing abilities of molecules to move on or near the surface. Consider an electroactive reactant near the opening of the large pore in Figure 27b. Such a molecule may have to wait for an electroactive product to diffuse out of the pore before the reactant can diffuse into it, whereas such a problem on the smooth surface would not exist. According to Mottola [91], kinetic behavior in constrained environments (where convective stirring is difficult and diffusion-controlled conditions predominate) can possess non-classical kinetic properties such as non-integral reaction orders, and rate coefficients that vary with time. Since many electrochemical techniques such as voltammetry occur with a passage of current

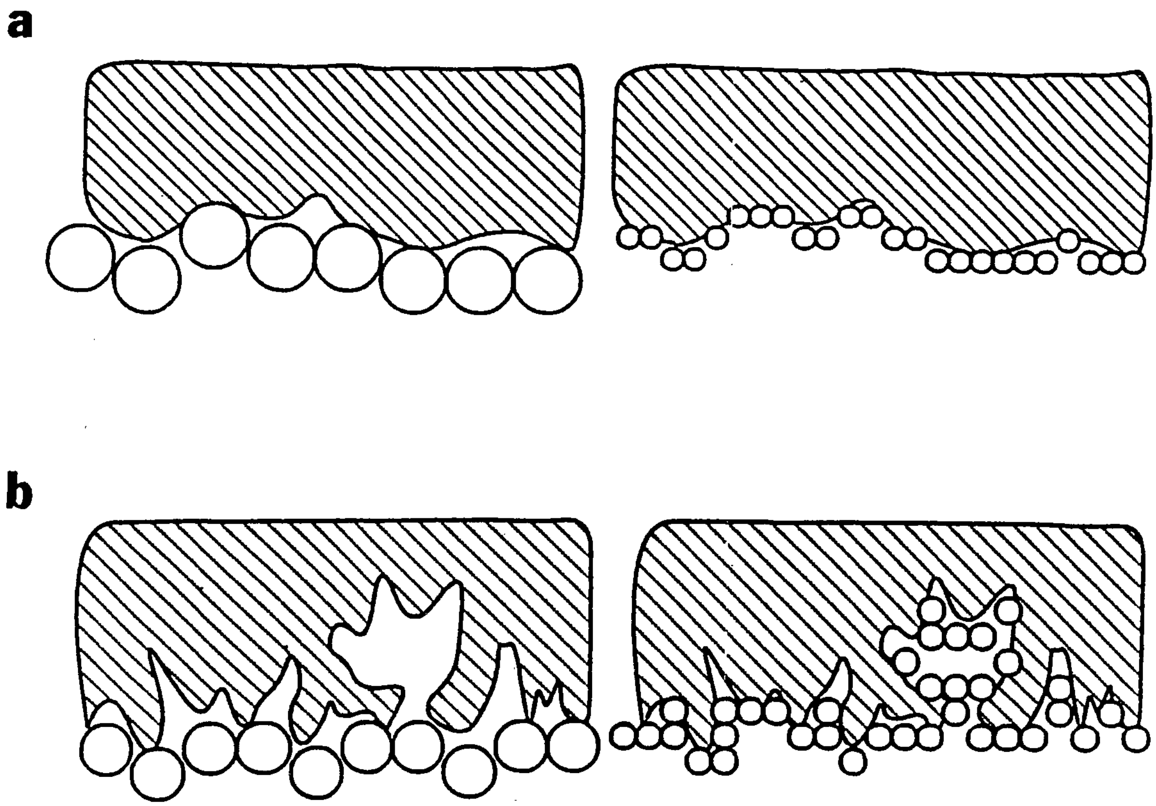

Figure 27. Illustration Showing Molecular Accessibility of Surfaces. a) relatively smooth surface; b) high degree of roughness. In each case, accessibility depends on molecular size as well as surface roughness.

under non-equilibrium conditions, such kinetic considerations must be taken into account.

One can also see in this discussion of molecular movement that the *size* of the individual species diffusing to and from the electrode surface can also give differences in electrode performance. Recall Figure 25 from Chapter III, where it was shown that large molecules will typically have more difficulty diffusing into and out of small pores. The accessible electrochemical area will be affected by the availability of reactive sites at which electron exchange can occur. In most cases, the accessible *electrochemical* surface area (the fraction of the total surface area accessible to a given electroactive species) of the electrode is generally lower than the *geometric* (total) surface area. This effect is more pronounced with electroactive species of increasing size and electrode surfaces of increasing irregularity.

Since the roughness of a conducting surface and the size of the electroactive species both dictate the current flow (analytical performance) of working electrodes, a set of electroactive molecules of differing size should give a means of quantifying electrode roughness and reactivity provided that they have similar electrochemical behaviors. For a family of electroactive probes containing the same redox center [namely the iron(II)/iron(III) couple in ligands of the 1,10- phenanthroline family], a scaling relationship between the apparent electrochemical surface area and the cross-sectional area of the electroactive species can be formulated. The scaling law is of the form:

$$A_E \propto \sigma^{[(2-D_E)/2]} \tag{1}$$

in which σ is the cross-sectional area of the electroactive species, A_E the apparent electrochemical area (obtained by chronocoulometric measurements), and D_E is defined here as an electrochemical dimension, which can be taken as a parameter providing information with regard to the roughness and electrochemical reactivity of a given conducting surface.

Experimental

The experimental details of the characterization of roughness and reactivity by the determination of the electrochemical dimension for glassy carbon and gold conductive surfaces are presented in this section. Although the work for the gold electrode was not done by this author [90], the experimental details and results were similar and are included to emphasize the validity of the overall approach.

Reagents and Solutions

All reagents were of analytical reagent grade, except as noted. All ligands used, L, form complexes with iron(II) in a 3:1 ligand-to-metal ion ratio and were purchased from GFS Chemicals (Columbus, OH). The complexes containing perchlorate as the counterion were prepared by mixing (in stoichiometric ratios) an aqueous solution of $Fe(NH_4)_2(SO_4)_2$ from Mallinckrodt (St. Louis, MO) with the ligand which had been dissolved in acetone. The complex was then precipitated as the perchlorate salt, $FeL_3 \cdot 2ClO_4$, by the addition of excess $NaClO_4$, which was also purchased from GFS Chemicals. Some of the FeL_3-perchlorate salts were directly purchased from GFS Chemicals and were used as received. The water used for solution preparation was deionized and further purified by distillation in an all-borosilicate-glass still with a quartz immersion heater. The supporting electrolyte solution, 0.0360 M in H_2SO_4, was prepared with a 74.6% acetonitrile/25.4% water medium. Acetonitrile (from EM Science, Cherry Hill, NJ) was required to solubilize some of the rather high molecular weight iron(II) complexes. The iron(II) complexes were prepared to be 1.00×10^{-3} M using the electrolyte solution described above as the solvent.

Instrumentation

All electrochemical measurements were made with a BAS-100 electrochemical analyzer (Bioanalytical Systems; West Lafayette, IN) equipped with an auto cell stand and utilizing a platinum wire pseudo-reference electrode, a platinum wire auxiliary electrode, and either a 3 mm diameter glassy carbon or a 3 mm diameter gold electrode as the working electrode.

Procedure for Electrode Polishing

The working electrode surfaces were prepared by rinsing the surface first with methanol, and then with purified water. The surfaces were then polished on a water-saturated felt pad onto which was placed a few drops of a suspension of 0.05 μm alumina particles obtained from Bioanalytical Systems. The electrodes were then thoroughly rinsed with distilled water. To remove any adsorbed alumina particles, the electrodes were placed into a sonicator with purified water for a few minutes. After a thorough rinsing with purified water one last time, the electrodes were ready for electrochemical measurements. In measurements with the gold electrode, nitrogen gas was gently bubbled through the solution for 5 minutes. There was no need for such a precaution when glassy carbon was used as the working conductive surface because there was no apparent interference from dissolved oxygen.

Procedure for Chronocoulometric Measurements

In order to set the initial and final potential step profile for the chronocoulometric measurements, cyclic voltammograms were recorded for each of the iron(II) complex solutions using potential limits of -0.10 V and 1.0 V with a sweep rate of 0.020 $V \cdot s^{-1}$. Quasi-reversible potential peaks for the $L_3Fe(II)/L_3Fe(III)$ couple, the anodic peak potential, E_{pa}, and the cathodic peak potential, E_{pc}, typically fell in the range 0.4 to 0.8 V versus the platinum reference. A cyclic voltammogram for the 1,10-phenanthroline iron(II) complex obtained with the glassy carbon working electrode is shown in Figure 28. The anodic and cathodic peaks that are evident around 0.05 V versus the platinum reference were due to the slight dissociation of the complex in the acetonitrile medium. Since this phenomenon was observed for the entire family of 1,10-phenanthroline iron(II) complexes studied, any small errors in concentration caused by the dissociation of the complexes should cancel in the final calculation of the electrochemical dimension, D_E.

Chronocoulometric potentials, E_i and E_f, were chosen as follows: $E_i = E_{pa} - 0.20$ V; $E_f = E_{pa}$. The duration of the potential pulse was fixed at 750 ms for glassy carbon and 250 ms for gold because these particular pulse times provided better regression coefficients in the plots of charge versus $(\text{time})^{1/2}$ (Anson plots). In an effort to increase reproducibility and to decrease the amount of adsorbed species on the electrode surface, the $L_3Fe(II)$ solutions were vigorously stirred for 30 s to 1 min after the completion of each chronocoulometric measurement. Prior to beginning the next measurement, the potential of the working electrode was poised at E_i for 30 s to 1 min without stirring to allow the solution to quiesce.

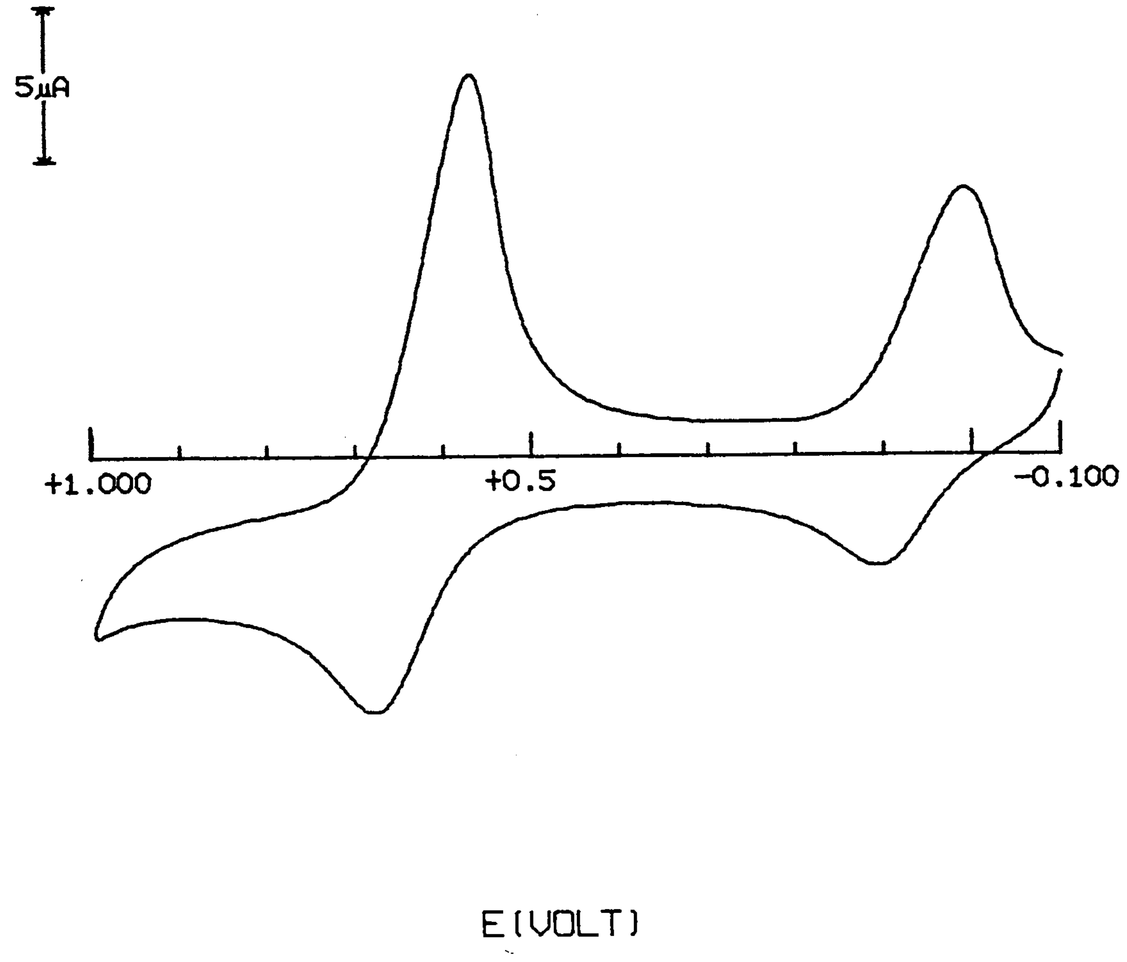

Figure 28. Typical Cyclic Voltammogram of 1 × 10^{-3} Tris(1,10-Phenanthroline)iron(II) Perchlorate. Initial potential: -0.1 V, high potential: 1.0 V, low potential: -0.1 V, sweep rate: 0.02 V/s, supporting electrolyte: 0.0360 M H_2SO_4 prepared with 74.6% acetonitrile/25.4% water. Potentials versus the platinum pseudo-reference electrode.

Determination of the Density of the Iron(II) Complexes Used for the Calculation of their Cross-Sectional Areas

The densities of the iron(II) complexes were determined for each of the FeL_3-perchlorate solids by use of the following procedure: (1) a clean, dry picnometer with a built in capillary and thermometer was dried to constant weight to the nearest 0.0001 g to give a value, w_2; (2) the picnometer was completely filled with *n*-decane and was again weighed to give the value w_1; the temperature of the *n*-decane, t_1, was also noted; (3) the picnometer was again dried to constant weight, was partially filled with the dried, solid iron(II) complex whose density was to be determined, and was weighed to give the value, w_3; (4) finally, the picnometer containing the solid was filled with *n*-decane and weighed giving the value, w_4; the temperature of the immersing liquid, t_2, was again noted. The density of the solid iron(II) complexes were calculated with the use of the following equation [92]:

$$d_{solid} = \frac{(w_3 - w_2)d_{liquid}}{(w_1 - w_2) - (w_4 - w_3)} \tag{2}$$

where d_{solid} denotes the density of the FeL_3-perchlorate salt and d_{liquid} denotes the density of the immersing liquid, *n*-decane, at the average temperature, $t_{average}$ =

$(t_1 + t_2)/2$. The density, d_{liquid}, of the *n*-decane was found by the use of an empirical equation relating density and temperature [93]:

$$d_{liquid}=0.7455-[(7.293\times10^{-4})t]-[(3.710\times10^{-7})(t)^2] \tag{3}$$

where d_{liquid} is the density of *n*-decane at temperature, t; the equation is valid in the 0-100°C temperature range.

Results and Discussion

No matter how much care that is exerted when polishing an electrode, the conducting surface is generally not "smooth" but "rough" and mostly not even "flat". Edgar [94] notes that "Roughly speaking, a fractal is a set that is more 'irregular' than the sets considered in classical geometry. No matter how much the set is magnified, smaller and smaller irregularities become visible". Considering a conductive electrode surface to be such a set, such self-similar fractal behavior should be apparent on conductive electrode surfaces at small scales approaching the molecular level.

As stated in Chapter III, the degree of irregularity (independent of reactivity) can be conveyed by a single quantity, known as the fractal dimension, D_f, and takes values between 2 and 3 for surfaces. The numerical value of the fractal dimension, however, is intimately related to the experimental approach utilized to extract it.

There are two basic ideas that are used to interpret the electrochemical dimension quantity, D_E, that is determined in this work for the glassy carbon and the gold electrode surfaces. One of these ideas is that the electrochemical dimension will describe to some extent the *roughness* of the surface. In Chapter III some discussion was made regarding the determination of fractal dimensions by covering the fractal object or surface with spheres of differing size. There it was shown that the number of spheres covering the object, n, and the radius of the spheres, R, obeyed the scaling law:

$$n \propto R^{-D_f} \tag{4}$$

The other idea that lends some meaning to the electrochemical dimension quantity is that this value is dependent on the *reactivity* of the glassy carbon surface. Recall the discussion in Chapter III that dealt with the reaction dimension, D_R. There, the work of Farin and Avnir [89] in the field of catalysis showed that catalytic activity, a (mole$\cdot$time$^{-1}\cdot$particle^{-1}) and the particle size of the catalyst (which is a function of the radius), r, also obey a simple scaling law:

$$a \propto r^{D_R} \tag{5}$$

This relationship assumes the approximation of ideally spherical particles.

Under the suspicion that "smooth" conducting surfaces would yield similar scaling relationships between the electrochemical area and the size of the electroactive species, the measurement and correlation of electrochemical areas of some conducting surfaces with the cross-sectional areas of a family of iron(II) ligands of roughly spherical geometry was studied. The family of ligands chosen for the correlation has, as the parent compound, tris(1,10-phenanthroline)iron(II) , which is shown in Table III. Molecular models reveal a roughly spherical architectural envelope for these chemical species, and that they allpresent the same redox center [the iron(II)/iron(III) couple] for electron exchange with a conducting surface.

Electrochemical Surface Areas

Electrochemical surface areas were determined by chronocoulometry using the "potential step" procedure described in Chapter III and under the experimental section. The charge produced as the potential is stepped up (or down) can be described by the integrated Cottrell equation [88]:

$$Q = \frac{2nFAD^{1/2}Ct^{1/2}}{\pi^{1/2}} + Q_{dl} + nFA\Gamma \tag{6}$$

where Q = charge in coulombs; n = number of electrons exchanged (equiv·mol^{-1}); F = Faraday constant (coulombs·mol^{-1}); A = apparent

TABLE III

CHEMICAL PROBES USED IN THE REPORTED STUDIES

Parent Ligand and Iron(II) Complex

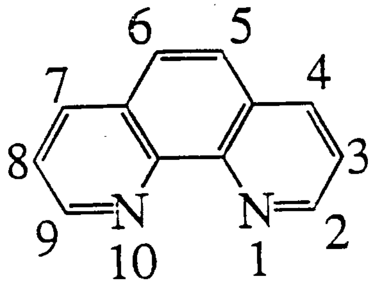

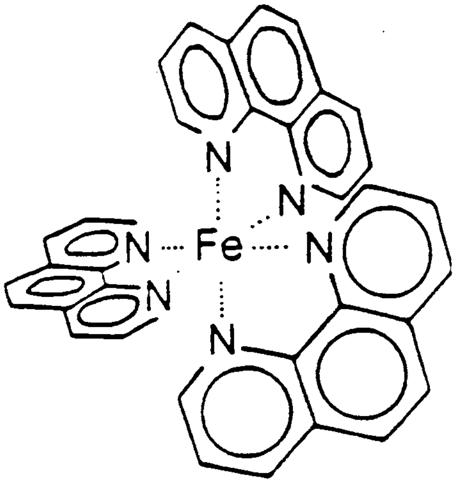

Other Derivative Ligands Used (Substitutions at positions 4, 5, 7, and 8 on the 1,10-Phenanthroline Moiety)

5-Methyl-1,10-phenanthroline

5-Chloro-1, 10-phenanthroline

5-Nitro-1,10-phenanthroline

5-Phenyl-1,10-phenanthroline

3,4,7,8-Tetramethyl-1,10-phenanthroline

4,7-diphenyl-1,10-phenanthroline

electrochemical surface area (cm^2), D = molecular diffusion coefficient ($cm^2 \cdot s^{-1}$); C^* = bulk concentration ($mol \cdot cm^{-3}$); t = time (s); Q_{dl} = charge contribution from the double layer capacitance (coulombs), and Γ = surface excess of reactant due to adsorption ($mol \cdot cm^{-2}$). The electrochemical surface area, A, can be extracted from the slope, $(2nFAC^*D^{1/2}/\pi^{1/2})$, of plots of Q versus $t^{1/2}$, if all the other terms in the slope are known. The values of the molecular diffusion coefficients for the probes used in this work were determined previously by Li and Mottola [95] using a continuous-flow procedure based on the original work of Taylor [96]. Typical values of the diffusion coefficients and of the electrochemical areas are shown in Table IV.

Cross-Sectional Areas of Electroactive Probes

Cross-sectional areas were determined by calculation of the radius for each complex obtained by molecular computer graphics (Poly Graf from Molecular Systems, Burlington, MA), and by independently using a method developed by McClellan and Harnsberger [97] with the help of the following equation:

$$\sigma = 1.091[M/(d_{solid} \times N_A)]^{2/3} \tag{7}$$

where σ is the cross-sectional area, M is the molecular weight, d_{solid} is the density of the solid, and N_A is Avogadro's number. It is of interest to point out that regardless of the approach used to obtain cross-sectional areas, there is good correlation between the two methods as Figure 29 shows. The cross-sectional areas obtained by computer modeling are, however, roughly 2 to 3 times larger than those obtained by picnometer. The absolute values, however, are not needed. It is the cross-sectional area *trends* of the homologous series of probe molecules that is important for this work.

The computer program used for dynamic computer graphics simulation, allows for random minimization of potential energy. The largest distance was found between the center of the iron(II) atom and the center of the most remote hydrogen atom on an adjoining ligand; the sum of this distance and the Van der Waals radius of the hydrogen atom was used as the radius of the iron(II)-ligand complex for the calculation of the cross-sectional area. Figure 30 shows the typical average model for the tris(5-phenyl-1,10-phenanthroline)-iron(II) species.

Log-Log Plots and Scaling Relationships

Although the probe species included in this study reveal a semi-spherical envelope by molecular modeling, the approach taken to arrive at a power law assumes irregular surfaces with non-spherical probes. This is done with the recognition that: (1) the scaling is guided not only by geometric considerations

TABLE IV

VALUES OF MOLECULAR DIFFUSION COEFFICIENTS [95] USED IN ARRIVING AT APPARENT ELECTROCHEMICAL AREAS FROM CHRONOCOULOMETRIC MEASUREMENTS, ANSON PLOT VALUES, AND ELECTROCHEMICAL AREAS FOR THE GLASSY CARBON ELECTRODE

Chemical Probe	Molecular Diff. Coeff. x10^6, cm^2s^{-1}	Slope of Anson plot, $\mu C(ms)^{-1/2}$	*A* x10^2 cm^2
1-10-Phenanthroline	6.13	1.036±0.018	12.1±0.8
5-Methyl-1,10-phenanthroline	5.66	1.133±0.062	13.8±0.1
5-Nitro-1,10-phenanthroline	5.24	0.868±0.012	11.0±0.6
5-Phenyl-1,10-phenanthroline	5.01	0.658±0.005	8.54±0.30
4,7-Diphenyl-1,10-phenanthroline	3.25	0.506±0.033	7.13±0.48

Uncertainties in slope values are based on sample standard deviations of 12 to 25 replicate measurements.

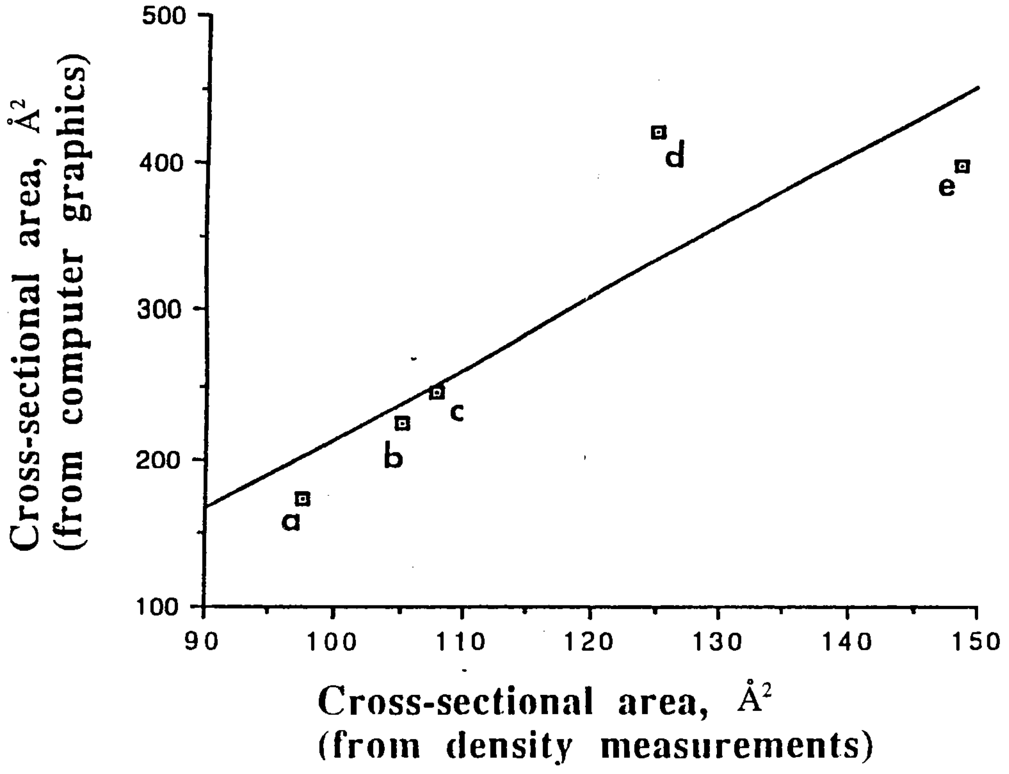

Figure 29. Comparison between Cross-Sectional Area Values for the Tris(1,10-Phenanthroline)Iron(II) Perchlorate Family of Compounds. Ligands: a) 1,10-phenanthroline; b) 5-methyl-1,10-phenanthroline; c) 5-nitro-1,10-phenanthroline; d) 5-phenyl-1,10-phenanthroline, and e) 4,7-diphenyl-1,10-phenanthroline.

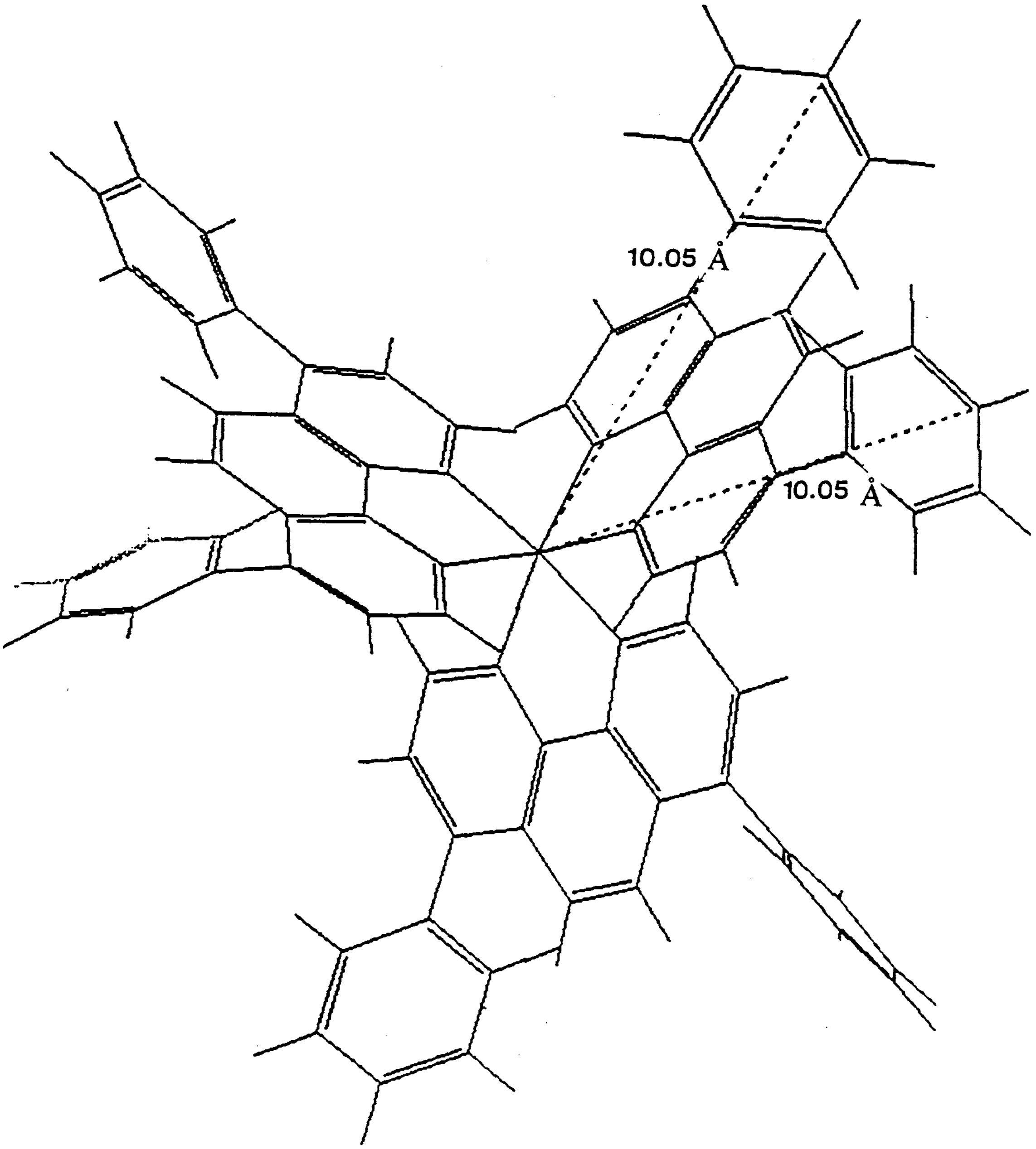

Figure 30. Two-Dimensional Projection of the Average Computer-Optimized, Atom-Based Structure of Tris(5-Phenyl-1,10-Phenanthroline)Iron(II) Cation. The dashed lines indicate, in Å, the largest distances from the center of the Fe-atom to the most distant hydrogen on the surface envelope.

(fractal power laws), but also by surface electroreactivity, (2) upon approaching the surface, the chemical probe may undergo distortion from the "pure" spherical form, and (3) the formulation used results in positive values for D_E.

From the fractal concept as applied to surfaces, the apparent (in this case electrochemical) area covered by N non-spherical species is [77]:

$$A = N\sigma \propto \sigma^{(2-D_E)/2} \tag{8}$$

and a plot of log A vs. log σ should be a straight line with slope equal to $(2-D_E)/2$. Hence, from this slope a value of D_E can be extracted. Figure 31 and Figure 32 show typical plots obtained for a "smooth" glassy carbon surface and a "smooth" gold surface, respectively. It is of interest to note that better linearity is observed by using cross-sectional area values that are obtained by density measurements rather than those obtained by computer modeling. In any event the trends are similar, and the average values of D_E are comparable. The average D_E for the glassy carbon surface was found to be 3.34 ± 0.12 (cross-sectional area by computer graphics) and 4.94 ± 0.06 (cross-sectional area from density measurements). The gold surface yielded values of 3.50 ± 0.10 (cross-sectional area by computer graphics) and 4.84 ± 0.08 (cross-sectional area from density measurements). Uncertainties are given in the

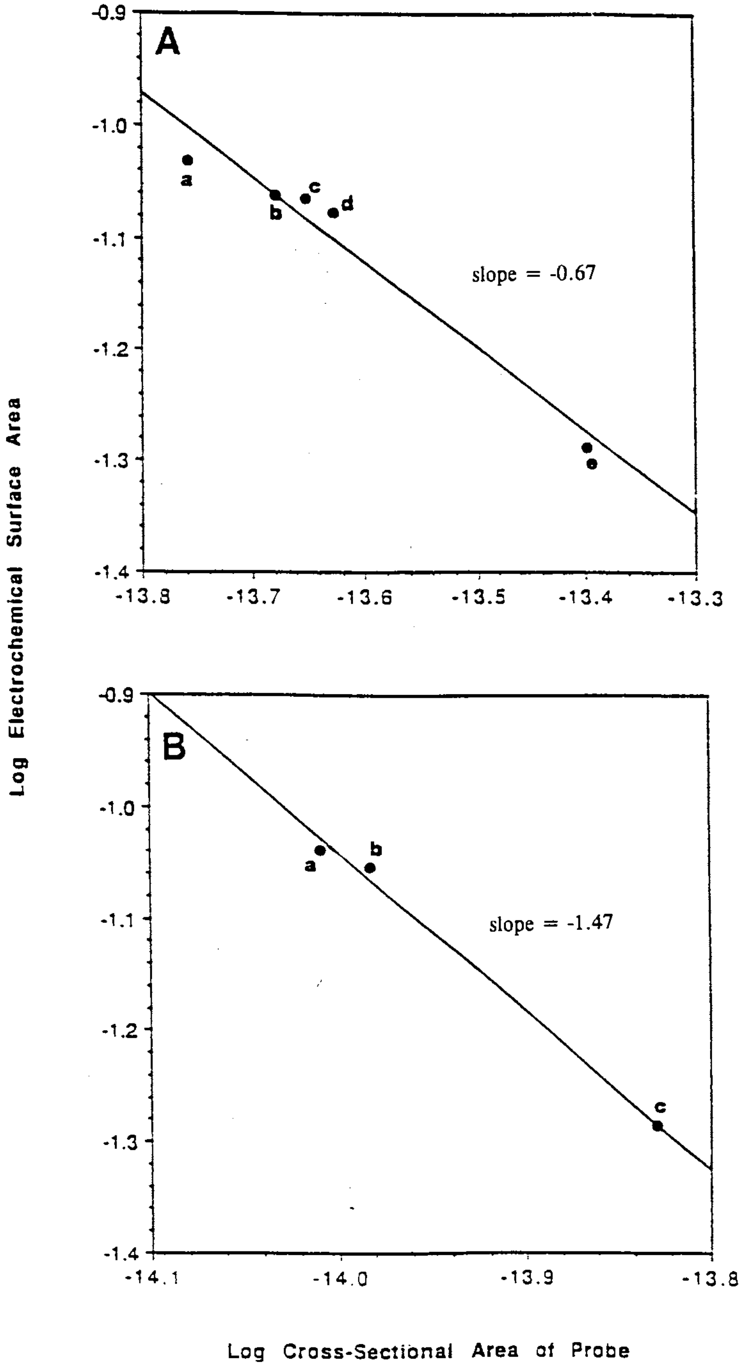

Figure 31. Typical Log-Log Plot of Electrochemical Surface Area Versus Cross-Sectional Area of Electrochemical Probe for a "Smooth" Glassy Carbon Surface. **A**) cross-sectional area estimated by computer modeling; **B**) cross-sectional area calculated via density measurements (see text for details). FeL_3^{+2} probe identification (via small letters) follows the listing given in Figure 29.

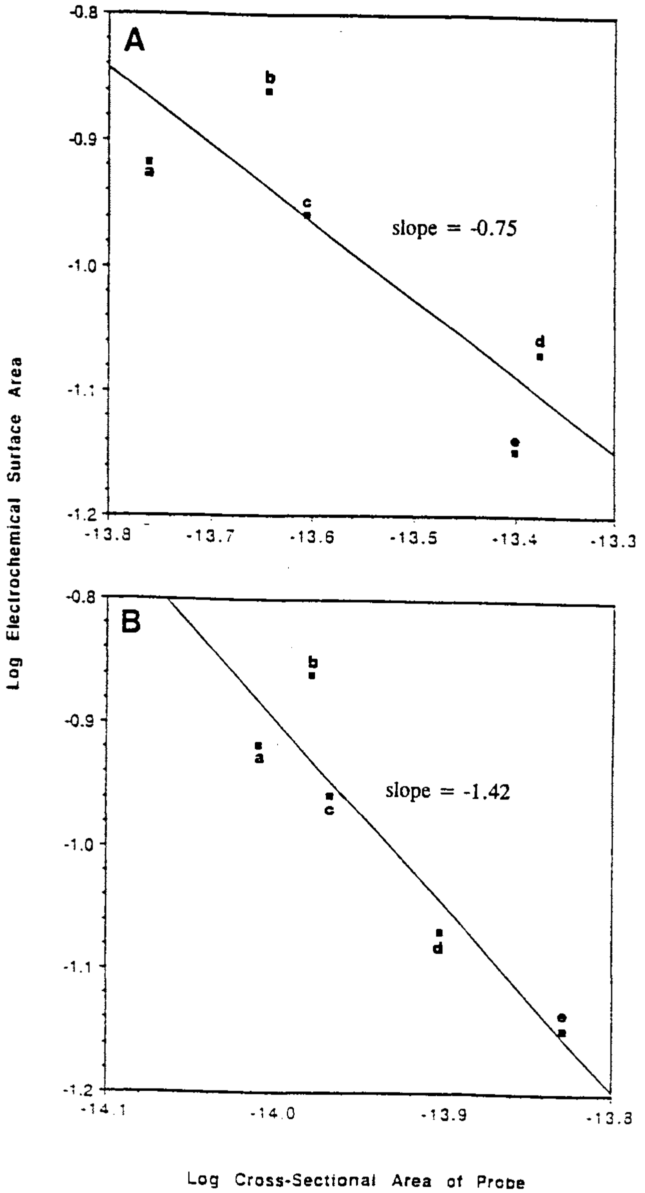

Figure 32. Typical Log-Log Plots of Electrochemical Surface Area Versus Cross-Sectional Area of Electrochemical Probe for a "Smooth" Gold Surface. Method of cross-sectional area determination (identified via large letters) and L_3Fe^{+2} probe identification (via small letters) follows. **A**: cross-sectional area estimated by computer modeling; *a*, 1,10-phenanthroline; *b*, 3,4,7,8-tetramethyl-1,10-phenanthroline; *c*, 5-methyl-1,10-phenanthroline; *d*, 5-chloro-1,10-phenanthroline; *e*, 4,7-diphenyl-1,10-phenanthroline; **B**: cross-sectional area calculated from density measurements (see text for details); *a*, 1,10-phenanthroline; *b*, 5-methyl-1,10-phenanthroline; *c*, 4,7-diphenyl-1,10-phenanthroline.

form of average deviations because they are based on triplicate values of slopes from log-log plots.

Conclusions

The results presented here are of exploratory nature, but point to power law trends from which a new parameter for electrode surfaces can be extracted. The basic idea of a log-log correlation between electrochemical area and cross-sectional area of a family of probes containing the same redox center seems substantiated. The main difficulty with the family of probes studied is their tendency to adsorb onto the electrode surface. By subtracting the intercept of the reverse step from the intercept of the forward step when plotting equation (6), the double layer capacitance, Q_{dl}, is eliminated (assuming that is the same for both steps) and the remaining value is a measure of $nFA(\Gamma_{red} - \Gamma_{ox})$. Although very good reproducibility was observed in values of the slopes, values of the intercepts were more poorly reproduced and seemed to decrease as polishing of the surface was repeated. Also evident is the fact that different approaches to the estimation of the cross-sectional area yield different values of D_E; this is, however, of no great concern since trends are similar, and the adoption of a single approach would standardize the values. Here again, Richardson's remark about the length of the coastline of Great Britain becomes evident. Research opportunities certainly remain for further measurements involving other families of probes and involving surfaces with different degrees of roughness based on the encouraging trends reported here.

CHAPTER V

SUMMARY AND CONCLUSIONS

This thesis dealt directly with the problem of characterizing both modified and unmodified electrode surfaces. Efforts to characterize both of these types of surfaces were discussed, as well as some of the implications that such information would have to the electroanalytical chemist.

Chapters I and II contained information pertinent to surface characterization of modified electrode surfaces. "Characterization was defined in these chapters as that process whereby one can locate or map the individual modifying centers on chemically-modified electrode surfaces. The importance of this information is that size and spacial distribution of the modifying centers is critical to electrode performance and reproducibility.

Chapter I began with a review of the broad field of chemically-modified carbon paste electrodes. Topics such as the advantages of the use of carbon paste electrodes (CPE's) over other materials, basic reasons for modification of CPE's, and the various means of modification were all covered. The chapter concluded with a brief overview of the current instrumental methods of surface analysis and characterization.

Chapter II presented the experimental details of the characterization of a CPE modified with tris-(4,7-diphenyl-1,10-phenanthroline)iron(II) perchlorate. The redox potentials of chloroauric and ferrous complexes showed that if an iron(II)-modified CPE were treated with $AuCl_4^-$ complexes in hydrochloric acid, mapping of the active iron(II) centers via backscattered electron microscopy could be done. It was shown that gold(0) (from the concomitant oxidation of the iron(II) complexes) and/or gold(III) (from anion exchange reactions of $AuCl_4^-$ with the iron(II) complex counterions) could both enhance the conductivity of the CPE surface at those points of modification and elucidate the locations of the modifying centers. This characterization approach was verified by cyclic voltammetry and energy-dispersive X-ray analysis.

Chapters III and IV were concerned with the characterization of the roughness and reactivity of electrode surfaces, both of which play an important role in the performance and reproducibility of various electrochemical techniques. Recall that the word "characterization" referred in these chapters and the quantification of surface roughness and reactivity by determination of a specific type of fractal dimension referred to as the electrochemical dimension.

Chapter III devoted a considerable amount of effort to introducing the concepts of fractal geometry and fractal dimensions. These concepts were illustrated by discussing the classic problem posed by L. F. Richardson: how long is the coastline of Great Britain? In addition, the chapter outlined various theoretical and experimental techniques for the determination of the fractal dimension of objects or surfaces. Finally, a few paragraphs introduced the idea of a reaction dimension to describe the reactivity of surfaces. In particular, how the activity of catalysts scales with particle size.

Chapter IV gave the experimental details of the determination of the electrochemical dimension of unmodified glassy carbon and unmodified gold electrode surfaces. This was done using a homologous series of probe molecules of differing sizes, yet having the same redox center. The idea was that the electrochemical behaviors of these probe molecules would be the same; only their sizes should differ. The near linear plots of log apparent electrochemical area vs. log cross-sectional area of the probe molecules proved that fractal scaling laws were being obeyed.

In general, this thesis hopefully explained the importance of the characterization of electrode surfaces, and the implications of such knowledge for the electroanalytical chemist. Future directions for this research could include the adaptation of these experimental characterization techniques for other types of electrode systems, molecular probe species, etc. It might also be interesting to study the effect of modification on surface roughness and reactivity, i. e. how would the attachment of an enzyme, say, affect the roughness, reactivity, and electrode performance? Work also needs to be directed in the area of *correlating* electrode surface character with its actual performance.

BIBLIOGRAPHY

1. Kalcher, K. *Electroanalysis* **1990**, *2*, 419-433.

2. Ulakhovich, N. A.; Medyantseva, E. P.; Budnikov, G. K., *Zhur. Anal. Khim.* **1993**, *48*, 980-998, *J. Anal. Chem. (Engl. Transl.)* **1993**, *48*, 682-694.

3. Adams, R. N. *Anal. Chem.* **1958**, *30*, 1576.

4. Adams, Ralph N. "Electrochemistry at Solid Electrodes", Marcel Dekker, Inc.: New York, 1969; pp 280-283.

5. Hynes, C. J., Ph.D. Dissertation, Oklahoma State University, Stillwater, Okla., 1991.

6. Sun, G., Ph.D. Dissertation, Oklahoma State University, Stillwater, Okla., 1991.

7. Murray, R.; Ewing, A.; Durst, R. *Anal. Chem.* **1987**, *59*, 379A.

8. Kuwana, T.; French, W. *Anal. Chem.* **1964**, *36*, 241-2.

9. Schultz, F.; Kuwana, T. *J. Electroanal. Chem.* **1965**, *10*, 95-103.

10. Hernández, L.; Hernández, P.; Blanco, M.; Sánchez, M. *Analyst* **1988**, *113*, 41-43.

11. Baldwin, R.; Christensen, J.; Kryger, L. *Anal. Chem.* **1986**, *58*, 1790-1798.

12. Gardea-Torresdey, J.; Darnall, D.; Wang, J. *J. Electroanal. Chem.* **1988**, *252*, 197-208.

13. Brainina, Z.; Tchernyshova, A.; Yu, N.; Kalnyshevskaya, S.; Kalnyshevskaya, L. N. *Analyst* **1989**, *114*, 173-180.

14. Abruña, H. *Coord. Chem. Rev.* **1988**, *86*, 135-189.

15. Bonakdar, M.; Mottola, H. A. *Anal. Chim. Acta* **1989**, *224*, 305-313.

16. Geno, P.; Ravichandran, K.; Baldwin R. *J. Electroanal. Chem.* **1985**, *183*, 155-166.

17. Linders, C. R.; Patriarche, G. J.; Kauffman, J-M.; Guilbault, G. *Anal. Lett.* **1986**, *19*, 193-203.

18. Bonakdar, M.; Yu, J.; Mottola, H. A. *Talanta* **1989**, *36*, 219-225.

19. Hynes, C. J.; Bonakdar, M.; Mottola, H. A. *Electroanalysis* **1989**, *1*, 155-160.

20. Matuszewski, W.; Trojanowicz, M. *Analyst* **1988**, *113*, 735-738.

21. Kubiak, W.; Wang, J. *Anal. Chim. Acta* **1989**, *221*, 43-51.

22. Abu Nader, P.; Vives, S. S.; Mottola, H. A. *J. Electroanal. Chem.* **1989**, *266*, 47-55.

23. Bonakdar, M.; Vilchez, J. L.; Mottola, H. A. *J. Electroanal. Chem.* **1989**, *266*, 47-55.

24. Wang, J.; Freiha, B. *Anal. Chem.* **1984**, *56*, 849-852.

25. Ravichandran, K.; Baldwin, R. P. *Anal. Chem.* **1984**, *56*, 1744-1747.

26. Engstrom, R.; Strasser, V. *Anal. Chem.* **1984**, *56*, 136-141.

27. Ormonde, D. E.; O'Neill, R. D. *J. Electroanal. Chem.* **1989**, *261*, 463-469.

28. Lyne, P. D.; O'Neill, R. D. *Anal. Chem.* **1989**, *61*, 2323-2327.

29. a) Abu Nader, P. R.; Ortiz, P. I.; Mottola, H. A. *Anal. Chim. Acta* **1991**, *249*, 395-404; b) Ortiz, P. I.; Nader, P. R.; Mottola, H. A. *Electroanalysis* **1993**, *5*, 165-169.

30. Hale, P. D.; Inagaki, T.; Karan, H. I.; Okamoto, Y.; Shotheim, T. A. *J. Am. Chem. Soc.* **1989**, *111*, 3482-3484.

31. Dicks, J. M.; Astron, W. J.; Davis, G. ; Turner, A. P. F. *Anal. Chim. Acta* **1986**, *182*, 103.

32. Ikeda, T.; Hamada, H.; Miki, K.; Senda, M. *Agric. Biol. Chem.* **1985**, *49*, 541-543.

33. Cheek, G. T.; Nelson, R. F. *Anal. Lett.* **1978**, *A11*, 393-402.

34. Kamin, R. A.; Wilson, G. S. *Anal. Chem.* **1980**, *52*, 1198-1205.

35. Albahadily, F. N., Ph. D. Dissertation, Oklahoma State University, Stillwater, Okla., 1989.

36. Murray, R. W. In "Electroanalytical Chemistry"; Bard, A. J., Ed.; Marcel Dekker: New York, 1984; Vol. 13, pp. 191-368.

37. Yao, M.; Musha, S. *Anal. Chim. Acta* **1979**, *110*, 203-209.

38. Almeida, N. F.; Mulchandani, A. K. *Anal. Chim. Acta* **1993**, *282*, 353-361.

39. Dominguez-Sanchez, P.; O'Sullivan, C. K.; Miranda-Ordieres, A. J.; Tuñon-Blanco, P.; Smyth, M. R. *Anal. Chim. Acta* **1994**, *291*, 349-356.

40. Andrieux, C. P.; Audebert, P.; Divisia-Blohorn, B.; Linquette-Maillet, S. *J. Electroanal. Chem.* **1993**, *353*, 289-296.

41. Yu, J., Ph.D. Dissertation, Oklahoma State University, Stillwater, Okla., 1991.

42. Wang, J.; Chen, Q. *Anal. Chem.* **1993**, *65*, 2698.

43. Wang, J.; Romero, E. G.; Reviejo, A. J. *J. Electroanal. Chem.* **1993**, *353*, 113-120.

44. Norton, H. "Electronic Analysis Instruments", Prentice Hall, Inc.: Englewood Cliffs, N. J., 1992; pp. 161-166.

45. Hayes, M. In "Techniques in Electrochemistry, Corrosion and Metal Finishing--A Handbook"; Kuhn, A. T., Ed.; John Wiley and Sons Ltd.: New York, 1987; Chapter 24.

46. Bockris, J. O.; Khan, S. U. M. "Surface Electrochemistry, A Molecular Level Approach", Plenum Press: New York, 1993; pp. 34-35, pg. 43.

47. Ingle, J. D.; Crouch, S. R. "Spectrochemical Analysis"; Prentice Hall: Englewood Cliffs, New Jersey, 1988; pp. 429-432, pp. 494-513.

48. Rüdenauer, F. G. *Anal. Chim. Acta* **1994**, *297*, 197-230.

49. Grimstone, A. V.; Skaer, R. J. "A Guidebook to Microscopical Methods", Cambridge University Press: London, 1972, pp. 1-6.

50. Marti, O.; Amrein, M. "STM and SFM in Biology", Academic Press, Inc.: San Diego, Calif., 1993; Chapter 1.

51. McDermott, M. T.; McDermott, C. A.; McCreery, R. L. *Anal. Chem.* **1993**, *65*, 934-44.

52. Freund, M. S.; Brajter-Toth, A; Cotton, T. M. *Anal. Chem.* **1991**, *63*, 1047-9.

53. Womelsdorf, J. F.; Ermler, W. C.; Sandroff, C. J. *J. Phys. Chem.* **1991**, *95*, 503-505.

54. Strong, L.; Evans, D. F.; Gladfelter, W. L. *Langmuir* **1991**, *7*, 442-443.

55. Mohanty, S. B. "Electron Microscopy for Biologists", Charles C. Thomas: Springfield, Ill., 1982; pp. 5-21.

56. Goldstein, J.; Newbury, D.; Echlin, P.; Joy, D.; Romig, A.; Lyman, C.; Fiori, C.; Lifshin, E. "Scanning Electron Microscopy and X-Ray Microanalysis", 2nd. ed.; Plenum Press: New York, 1992.

57. Postek, M. T.; Howard, K. S.; Johnson, A. H.; McMichael, K. L. "Scanning Electron Microscopy: A Student's Handbook"; Ladd Research, Inc.: Burlington, Vt., 1980; Chapters 2, 3, and 4.

58. (a) Wang, J.; Brennsteiner, A.; Angnes, L.; Sylwester, A.; LaGasse, R.; Bitsch, N. *Anal. Chem.* **1992**, *64*, 151-155; (b) Wang, J.; Angnes, L.; Tobias, H. *Anal. Chem.* **1993**, *65*, 2300-2303.

59. Bodalbhai, L.; Brajter-Toth, A. *Anal. Chim. Acta* **1990**, *231*, 191-201.

60. Pantano, P.; Kuhr, W. *Anal. Chem.* **1991**, *63*, 1413-1418.

61. Charlot, G. "Theorie et Methode Nouvelles d'Analyse Qualitative", 3rd ed.; Casa Masson: Paris, 1954; Chapter XXX.

62. Fiori, C. E.; Newbury, D. E. "SEM/1978/I"; SEM, Inc.: AMF O'Hare, Ill., 1978; pg. 401.

63. Preining, O. *Fresenius' Z. Anal. Chem.* **1990**, *337*, 172-175.

64. Vicsek, T. "Fractal Growth Phenomena", 2nd ed.; World Scientific Publishing Co.: River Edge, New Jersey, 1992, Chapter 2 and 4.

65. Mandelbrot, B. B. "The Fractal Geometry of Nature", W. H. Freeman and Company: New York, 1977.

66. Richardson, L. F. *Gen. Sys. Yearb.* **1961**, *6*, 139.

67. Pfeifer, P.; Obert M. In "The Fractal Approach to Heterogeneous Chemistry"; Avnir, D., Ed.; John Wiley and Sons Ltd.: New York, 1990; Chapter 1.2.

68. Avnir, D.; Farin, D.; Pfeifer, P. *New J. Chem.* **1992**, *16*, 439-449.

69. Huang, J.; Tucotte, D. L. *J. Optical Soc. America*, **1990**, *7*, 1124-30.

70. Rigaut, J. P., Paris, France, 1988, Equipe Analyse d'Images Report.

71. Williams, J. M.; Beebe, T. P., Jr. *J. Phys. Chem.* **1993**, *97*, 6249-54.

72. Skatkov, L. I.; Konotop, V. V.; Cheremskoy, P. G.; Gomozov, V. P.; Bayrachny, B. I. *Appl. Surface Sci.* **1994**, *81*, 427-429.

73. Schmidt, P. W.; Hohr, A.; Neuman, H. B.; Kaiser, H.; Avnir, D.; Lin, J. S. *J. Chem. Phys.* **1989**, *90*, 5016-5023.

74. Bonczyk, P. A.; Hall, R. J. *Langmuir*, **1992**, *8*, 1666-1670.

75. Pfeifer, P.; Avnir, D. *J. Chem. Phys.* **1983**, *79*, 3558-3565.

76. Avnir, D.; Farin, D. *Nature* **1984**, *308*, 261-263.

77. Avnir, D.; Pfeifer, P. *Nouv. J. Chim.* **1983**, *7*, 71-72.

78. Ismail, I. M. K.; Pfeifer, P. *Langmuir* **1994**, *10*, 1532-1538.

79. Goodwin, A. E. Ph.D. Dissertation, Oklahoma State University, Stillwater, Okla., 1988.

80. Bowden, F. P.; Rideal, E. K. *Proc. Roy. Soc.* **1928**, *A120*, 59-79.

81. Nyikos, L.; Pajkossy, T. *Electrochim. Acta* **1985**, *30*, 1533-1540.

82. Pajkossy, T. *J. Electroanal. Chem.* **1991**, *300*, 1-11.

83. Nyikos, L.; Pajkossy, T. *Electrochim. Acta* **1986**, *31*, 1347-1350.

84. Nyikos, L.; Pajkossy, T. *Electrochim. Acta* **1989**, *34*, 171.

85. Wu, W-T.; McEvoy, A. J.; Grätzel, M. *J. Electroanal. Chem.* **1990**, *291*, 235-242.

86. Crevs, A. H.; Carro, P.; González, S.; Salvarezza, R. C.; Arvía, A. J. *J. Electrochem. Soc.* **1992**, *139*, 1064-1070.

87. Chen, C. P.; Jorné, J. *J. Electrochem. Soc.* **1990**, *137*, 2047-2051.

88. Bard, A. J.; Faulkner, L. R. "Electrochemical Methods: Fundamentals and Applications"; John Wiley and Sons, Inc.: New York, 1980; Chapter 5.

89. Farin, D.; Avnir, D. *J. Am. Chem. Soc.* **1988**, *110*, 2039-2045.

90. Howard, R., Oklahoma State University, personal communication, 1995.

91. Mottola, H. A. *Trends Anal. Chem.* **1990**, *9*, 297-302.

92. a) Bauer, N. In "Techniques of Organic Chemistry: Physical Methods of Organic Chemistry", 2nd ed.; Weissberger, A., Ed.; Wiley Interscience: New York, 1949; Vol. I, pp. 99-102; b) Reilly, J.; Rae, W. N. "Physico-Chemical Methods", 5th ed.; Van Nostrand: New York, 1954; pp. 586-592.

93. Brunel, R. F.; Bibber, K. In "International Critical Tables of Numerical Data: Physics, Chemistry and Technology"; Washburn, E. W., Ed.; McGraw-Hill: New York, 1928; pp. 27-30.

94. Edgar, G. A. "Measure, Topology, and Fractal Geometry"; Springer-Verlag: New York, 1990, p. v.

95. Li, S.; Mottola, H. A. *Anal. Chim. Acta* **1994**, *289*, 79-85.

96. (a) Taylor, G. *Proc. R. Soc. London, Ser. A* **1953**, *219*, 186; (b) Taylor, G. *Proc. R. Soc. London, Ser. A* **1954**, *225*, 473.

97. McClellan, A. L.; Harnsberger, H. F. *J. Colloid. Interfac. Sci.* **1967**, *23*, 577.

2

VITA

Dale William Harak

Candidate for the Degree of

Doctor of Philosophy

Thesis: CHARACTERIZATION STUDIES OF UNMODIFIED AND CHEMICALLY MODIFIED ELECTRODE SURFACES

Major Field: Chemistry

Biographical:

Personal Data: Born in Enid, Oklahoma, July 22, 1965, the son of Henry R. and Maxine L. Harak.

Education: Received Bachelor of Science Degree in Chemistry from Phillips University, Enid, Oklahoma, May, 1989; completed the requirements for the Doctor of Philosophy degree at Oklahoma State University, Stillwater, Oklahoma in December, 1995.

Professional Experience: principal clarinet, Enid-Phillips Symphony Orchestra, Enid, Oklahoma, August, 1983 to May, 1995; church organist, First United Methodist Church, Crescent, Oklahoma, July, 1987 to August, 1995; church musician, St. Camillus Catholic Church, Marshall, Oklahoma, July, 1988 to August, 1995; teaching/research assistant, Dept. of Chemistry, Oklahoma State University, Stillwater, Oklahoma, June, 1989 to August, 1995; assistant professor, Dept. of Chemistry, Rockhurst College, Kansas City, Missouri, August, 1995 to present.